THE UNIVERSITY *of* EDINBURGH

Satellite investigations of ice dynamics and supraglacial lake development in Greenland

Kate H. Briggs

PhD

University of Edinburgh

School of Geosciences

College of Science and Engineering

2011

Declaration

This thesis embodies 4.5 years of my life. It was composed by myself and the work contained herein is my own, and where chapters have been prepared for submission to journals the authorship and contributions are noted appropriately. This thesis has not been submitted for any other degree or professional qualification.

Kate H. Briggs

Acknowledgements

I have rather a lot of people to thank for the guidance, support and kindness they have shown me throughout the past four (and the rest) years of my PhD. First of all, I am thankful to my supervisors, Andy Shepherd and Pete Nienow, for both their academic guidance and for giving me patience and understanding when I really needed it. Beyond the guidance of my supervisors I have had many useful discussions with, and advice from, the members of the glaciology group in Edinburgh (and now Leeds) past and present - Malcolm McMillan, Steve Palmer, Eero Rinne, Aud Sundal, Ian Bartholomew, Tom Cowton, Stew Jamieson, Vicki Parry, Andy Hein, Mehmet Karatay, Andy Sole, Andy Wright, Neil Ross, Santiago de la Pena and Noel Gourmelen. I want to extend special thanks to Steve Palmer, Eero Rinne and Malcolm McMillan for all the help they have given me. I am grateful to IT help at Edinburgh, in particular Chris Place and Steve Dowers, for resolving my computing woes.

As important as the academic support received during my PhD has been the support provided by friends and family. To my office mates Lynsey Callaghan, Michaela Newton, Ian Bartholomew, Matthew Brolly, Martin Hurst, Steve Palmer, Richard Streeter, Eero Rinne, Tom Cowton, Ed Mitchard, Mal McMillan and Katharine Fitzpatrick, who I shared the PhD experience with, for general advice, the occasional rant and a lot of the all important banter- thank you! Thanks to my good friends, Katharine Fitzpatrick, Elizabeth Richardson, Carolyn Anderson, Anna Jagan, Mal McMillan, Rik Higham, Eero Rinne, Tom Russon, Steve Palmer, Innes Keighren, Richard Phillips, Steve Binnie, Addy Pope, Raph Bleakley, Mehmet Karatay, Hannah Mathers and Jennifer Wyllie with whom I have shared many good chats, tasty meals, ESSENTIAL tea and cake breaks, cinema trips, great runs, climbs and walks, and lovely holidays throughout my PhD, all of which have kept me smiling! Thanks to my family; Mum, Adam, Lynda, Pam, Vicky, Daisy, Grandma and Aunty Joan, for being generally wonderful and making me feel so secure. And last, but not least, to my Dad, who in my opinion IS the best Dad in the world – your love and support made this possible for me- thank you!

Contents

List of figures

List of tables

Abstract

This thesis aims to improve the current understanding of the processes which control the flow variability of Greenland Ice Sheet (GrIS) outlet glaciers. The most recent Intergovernmental Governmental Panel on Climate Change (IPCC) report (Meehl *et al.,* 2007) identifies that a critical limitation to forecasts of sea-level rise are uncertainties in modelling the ice dynamics of the GrIS. Using Synthetic Aperture Radar (SAR) feature tracking, seasonal velocities of land- and marine- terminating glaciers in a region in the northeast of Greenland are measured. Records of air temperature in conjunction with seasonal observations of supraglacial lake development, sea ice conditions and ice front positions, derived from SAR imagery, are used to investigate the controls on the observed variations in ice velocity. A clear link between ice velocities and glacier hydrology is found. These findings are consistent with observations from other glaciers in Greenland and are suggestive of a universal hydrological forcing of ice velocity for the whole of the GrIS ablation zone.

Lake drainage events have been identified as a key factor in linking atmospheric changes, glacier hydrology and ice velocities in Greenland. For modelling purposes, a means of parameterising the distribution and evolution of supraglacial lakes is therefore needed. Assuming that water will pond in surface depressions, this thesis assesses the ability of using Digital Elevation Models (DEMs) for this purpose. High resolution DEMs are created using Interferometric SAR (InSAR) for two, separate regions of the GrIS. The positions and areal extent of surface depressions are compared with those of lakes observed in optical satellite imagery. The level of correspondence between the two datasets is found to be poor as a result of the resolution of the DEMs and the physical differences between surface depressions and lakes (e.g. lakes may not fill the capacity of the depression). An alternative method for parameterising the seasonal distribution of supra-glacial lakes, by extrapolating trends observed in current lake distributions, is investigated. The locations and evolution of lakes in the west of Greenland during the summer of 2003 are mapped using 47 Moderate Resolution Imaging Spectroradiometer (MODIS) images. Clear

trends are identified in the distributions of lakes with elevation and are linked to the seasonal melt-cycle and to changes in ice thickness and its influence on surface depressions, tensile stresses and hydrofracturing. It may be possible to extrapolate these trends to other regions and higher elevations on the ice sheet, thereby enabling the distribution of lakes to be parameterised in ice sheet models. The findings of this thesis help to contribute to the understanding of the interaction between climate and ice dynamics in the context of the GrIS.

Chapter 1: Introduction

1.1 Aim

This thesis aims to provide an improved understanding and parameterisation of processes linking climate change to the dynamics and mass loss of the Greenland Ice Sheet (GrIS). This is achieved using a range of remotely sensed images and techniques, including optical and Synthetic Aperture Radar (SAR) data and Interferometric SAR (InSAR) and SAR feature tracking methods. This chapter outlines the broad motivation for this research and the structure of this thesis.

1.2 Motivation

Sea level rise poses a major threat to life and livelihoods in coastal regions across the globe (Parry *et al.*, 2007). Between 1961 and 2003 global sea level rose at an average rate of between 1.3 and 2.3 mm per year (Meehl *et al.*, 2007) (Figure 1.1). Forecasts suggest that sea level will continue to rise over the coming centuries and millennia (Meehl *et al.*, 2007). The most up to date projections predict an overall increase in sea level of 32 ± 5 cm by 2050 (Rignot *et al.*, 2011).

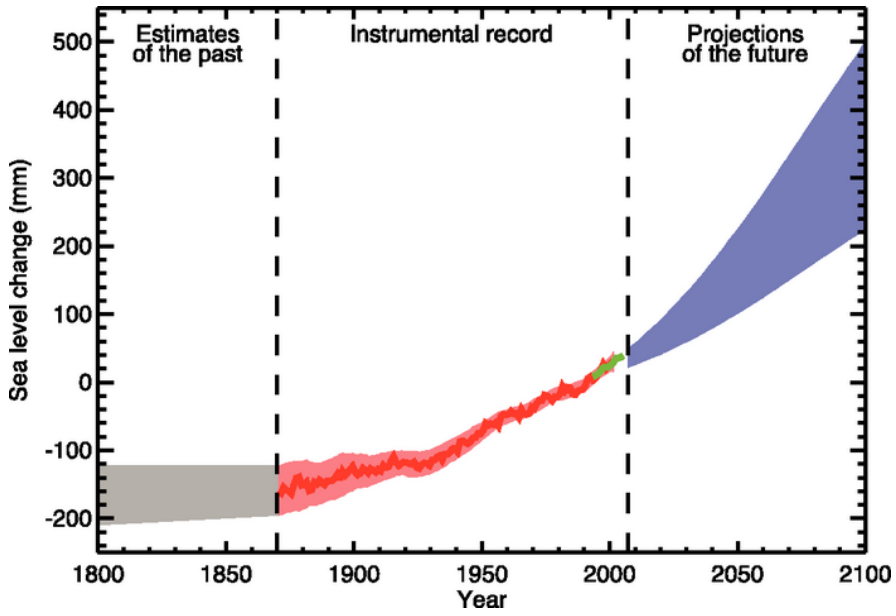

Figure 1.1: Global mean sea level (deviation from the 1980-1999 mean) in the past and projected for the future. Before 1870 global measurements of sea level are not available and the grey shading represents the uncertainty in the estimated long-term rate of sea-level change. From 1870, the red line shows a reconstruction of global mean sea level from tide gauges and the green line, from satellite altimetry. The 21st century Intergovernmental Panel on Climate Change (IPCC) projections for sea level rise are in blue and represent a range of model projections. (Taken from Meehl *et al.*, 2007).

Changes in sea level are mostly related to climate change and occur due to changes in the volume of water in the oceans (eustatic sea level changes) and vertical land movements (isostatic sea level changes). Eustatic sea level changes occur as a result of thermal expansion of the oceans and the exchange of water between oceans and other reservoirs (e.g. glaciers, ice caps and ice sheets). Isostatic sea level changes result from, for example, glacial isostatic adjustments and sedimentation. In the latter part of the 20th century, the largest contributions to sea level rise were from thermal expansion of the oceans and melting of small glaciers and ice caps (Meehl *et al.*, 2007). However, forecasts suggest that over the next few decades sea level rise will be dominated by the contributions from the Greenland and Antarctic ice sheets (Rignot *et al.*, 2011).

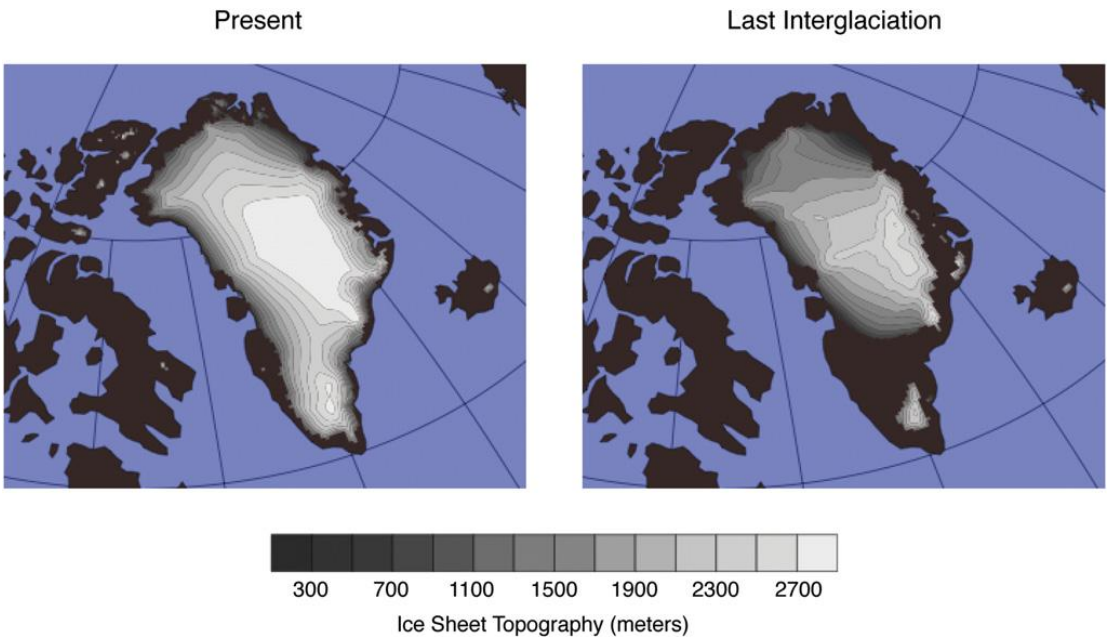

Figure 1.2: The GrIS today (left) and during marine isotope stage (MIS) 5e, the last interglacial, (right) from the ice sheet modelling study of Otto-Bliesner *et al.*, (2006).

The GrIS has the potential to raise sea level by 7 m if it disappears entirely (Bamber *et al.*, 2001a). Records and modelling of past interglacials suggest that mass losses from the GrIS may have made substantial contributions to sea level rise. For example, during the last interglacial (the Eemian, ~130 ka), when global sea levels were 4-6 m higher than at present (Overpeck *et al.*, 2006), losses from the GrIS (e.g. Otto-Bliesner *et al.*, 2006) (Figure 1.2) may have contributed up to 5.5 m to sea level rise (e.g. Letreguilly *et al.*, 1991; Ritz *et al.*, 1997; Cuffey and Marshall, 2000). In the future, model predictions indicate that forecasted warming will lead to shrinking of the ice sheet (e.g. Huybrechts and de Wolde, 1999; Gregory *et al.*, 2004; Alley *et al.*, 2005a) (Figure 1.3) and the most extreme scenarios have suggested that the ice sheet may disappear in as little as 1000 years (e.g. Greve *et al.*, 2000; Gregory *et al.*, 2004).

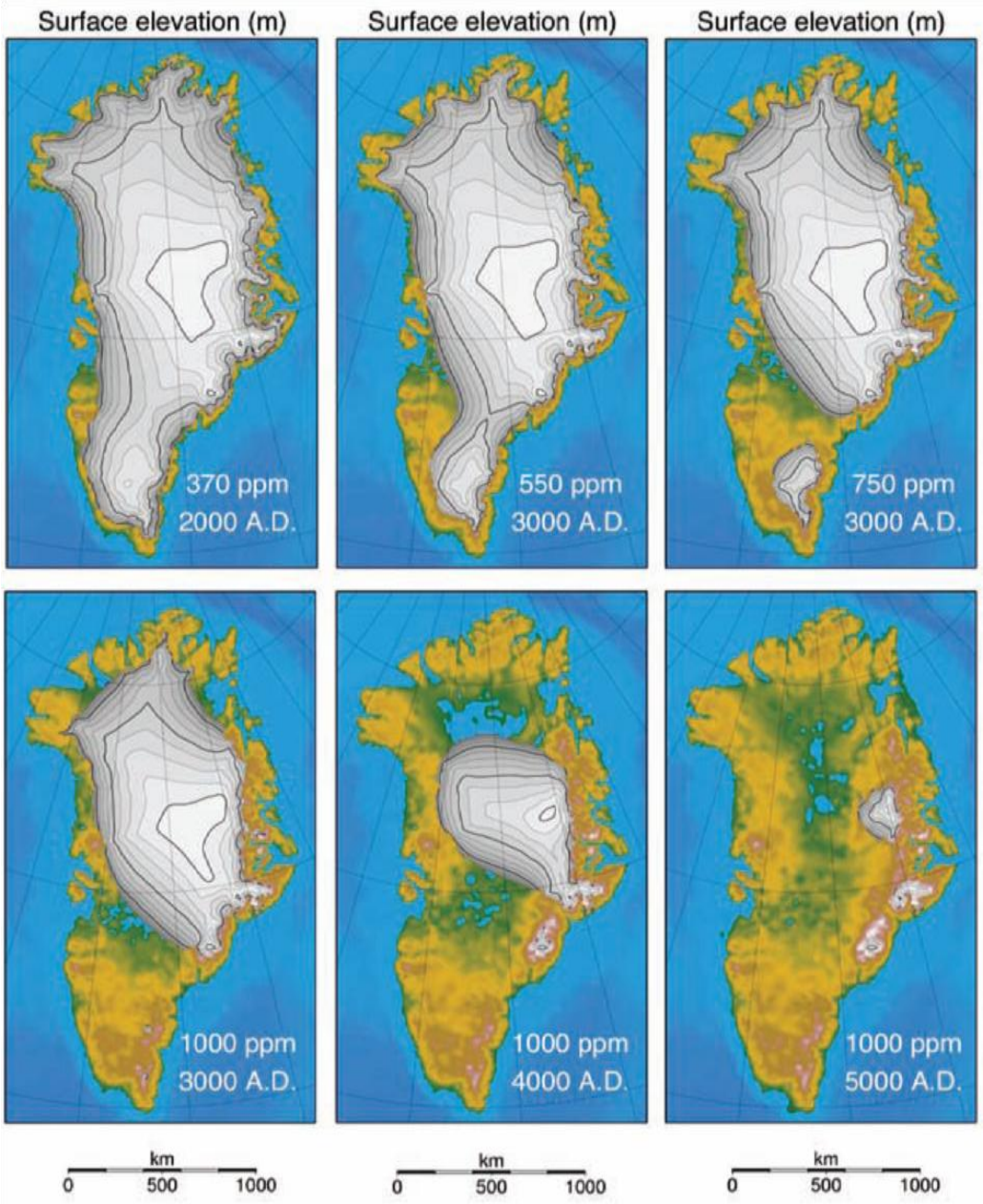

Figure 1.3: The modelled future evolution of the GrIS based on a range of IPCC warming scenarios forced by different atmospheric carbon dioxide concentrations (Church *et al.*, 2001). Taken from Alley *et al.*, 2005a.

At present, observations show that the GrIS is losing mass (e.g. Krabill *et al.*, 2000, 2004; Luthcke *et al.*, 2006; Rignot and Kanagaratnam, 2006; Thomas *et al.*, 2006; Rignot *et al.*, 2008; Wouters *et al.*, 2008; Velicogna, 2009; Slobbe *et al.*, 2009; Zwally *et al.*, 2011) (Figure 1.4) at a rate which has increased over the past decades (e.g. Thomas *et al.*, 2008; Zwally *et al.*, 2011) (Figure 1.4). The ice sheet is losing

mass primarily as a result of increasing rates of surface melting and ice discharge to the oceans. The increase in the rate of mass loss due to surface melting is the direct result of an increase in surface temperatures (e.g. Hall *et al.*, 2008; Box *et al.*, 2009). Increasing rates of ice discharge have resulted from increased outlet glacier flow rates (e.g. Rignot and Kanagaratnam, 2006; Rignot *et al.*, 2008; van den Broeke *et al.*, 2009). However, the causes of the increased outlet glacier flow rates are not fully understood.

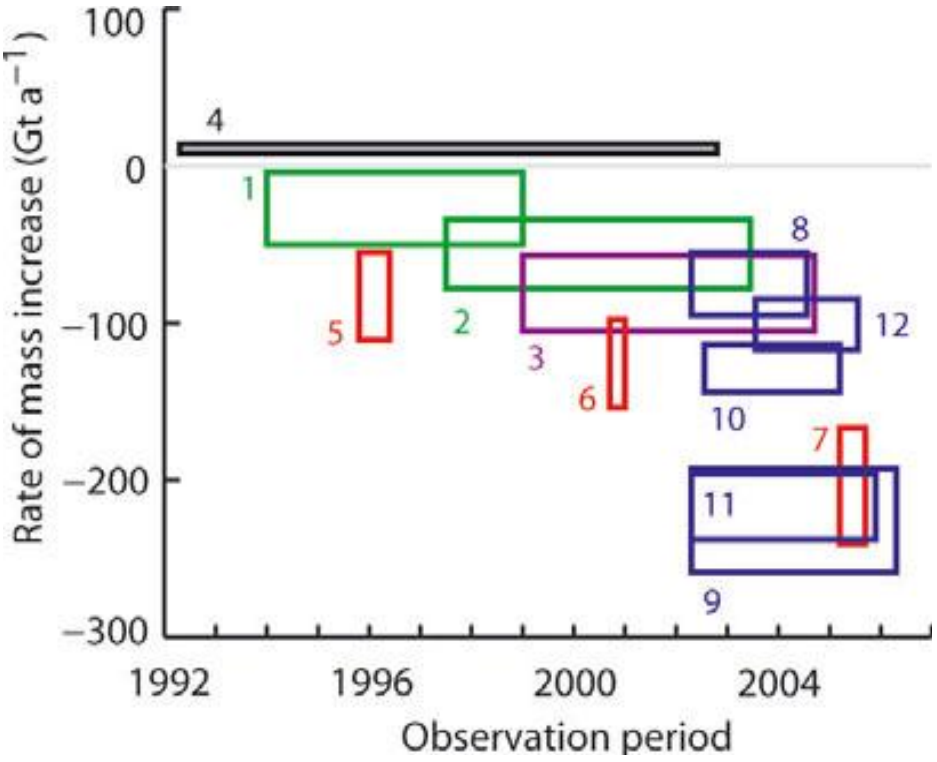

Figure 1.4: Estimates of the rate of GrIS mass change based on European Remote Sensing (ERS) satellite radar altimeter data (black), airborne laser altimeter surveys (green), airborne/satellite laser altimeter surveys (purple), massbudget calculations (red) and temporal changes in gravity (blue). Rectangles depict the time periods of observations (horizontal) and the upper and lower estimates of mass balance (vertical). Sources (corresponding to numbers on rectangles): 1 and 2: Krabill *et al.*, (2000, 2004); 3: Thomas *et al.*, (2006); 4: Zwally *et al.*, (2005); 5–7: Rignot and Kanagaratnam (2006); 8 and 9: Velicogna and Wahr (2005, 2006); 10: Ramillien *et al.*, (2006); 11: Chen *et al.*, (2006); 12: Luthke *et al.*, (2006). (Taken from Thomas *et al.*, 2008)

For society to be able to most effectively mitigate for the potential impacts of sea-level rise, accurate predictions of the rate at which it may occur must be made. The accuracy of these predictions is controlled by the reliability of the models we use to make the forecasts, which in turn is a product of our knowledge of the physical

systems they aim to represent. The most recent Intergovernmental Panel on Climate Change (IPCC) report from 2007 (Lemke *et al.*, 2007) identified that a key limitation to forecasts of sea level rise stems from a high level of uncertainty in the predictions of future mass losses from the GrIS. This is the result of the uncertainties in the links between climate and the mechanisms controlling ice flow rates and therefore ice discharge and mass loss. It is critical for the accuracy of forecasts of ice sheet mass loss and sea level rise, that we are able to improve our understanding of these links. Therefore this has become a key focus of glaciologists and this thesis.

1.3 Thesis Structure

The following chapter will outline the recent dynamic changes in Greenland and their causes, providing a background for this thesis and justification for the key objectives set out therein. Chapter 3 provides a review of the methods used to achieve these objectives. Chapters 4, 5, and 6 present the methods, results and discussion of this thesis in the format of papers prepared for submission to scientific journals. The final chapter, Chapter 7, provides a synthesis of the findings of this thesis, placing our results into a wider context, discussing any limitations and outlining the potential for future research.

Chapter 2: Greenland Ice Sheet flow dynamics

2.1 Introduction

The motion of ice under the force of gravity is a basic characteristic of all glaciers and ice sheets. The degree of movement of glaciers is a balance between driving stresses (i.e. gravity, ice thickness and surface slope), resisting frictional forces at the lateral margins and the bed, and the longitudinal stress gradient (van der Veen, 1999). There are three principal mechanisms by which glacier flow occurs; these are internal deformation, deformation of the glacier bed and basal sliding (Paterson, 1994).

Internal deformation results from movement within or between individual ice crystals and brittle failure of the ice. In regions where the ice sheet is frozen to its bed (e.g. in the interior), ice sheet flow will be dominated by internal deformation. Ice velocities resulting from internal deformation are controlled by ice temperature, particles in the ice, ice thickness and surface slope which are relatively slow to change, therefore changes in ice velocities resulting from changes in internal deformation occur slowly. Deformation of subglacial till is thought to occur when the critical shear stress of the sediment is exceeded and this is dependent on the shear strength (or material composition) of the till, saturation and the pressure exerted by the overlying ice (Paterson, 1994). Due to the difficulties in monitoring the bed of an ice sheet, little is known about bed deformation. Basal sliding of the glacier at the ice-bed interface responds to changes in subglacial effective pressures (Paterson, 1994), often as a result of changing water pressure, and is also sensitive to changes in the longitudinal stress gradient (e.g. from glacier calving or buttressing). Changes in both the basal sliding and subglacial till deformation rates can occur rapidly.

Until recently changes in the dynamics of ice sheets were considered to occur over millennial timescales (Houghton *et al.,* 2001). However, observations over the course

of the past decade have revealed major changes in the flow of outlet glaciers that occur over timescales of hours to years (e.g. Rignot and Kanagaratnam, 2006; Howat *et al.,* 2007; Das *et al.,* 2008; Joughin *et al.,* 2008a,b; Shepherd *et al.,* 2009). In Greenland, Rignot and Kanagaratnam (2006) showed that, due to a widespread acceleration of glaciers, the rate of ice discharge tripled between 1996 and 2005 and several authors have reported a rapid switching between accelerating and decelerating flow at a number of marine-terminating glaciers in the southeast and west of the ice sheet (e.g. Luckman *et al.,* 2006; Rignot and Kanagaratnam, 2006; Howat *et al.,* 2007; Howat *et al.,* 2008). Initially it was not known what was driving these changes and whether they represented short term changes or were part of long term ice sheet instability. Although considerable progress has been made in understanding the forces and mechanisms controlling these changes, our knowledge remains incomplete. The following sections will outline the current state of our knowledge.

Some evidence exists for GrIS sliding variability resulting from glacier surging (e.g. Weidick, 1988; Jiskoot *et al.,* 2003) and geothermal heat fluxes (e.g. Fahnestock *et al.,* 2001), however, the widespread and synchronous nature of the recent dynamic changes are suggestive of regional climatic forcing (Luckman *et al.,* 2006; Howat *et al.,* 2008). Climate forcing has been linked to GrIS dynamic changes in two ways: 1) through ice-ocean interactions in ocean-terminating outlet glaciers (e.g. Holland *et al.,* 2008; Sole *et al.,* 2008; Howat *et al.,* 2008) and 2) with increased surface meltwater supply to the bed of inland ice (e.g. Zwally *et al.,* 2002; Parizek and Alley, 2004; van de Wal *et al.,* 2008; Shepherd *et al.,* 2009).

2.2 Dynamic changes at marine margins due to ice-ocean interactions

Recent studies show that the most substantial velocity changes and thinning due to increased ice velocities, have occurred at the marine-terminating margins (e.g. Abdalati *et al.,* 2001; Krabill *et al.,* 2004; Sole *et al.,* 2008; Thomas *et al.,*2009; Pritchard *et al.,* 2009; Joughin *et al.,* 2010a). The contrast between the magnitude of dynamic changes seen at marine- and land-terminating outlet glaciers suggests that either the forcing mechanisms driving the recent velocity variations are specific to

marine-terminating margins and/or that marine based glaciers are more sensitive to perturbations to the ice sheet. It has been suggested that tidewater glaciers may be responding to changes in the ocean and/or the atmosphere.

The stability of tidewater glaciers is very sensitive to changes at their fronts (Meier and Post, 1987; Pfeffer, 2007). A tidewater glacier in a stable state (i.e. neither advancing nor retreating) is grounded at its terminus; perturbations of conditions at the terminus which lead to flotation will cause the glacier to become unstable, accelerate and undergo rapid retreat (Meier and Post, 1987; Pfeffer, 2007). Observations have shown that that the retreats and accelerations of many of the tidewater glaciers in Greenland began with changes to the front of the glaciers (Howat *et al.,* 2007, 2008; Joughin *et al.,* 2004, 2008b; Thomas, 2004; Sole *et al.,* 2008), a finding confirmed by the recent modelling experiments of Nick *et al.,* (2009). There are a number of suggestions as to what could have forced these changes which include reductions in sea ice (Amundson *et al.,* 2010), increased undercutting at calving fronts (Motyka *et al.,* 2003; Nick *et al.,* 2009) and increased basal melting and thinning of floating ice tongues (Holland *et al.,* 2008) due to warming ocean temperatures, and higher rates of calving caused by the increases in surface meltwater resulting from atmospheric warming (Motyka *et al.,* 2003; Benn *et al.,* 2007).

2.2.1 Ocean induced acceleration of marine- terminating glaciers

Oceanographic data suggests that the recent perturbations at Greenland tidewater glacier termini may be linked to an increase in ocean temperatures. Records show that ocean temperatures on the continental shelf to the Southeast and West of Greenland have been warming since the mid 1990's (Figure 2.1) (Holland *et al.,* 2008; Hanna *et al.,* 2009; Murray *et al.,* 2011). This warming in ocean temperatures occurred as a switch in the phase of the North Atlantic Oscillation (NAO) in 1995/1996 weakened the subpolar gyre allowing the warm, subpolar Irminger Current to spread westward under the cold polar waters and onto the Greenland continental shelf (Holland *et al.,*2008). Holland *et al.,* (2008) report a rise in the temperature of bottom waters (150-600 m depth including warm Irminger waters and

overlying mixed waters) over much of the West Greenland continental shelf from 1.7˚C in 1995 to 3.3˚C from 1998 and thereafter (Figure 2.1). For this rise in ocean temperatures to have had a direct impact on marine-terminating glaciers, the warm waters must have been able to be transmitted into the fjords and to the ice fronts. On the continental shelf, the warm Irminger waters are found at depths of between 400-600 m and are separated from the overlying cold polar waters (50-100 m depth) by a layer of mixed water (Hanna *et al.,* 2009) (Figure 2.2). Most of the fjords in Greenland contain sills at depths ranging from nearly 0 m to over 500 m (Hanna *et al.,* 2009); therefore, with the exception of the shallowest fjords, the warm mixed waters are able to penetrate into the fjords. These warm waters are drawn into the fjords and then transported to the glacier front by circulation in the fjord. The circulation may be driven by a combination of outflow of large inputs of glacier meltwater at the head of the fjord and balanced by a saltier inflow at depth (Ribergaard, 2007; Straneo *et al.,* 2011), and by pressure gradients between the fjord and the shelf as a result of alongshore winds (see Straneo *et al.,* 2010).

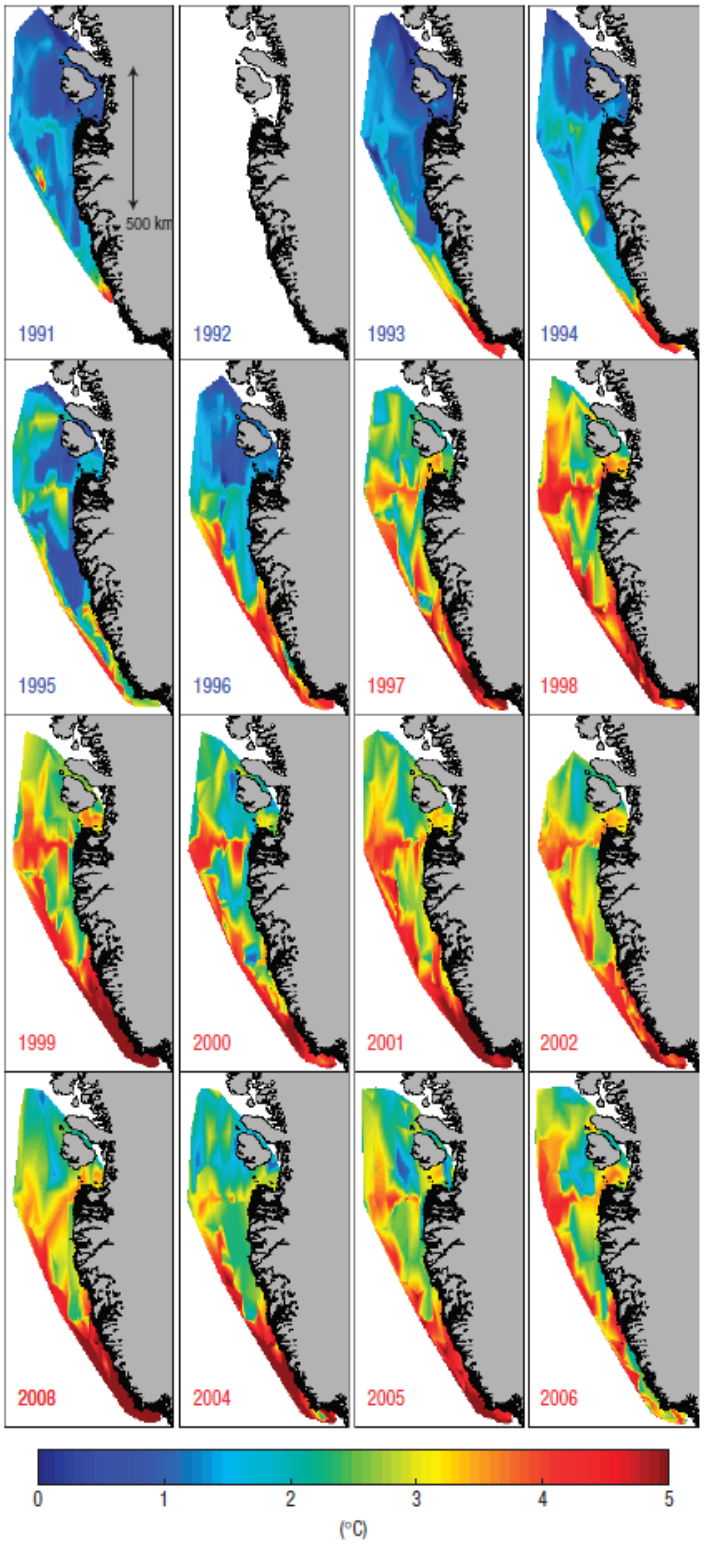

Figure 2.1: Subsurface ocean temperatures over the west Greenland continental shelf from 1991-2006. A sudden increase in subsurface water temperatures occurred in 1997, when warm waters flooded into Disko Bay and the Jakobshavn fjord. Taken from Holland *et al.*, (2008).

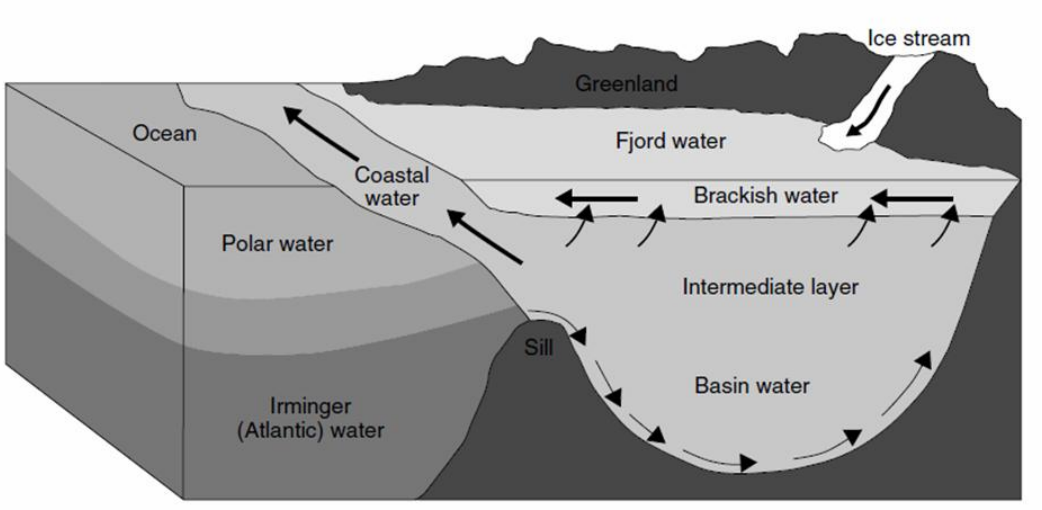

Figure 2.2: Circulation in a West Greenland fjord. Taken from Hanna *et al.*, (2010).

The precise mechanism by which the increased ocean temperatures may have affected thinning, retreat and acceleration of the glacier termini is still unproven, however, a number of theories exist. Rignot *et al.*, (2010) calculated the melt rates of four grounded tidewater glaciers in three different fjord systems in central West Greenland using oceanographic data, bathymetry and modelled convective flow at the ice fronts. They found rates of submarine melting at the calving front ranging from 0.7 ± 0.2 to 3.9 ± 0.8 m d^{-1}, which are two orders of magnitude larger than surface melt rates and comparable to ice loss from iceberg discharge. They postulate that these melt rates could lead to destabilisation of the ice front in two ways; firstly, by melting at the calving front of grounded ice directly, submarine melting will lead to grounding line retreat, or secondly, by increased calving as the warm waters undercut the submerged ice face, promoting calving below the water surface and causing ice front retreat. Holland *et al.*, (2008) examined the impact of submarine melting on Jakobshavn Isbrae, which was until the early 2000's buttressed by a permanent floating ice tongue. They suggest that the floating ice tongue disintegrated as a result of rapid submarine melt-induced thinning. The initial thinning of the tongue would have decreased its buttressing effect and in turn, reduced the backpressure on the upstream ice, increasing rates of longitudinal

stretching and velocity. The complete breakup of the tongue would have caused an immediate increase in longitudinal stretching and therefore velocity.

Warmer ocean temperatures also cause a decrease in sea ice. Calving rates, and therefore glacier flow rates, of floating tidewater glaciers have been linked with seasonal and interannual fluctuations in concentrations of sea ice (e.g. Higgins, 1991; Sohn *et al.,* 1998; Reeh *et al.,* 2001; Copland *et al.,* 2007; Joughin *et al.,* 2008a; Amundson *et al.,* 2010; Howat *et al.,* 2010). The seasonal advance and retreat of glacier calving fronts on the west coast have been correlated with growth and decay of sea ice in proglacial fjords (Sohn *et al.,* 1998; Joughin *et al.,* 2008a; Amundson *et al.,* 2010; Howat *et al.,* 2010) and multi-year retreats and flow accelerations at some tidewater glacier have been attributed to a lack of spring readvance and expanded calving seasons due to a decline in winter sea ice concentrations (Joughin *et al.,* 2008a) and early melange clearing (Howat *et al.,* 2010). Amundson *et al.,* (2010) propose that sea ice acts to bind the mélange of icebergs together which is then strong enough to inhibit calving and enables the terminus to advance. This then reduces the longitudinal strain rates at the grounding line, resulting in ice thickening and increased effective pressure which causes a decrease in the velocity of the ice. Therefore a decrease in sea ice concentrations would remove this buttressing effect and allow the glacier to accelerate. Although a correlation between sea-ice break-up and increased calving rates and ice velocity has been observed at a number of glaciers in Greenland (Higgins, 1991; Reeh *et al.,* 2001; Joughin *et al.,* 2008a; Howat *et al.,* 2010), at present data does not exist that can prove the causal relationship proposed by Amundson *et al.,* (2010). Therefore the possibility remains that sea ice and glacier calving fronts and speeds are responding independently to some other factor, for example ocean circulation and/or subglacial drainage.

2.2.2 Atmosphere induced acceleration of marine-terminating glaciers

It has been suggested that a frontal perturbation to Greenland's tidewater glaciers may have originated from an increase in air temperatures. Since the mid 1990's there has been an accelerating trend of rising air temperatures in Greenland (e.g. Hanna *et al.,*2005; Chylek *et al.,*2006; Box *et al.,* 2006). This has led to increases in surface

ablation (e.g. Hanna *et al.,* 2008; van den Broeke *et al.,* 2009), melt area extent (e.g. Steffen *et al.,* 2004; Fettweis *et al.,* 2007; Tedesco, 2007) and runoff rates (Ettema *et al.,* 2009). Higher rates of surface ablation have led to ice sheet thinning (Sole *et al.,* 2008; Thomas *et al.,* 2009). This may have led marine-terminating glaciers to approach flotation and a state of instability which was followed by increased velocities and frontal retreat (Sohn *et al.,* 1998). It has also been proposed that increased surface melting may also increase calving rates through an increase in hydrofracturing of water-filled crevasses (section 2.3.1) near the ice front (Sohn *et al.,* 1998; Benn *et al.,* 2007). Furthermore, it has been proposed that because increased temperatures and surface melt rates would raise the flow of subglacial water entering a fjord, this would strengthen the circulation of water within the fjord (Figure 2.2) and thereby enhance oceanic melt rates of the glacier face, causing increased calving and frontal retreat (Rignot *et al.,* 2010). However, in studying the glacier accelerations of the south-eastern region of the GrIS in the 2000's, Murray *et al.,* (2011) discount the idea that glacial accelerations were forced by increased air temperatures and surface runoff as they find no correlation between air temperatures and glacier dynamic changes. Further investigations are needed to improve our understanding of the link between atmospheric forcing and marine-terminating glacier flow rates.

2.2.3 Deceleration and stabilisation of marine- terminating glaciers

It is important to stress that a key characteristic of dynamic tidewater behaviour is that it is often cyclical. Following a period of retreat and acceleration tidewater glaciers will often stabilise and decelerate (Meier and Post, 1987). Classically this has been proposed to occur when a glacier retreats to a pinning point where resistive stresses exceed driving stresses (i.e. at a submerged topographic high or a constriction in the fjord – Meier and Post, 1987). Such behaviour was observed at Helheim and Kangerdlugssuaq glaciers in the southeast of Greenland, as after initial accelerations of 100% and 40% respectively between 2003 and 2005 they both decelerated in the summer of 2006 (Howat *et al.,* 2007). It has been suggested that this occurred as the front of the glaciers regrounded on bathymetric highs (Howat *et al.,* 2007; Joughin *et al.,* 2008b). Because such pinning points are external to the ice

sheet and therefore vary from glacier to glacier the degree of retreat and timing of restabilisation may be expected to vary between glaciers. However, Howat *et al.,* (2008) and Murray *et al.,* (2011) generated velocity datasets of many of the tidewater terminating glaciers in the southeast of Greenland, including Helheim and Kangerdlugssuaq glaciers for much of the 2000's. They found near synchronous speed-up and slow downs at most of the glaciers. Murray *et al.,* (2011) propose that the synchronous nature of this stabilisation rules out any local controls i.e. regrounding and instead suggest that the speed up and slow down occurred in response to warming and cooling ocean temperatures respectively. Furthermore, a study by Nick *et al.,* (2010) which models marine-terminating glacier retreat based on the penetration of surface and basal crevasses suggests that tidewater glacier retreat may achieve stability on reverse slopes. Restabilisation is a very important characteristic of marine-terminating glaciers as it affects long-term ice velocities and therefore rates of discharge and mass loss. Hence it is important to understand and parameterise the processes which govern it in future ice sheet models.

2.3 Surface meltwater forcing of inland ice dynamic changes

Ice velocities of inland ice in Greenland have been observed to exhibit variability at daily (e.g. Das *et al.,* 2008; Shepherd *et al.,* 2009; Bartholomew *et al.,* 2010), seasonal (e.g. Joughin *et al.,* 2008c; Bartholomew *et al.,* 2010) and interannual timescales (e.g. Zwally *et al.,* 2002; van de Wal *et al.,* 2008; Sundal *et al.,* 2011) in response to the delivery of surface meltwater to the bed of the ice. Similar daily and seasonal velocity variations have also been observed at tidewater glaciers and are linked to the input of surface runoff to the bed (Howat *et al.,* 2010; Stearns *et al.,* 2010). However, the overall percentage increase in seasonal velocities (away from the calving front) is much lower (10-15%) than at slower land- terminating glaciers and inland ice (Joughin *et al.,* 2008c) and contributes only a small amount to the overall annual discharge from the ice sheet. Nonetheless this mechanism is significant in terms of mass loss at land-terminating margins. This is because ice motion controls the transport of mass from high elevations to low elevations where

surface melt rates are higher. Therefore an increase in ice velocities at land-terminating margins due to increased surface melting would effect a positive feedback mechanism as the ice sheet would thin and further increase melt rates (Parizek and Alley, 2004).

2.3.1 Daily to seasonal velocity variations of inland and land-terminating ice

There have been a number of studies which identify velocity variations at daily to seasonal timescales on the GrIS and which have been linked to surface meltwater inputs. Diurnal velocity measurements were acquired by Shepherd *et al.,* (2009) using 3 GPS (Global Positioning System) sensors situated between 37 and 72 km inland of the western ice margin, where the ice is between 890 and 1120 m thick. Measurements were taken over a 5 day period in late summer 2007. They recorded an average daily speed up of 55% over the three sites which occurred roughly 2 hours after the daily peak in melt. Short term velocity increases have also been associated with the drainage of supraglacial lakes (see below). Das *et al.,* (2008) recorded a substantial surface displacement (<0.8 m in a few hours) which coincided with the rapid (~1.4 hours) drainage of a 0.044 ± 0.01 km^3 lake through ice 980 m thick at the western margin in the summer of 2006. Over a seasonal timescale, ice is observed to flow faster during the summer than the winter. Over the land-terminating margins and the inland ice, seasonal summer speed ups of up 125% have been recorded (e.g. Zwally *et al.,* 2002; van Joughin *et al.,* 2008c; Bartholomew *et al.,* 2010; Palmer *et al.,* 2011; Sundal *et al.,* 2011). The seasonal acceleration of the ice has been correlated with the onset of surface melting (e.g. Van de Wal *et al.,* 2008; Bartholomew *et al.,* 2010). Van de Wal *et al.,* (2008) report that velocity increases occurred less than a week after the onset of melt in a region of the ice sheet where the ice thickness exceeds 1000m. However, following the initial speed up of the ice, velocity and surface ablation are found to decorrelate throughout the melt season and late summer velocities have been found to be lower than winter velocities (e.g. Zwally *et al.,* 2002; Bartholomew *et al.,* 2010).

The observations outlined above and the widely reported coincidence of velocity increases with vertical surface uplift (e.g. Zwally *et al.,* 2002; Das *et al.,* 2008; Shepherd *et al.,* 2009; Bartholomew *et al.,* 2010) are consistent with observations at Alpine and small Arctic glaciers where velocity variability has been found to result from changes in basal water pressures and sliding in response to meltwater inputs and the seasonal reconfiguration of the subglacial drainage system (e.g. Iken *et al.,* 1983; Iken and Bindschadler, 1986; Mair *et al.,* 2001, 2002; Bingham *et al.,* 2003, 2005). At the end of spring and beginning of summer, as the surface of the glacier begins to melt, water is routed through the ice to the bed via moulins and crevasses. Upon reaching the glacier bed the water is fed into a hydraulically inefficient, distributed drainage system which is composed of water films, cavities downstream of bedrock obstacles, canals and flow through sediment (Sharp, 2005). Water travels slowly in such systems resulting in high subglacial water pressure. Increasing volumes of water input leads to water pressures capable of 'hydraulically jacking' the ice from the glacier bed (Iken and Bindschadler, 1986) which causes decreased levels of friction and increased ice velocities. As the transient snow line retreats up-glacier throughout the melt season, the production of surface melt water grows. This leads to an increase in the flux of water to the bed, resulting in rising water pressures, which forces the development of a hydraulically efficient, channelized system (Mair *et al.,* 2001). The water pressure in channelized drainage systems is low and therefore ice velocities decrease (Fountain and Walder, 1998). Late summer velocity increases are observed in lower portions of glaciers in response to high magnitude melt water inputs (i.e. following supraglacial lake drainage or large rain events) (e.g. Iken and Bindschadler, 1986; Bingham *et al.,* 2005) which overcome the capacity of the channelised system and forces water into the peripheral distributed system, where subglacial water pressure becomes high and sliding velocities increase (Bartholomaus *et al.,* 2008). At the end of summer when the energy available for surface melting decreases, water input to the bed declines, channels are no longer filled by water and so they begin to close by ice creep (Cutler, 1998). Initially water pressure falls but the drainage system then contracts to the point that water pressure begins to rise again (Hubbard and Nienow, 1997) and a distributed drainage system dominates.

The mechanism outlined above has been used to explain daily and seasonal velocity variability of inland ice and outlet glaciers in Greenland (e.g. Zwally *et al.*, 2002; van de Wal *et al.*, 2008; Bartholomew *et al.*, 2010; Howat *et al.*, 2010; Sundal *et al.*, 2011). However, it must be noted that at present such an explanation remains theoretical, as due to the inaccessibility of the subglacial environment, no direct measurements of the subglacial drainage system of the GrIS has been made. This is a key limitation to ice sheet model parameterisation, although projects which intend to measure the subglacial environment in Greenland are underway (e.g. the 'Cryo-egg' project at the University of Bristol, see http://seis.bris.ac.uk/~ggbsrl/Cryoegg/home.html for further information).

Unlike at small Alpine and Arctic glaciers, away from the margin of the GrIS surface crevasses and moulins are unable to penetrate to the bed under extensional stress alone due to the compressive effect of ice overburden pressure at depth. However, theoretical and observational studies from the western margin of the ice sheet suggest that a hydrofracturing mechanism provides a pathway for surface water to reach the bed of the ice (Van der Veen, 2007; Das *et al.*, 2008). The theory of hydrofracturing suggests that if the volume of water within a crevasse exerts enough pressure to overcome the ice overburden pressure along with tensile stresses a crevasse may propagate through over 1km of cold ice (e.g. Weertman, 1978; van der Veen, 1998a, b; Alley *et al.*, 2005b). Alley *et al.*, (2005b) propose that supraglacial lakes are significant for hydrofracturing as they warm ice, supply water and increase the pressure driving water flow and ice cracking. Das *et al.*, (2008) observed a lake drainage event on the western margin of the GrIS and found that the volume of water collecting in supraglacial lakes is sufficient to exert enough extra pressure on a fracture to overcome the ice overburden pressure of 980 m thick ice and allow ice fracturing and lake drainage. They also found that a continued supply of melt water from surface streams allowed some fractures to remain open and form discrete moulins which remained open until the end of the melt season (Das *et al.*, 2008). Using ice-penetrating radar surveys covering an area of the GrIS near Jakobshavn Isbrae, Catania, *et al.*, (2008) mapped the locations of englacial pathways. They found only a moderate correlation between lake locations and moulins suggesting that many lakes may drain overland and that moulins form in the absence of lakes.

They found a strong correlation between moulin locations and regions of longitudinal extension, which suggests that surface crevassing may exert a primary control on moulin locations in the ablation zone. They also found that in ice thicker than 800 m the locations of lakes and moulins are more closely tied and therefore propose that in thicker ice lakes may be required for moulins to form.

During the summer supraglacial lakes (Figure 2.3) are observed to form across the whole of the GrIS below the limit of melting (e.g. Echelmeyer *et al.,* 1991; Luthje *et al.,* 2006; Box and Ski, 2007; McMillan *et al.,* 2007; Sneed and Hamilton, 2007; Sundal *et al.,* 2009). It has been found that lakes form in the same locations each year (e.g. Echelmeyer *et al.,* 1991; Luthje *et al.,* 2006; Sundal *et al.,* 2009) and this is because the surface depressions in which lakes develop are surface expressions of subglacial topography (Echelmeyer *et al.,* 1991). Using a range of remote sensing and field based techniques the area and depth of lakes have been measured by a number of authors in the west of Greenland and it has been found that lake areas range from a few 10's of metres to 10 km^2 and depths between <1 and 20 m (e.g. Echelmeyer *et al.,* 1991; Box and Ski, 2007; Georgiou *et al.,* 2009). The distribution of lakes has been observed to evolve seasonally (e.g. Box and Ski, 2007; McMillan *et al.,* 2007; Sneed and Hamilton, 2007; Sundal *et al.,* 2009). Throughout the melt season, lakes begin to develop further inland and at higher elevations, tracking the expansion of the region of surface melting (e.g. Box and Ski, 2007; McMillan *et al.,* 2007; Sundal *et al.,* 2009). As previously mentioned, lakes can episodically drain rapidly. McMillan *et al.,* (2007) show that lake drainage events occur on a wide scale in the west of Greenland. By mapping seasonal development they showed that lakes covered a total area of 75 ± 5 km^2 in early July 2001 but lost 36 ± 3.5 km^2 throughout the following 25 days. By comparing the extents of lakes on different years, Sundal *et al.,* (2009) found that lake area extents could be up to 50% lower in years with low runoff compared to a high runoff year and that this was the result of lakes forming at higher elevations. It has therefore been suggested that, as climate warms, lakes will form higher on the ice sheet surface. Furthermore, Luthje *et al.,* (2006) postulate that lakes forming at higher elevations will be larger in size due to more shallow slopes favouring larger surface depressions. Therefore, melt-water inputs to the bed resulting from supraglacial lake drainage may increase in the future and the

associated increase in ice velocities has the potential to increase mass loss. The potential for this remains to be investigated.

Figure 2.3: Supraglacial lakes on the surface of the Greenland Ice Sheet (Photo by Sarah Das of WHOI).

2.3.2 Interannual velocity variations of inland and land-terminating ice

Several studies have investigated the longer-term (interannual) relationship between ice velocities and surface melt rates, the findings of which have been equivocal. Zwally *et al.*, (2002), looked at the relationship between ice velocities and surface melting using in situ GPS measurements from 1996 to 1999 and contemporaneous passive microwave data of melt extent and positive degree day (PDD) calculations at a location 35 km from the margin near the equilibrium line altitude (ELA) where the ice thickness is 1220 m. They discovered that there is a significant positive correlation between interannual surface melt volumes and glacier velocities. From this they suggest that with atmospheric warming and increasing amounts of surface melting, GrIS outlet glaciers and ice discharge would accelerate. Parizek and Alley (2004) conducted a modelling experiment linking surface melting with a sliding law

based on the finding of Zwally *et al.,* (2002) in order to investigate its effect on ice sheet mass loss under different warming scenarios. They propose a positive feedback mechanism of ice loss. Increased sliding from enhanced surface melt leads to a reduction in the overall thickness of the ice sheet and therefore a greater penetration of melting inland as temperatures are warmer at lower elevation. They conclude that volume reductions from increased sliding will be substantial, ranging between 2.6-9.9% by 3000 AD under different CO_2 scenarios.

Price *et al.,* (2008) refute the findings of Zwally *et al.,* (2002) and suggest that seasonal velocity variations observed by Zwally *et al.,* (2002) near the ELA can be explained by longitudinal coupling with perturbations in ice flow towards the margin and that these conditions are normal and therefore may have limited impact on the ice sheet in a warming climate. Similar occurrences have been observed at Alpine glaciers where small velocity differences in the upper accumulation zone where there is no melt water input from the ice surface, is the result of longitudinal coupling with velocity changes downstream (Mair *et al.,* 2002; Bingham *et al.,* 2003). However, the findings of Shepherd *et al.,* (2009) and Bartholomew *et al.,* (2010) oppose the suggestion of Price *et al.,* (2008) suggesting that longitudinal coupling only occurs locally on the GrIS (<10km -Bartholomew *et al.*, 2010).

Furthermore, in opposition to the suggestion of Zwally *et al.,* (2002) that ice velocities will increase with increasing temperatures, van de Wal *et al.,* (2008) report that there is no correlation, and Sundal *et al.*, (2011) report that there is a negative correlation between years of increased surface melting and mean summer velocity. Both suggest that this occurs as the subglacial drainage system adapts to changes in meltwater inputs. Van de Wal *et al.,* (2008) suggest that long term changes in ice velocity are responding to changes in ice thickness and surface slope. However, Sundal *et al.,* (2011) report that although the maximum annual recorded velocities correlate with surface melt rates interannually, the duration of rapid velocities is three times shorter in warmer summers than colder ones. They suggest that in years of high seasonal melt the subglacial hydraulic system adjusts rapidly so that the average seasonal velocity of the glacier is no higher than a lower melt year.

Consequently, both propose that the long-term impact of a warming climate on melt induced velocity variations will not lead to increased flow rates.

A recent modelling study by Schoof (2010) suggests that it is the variability in meltwater input as opposed to the total water volume which may drive ice sheet acceleration. He suggests that an increased rate of steady water supply has a limited potential to increase seasonal velocities because the seasonal evolution of the subglacial drainage system enables greater volumes of water to be accommodated and this suppresses water pressures and acceleration. Conversely, if water is released in brief pulses to the bed as a result of, for example a rainfall or lake drainage event, the capacity of the channelised system will be exceeded and water will be pushed into surrounding distributed systems, thus causing pressure and basal sliding increases. Therefore, it is important that models are able to capture the variability of meltwater inputs to the subglacial system.

2.4 Summary

Glacier discharge is an important component of GrIS mass loss. Recent observations have revealed rapid and substantial variability in discharge rates as a result of large changes in the flow dynamics of a number of outlet glaciers of the GrIS. These dynamic changes have been linked to climate forcing in 2 key ways; firstly, through ice-ocean interactions at the ice sheets marine margins and secondly through the transfer of surface meltwater to the glacier bed.

It has been identified that the majority of the major dynamic changes occurring recently have been almost exclusively at marine-terminating glaciers. Accelerated velocities have been linked to perturbations at the front of tidewater glaciers and have been connected to both changes in ocean and atmospheric temperatures. Increases in ocean temperatures have been recorded off the coast and in the fjords of East and West Greenland during the late 1990's and 2000's. It is suggested that these temperature increases may have increased basal melting and therefore calving at glacier termini, and decreased the sea ice concentrations abutting glaciers and reducing its buttressing effects on ice flow. Frontal perturbations may also have

resulted from increased atmospheric temperatures and surface melting. It is proposed that this may have increased calving rates due to increased hydrofracturing in crevasses near the termini and also due to increased freshwater input to the head of fjords may have strengthened circulation in the fjords, bringing more warm water to the ice fronts. A number of glaciers which were observed to accelerate in the mid-2000's were also found to restabilise a few years later in a synchronous manner which may be indicative of a climate forcing. It is apparent that the behaviour of tidewater glaciers is highly complex due to the interplay of a large number of potential forcing mechanisms and boundary conditions. Due to our limited understanding of the mechanisms controlling tidewater glacier behaviour it remains unclear whether the recently observed dynamic changes to tidewater glaciers are short-term or part of a longer trend. Further observations and longer term trends are required in order to further our understanding.

The transfer of surface meltwater to the bed of the ice sheet has been identified as a key control for short-term changes in ice velocities at land-terminating outlet glaciers and the inland ice of the ice sheet. Clear daily and seasonal patterns in ice velocities have been identified on the ice sheet and are linked to changes in basal water pressures and basal sliding governed by surface meltwater inputs and variability of the configuration of the subglacial drainage system in time and space. The drainage of supraglacial lakes has been identified as an important factor in transferring water to the bed of the ice sheet, especially higher on the ice sheet where the ice is thicker (>800 m). Studies have revealed their formation and drainage is widespread throughout the summer months and that in warmer years lakes form higher on the ice sheet. Thus it has been suggested that in future, warmer climates, lakes will form at higher and higher elevations and their drainage may lead to an increase in ice velocities. The observed interannual response of ice velocities to differences in rates of surface melting are less clear, as studies have suggested that increased surface melting has led to both increased and decreased summer surface velocities. This interannual response does however, appear to be regulated by the subglacial drainage system although at present no direct observations exist.

Although the recent major dynamic changes to the GrIS appear to have been governed by factors perturbing the front of tidewater glacier, the relative importance of this variability in comparison to that of surface melt induced dynamic changes and mass loss from surface ablation, will decrease in the future if the ice sheet continues to retreat. This is because much of the GrIS rests on bedrock topography that is above sea-level (Bamber *et al.,* 2001b) and so continued retreat will result in an ice sheet predominantly grounded above sea-level and therefore insensitive to oceanic forcings. The transition from ocean- to land based-margins will thereby render the component of mass loss from ice discharge to the oceans irrelevant and mass loss from surface ablation more prevalent. Surface velocities will be governed by surface melt induced basal sliding and although no longer important in terms of discharge, the ice dynamics of Greenland's glaciers will be important as a means of transporting mass to lower elevations where temperatures are warmer and ablation greater (Parizek and Alley, 2004). Therefore to forecast the response of the ice sheet to climate changes and the potential contribution to sea level changes over the coming centuries to millennia we must be able to model dynamic losses from tidewater glaciers in the short-term, predict the nature and timing of the transition of the ocean margins to land-based margins and forecast the influence of rising temperatures on surface melt induced basal sliding on ice sheet velocities and surface ablation rates.

2.5 Thesis objectives

This chapter has identified many gaps in the current state of understanding of the present and future dynamics of the GrIS; to address all of these gaps is beyond the scope of one PhD. The key objectives of this thesis are as follows:

1. To establish the different factors forcing seasonal velocity variations at land and marine-terminating glaciers in the northeast of Greenland.

2. To investigate the distribution and factors controlling supraglacial lake formation and drainage, and to explore methods for predicting the spread and behaviour of lakes in a warming climate. Specifically the objectives are:

i) To assess the ability of using a high resolution Digital Elevation Model (DEM) to identify and therefore predict the location of supraglacial lakes in the northeast of Greenland.

ii) To investigate current spatial and temporal trends in the formation and drainage of lakes in the west of Greenland to predict the future potential for lake drainage events at elevations beyond which they currently form.

Chapter 3: Review of methods

To fulfil the objectives outlined in Chapter 2, this thesis utilises remotely sensed data for retrieving ice velocities, building ice surface DEMs and mapping supraglacial lakes. This chapter provides both a review and an assessment of effectiveness of the methods previously applied in glaciology to acquire these datasets. More specific details of the methods applied within this thesis are found in Chapters 4, 5 and 6.

3.1 Ice velocity retrieval methods

In situ measurements of glacier motion began over 200 years ago with observations of terminus positions and the gradual deformation of a straight line of painted rocks placed on the ice surface (e.g. Forbes, 1859; Meier, 1960). Developments in such early practices have led to current methods of field-based ice velocity measurements where GPS point surveys are capable of delivering very precise results (mm scale accuracy) with repeat measurements every few seconds (e.g. van de Wal *et al.*, 2008; Shepherd *et al.*, 2009). However, in situ methods are both spatially and temporally constrained: they are labour intensive, time consuming and, because many glaciated areas are often inherently inaccessible, they can be physically unattainable. Such restrictions to velocity monitoring can nevertheless be overcome through the use of remote sensing data. Following the initial outlay of producing and launching a sensor, data can be acquired regularly and over vast areas at relatively little cost, thus making remote sensing an ideal medium for studying ice velocity changes over large ice masses such as the GrIS. Several methods of deriving ice velocities have been developed using remote sensing imagery, including interferometry and offset tracking with optical and SAR data. These techniques will now be discussed in more detail.

3.1.1 Interferometric SAR (InSAR)

InSAR combines two complex SAR images of the same region acquired from positions separate in both space and time. Differencing the phase signal allows the difference in the range from each antenna to a point on the ground to be inferred (Figure 3.1). The signal acquired contains components of topography and of surface displacement. Therefore, to acquire surface velocity estimates, the signal due to topography must be removed (Figure 3.2). This can be achieved either by subtracting a simulated topographic phase signal from an external DEM (e.g. Mohr *et al.,* 1998; Alsdorf and Smith, 1999) or through the differential use of two interferograms (e.g. Kwok and Fahnestock, 1996). A more detailed description of InSAR is given in Section 3.2.3.

The first application of interferometry in glaciology was that of Goldstein *et al.,* (1993) who investigated the ice flow velocity and grounding line position of the Rutford Ice Stream, West Antarctica. Since then, InSAR has become an invaluable tool for glaciologists, providing a means of measuring surface displacements at centimetre scale accuracy over vast regions. In Greenland, InSAR has provided many key glaciological insights including mapping of ice velocity fields (e.g. Rignot *et al.,* 1995; Joughin *et al.,* 1999; Fahnestock *et al.,* 2001), velocity variability (e.g. Joughin *et al.,* 1996a; Mohr *et al.,* 1998; Joughin *et al.,* 2004; Rignot and Kanagaratnam, 2006; Palmer *et al.,* 2011), mass balance (e.g. Rignot *et al.,* 1996; Joughin *et al.,* 1997; Rignot *et al.,* 2001) and grounding line positions (e.g. Rignot, 1996; Rignot *et al.,* 1997).

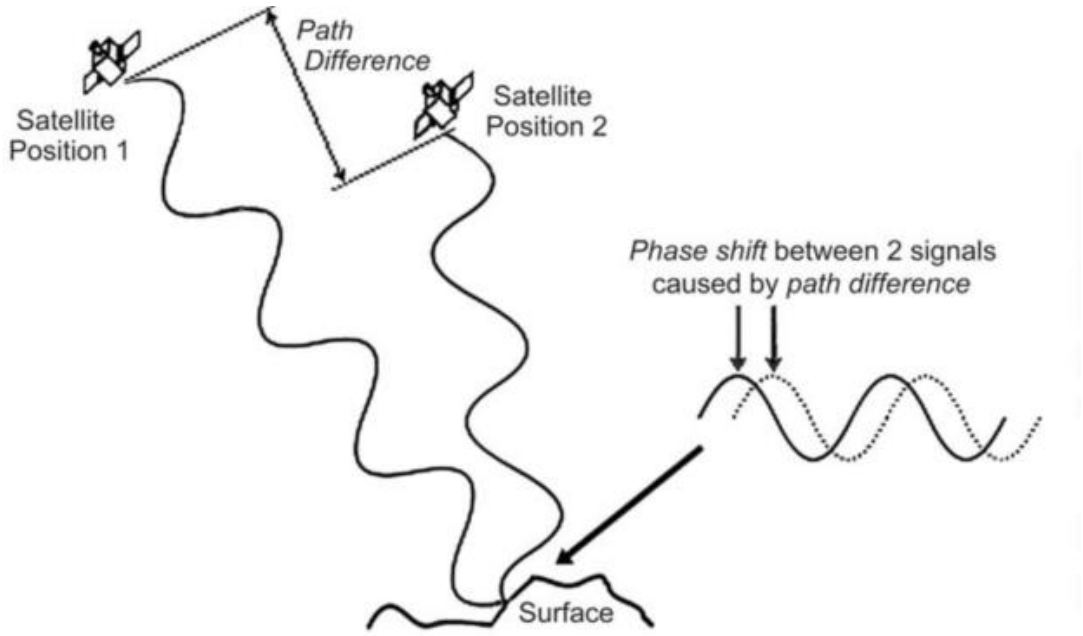

Figure 3.1: Schematic showing phase shift between backscattered signals received at 2 locations caused by the radar path difference. Taken from Massom and Lubin (2006).

Surface features are not required in order to derive velocity measurements from InSAR enabling the measurement of surface displacements in the featureless interiors of the ice sheets (e.g. Goldstein *et al.*, 1993). However, in order to derive usable phase information in an interferogram, the phase signal in the two SAR images must remain sufficiently correlated (coherent). Coherence may be lost as a result of surface change, due, for example, to snowfall or melting, or rotation or displacement due to flow. Both factors, and therefore loss of coherence (decorrelation), increase with time between image acquisitions. As a result, InSAR has only successfully been applied in Greenland using images separated by 3 days or less. Most SAR missions have a repeat period of greater than 24 days which is a major limitation of the application of InSAR to glaciology. The only data found to be suitable for glaciological applications of interferometry in Greenland was acquired between 1995 and 1997 when the ERS-1 and ERS-2 satellites were flown on the tandem (1-day separation) and ice (3-day separation) missions. Furthermore, the use of this data for time series analysis of velocity changes (seasonally and annually) is limited, as the one- or three-day averaged ice velocity measurements are separated by the 35 day repeat period of the satellite. At present there are no plans for any future

missions which will provide data suitable for ice applications of InSAR. InSAR is also subject to a number of further limitations that restrict it's applicability in glaciology, these include insensitivity to displacement in the azimuth direction and problems in converting the relative phase measurements to absolute height or displacement estimates. A more comprehensive review of InSAR errors is provided by Massonnet and Feigl (1998) and Massom and Lubin (2006).

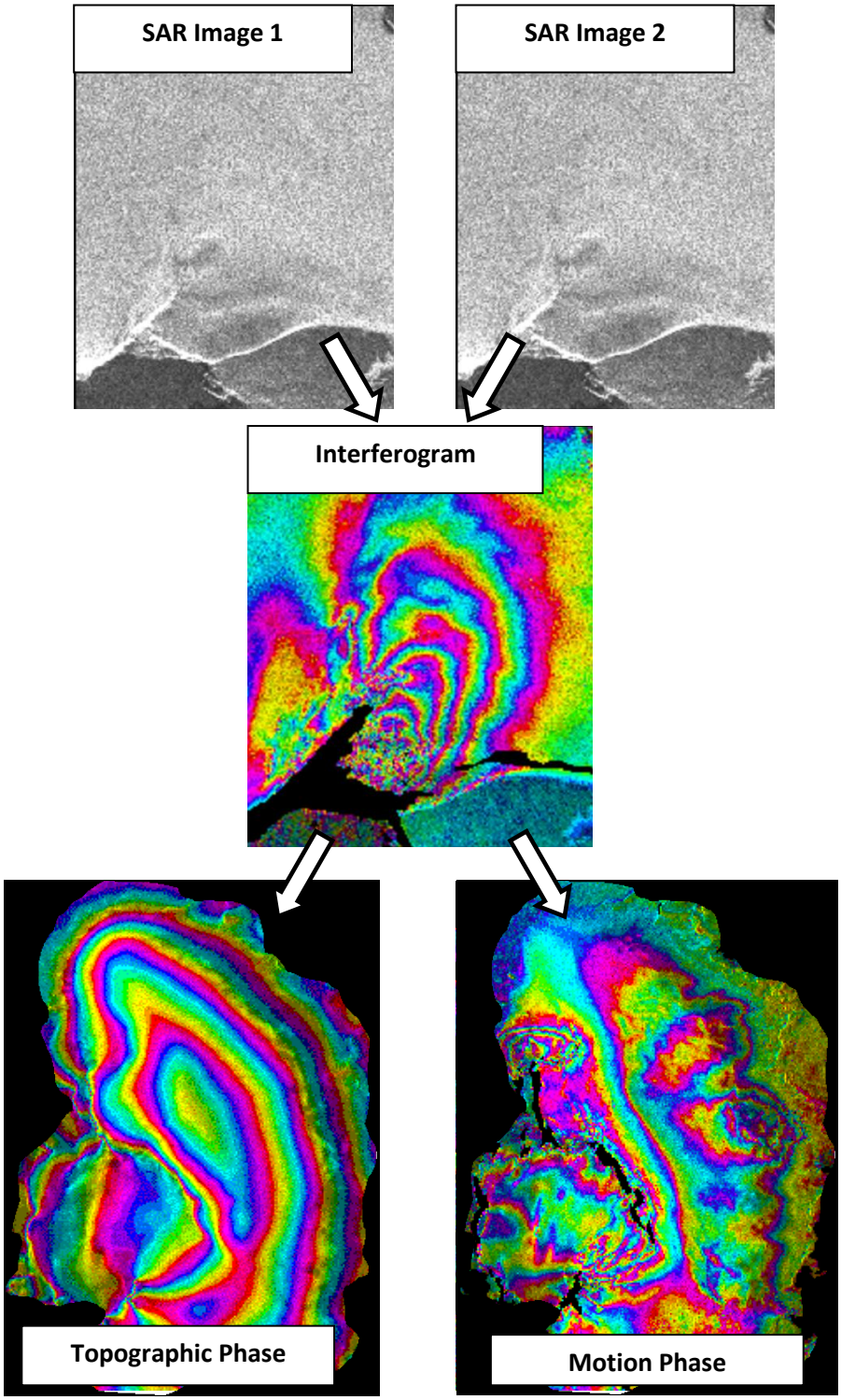

Figure 3.2: Two temporally separate SAR images of the same scene are differenced to produce an interferogram. Using differential InSAR the signals of phase due to motion and to topography can be isolated to produce individual interferograms. (Images courtesy of Professor Andrew Shepherd)

3.1.2 Feature tracking with optical images

Calculations of ice motion using feature tracking are derived by mapping the displacement of features, such as moraines and crevasses, on the glacier surface between 2 images which are separated by a known amount of time (Figure 3.3). Early applications of feature tracking determined ice motion by co-registering image pairs using common fixed points such as mountain peaks and tracking persistent features using manual picking (Lucchitta and Ferguson, 1986). However, this technique could not be applied to the ice sheet interior where features suitable for manual co-registration are not available. Development of an automated cross-correlation algorithm by Bindschadler and Scambos (1991) which identifies surface displacements by matching image brightness values, led to an improvement in the accuracy (± 2.3 m/yr compared to ± 20 m/yr) and breadth of applicability of the feature tracking technique. The area over which velocity measurements were derived was expanded as the algorithm allowed diffuse or subtle features, such as broad dunes and crevasse scars, to be tracked successfully.

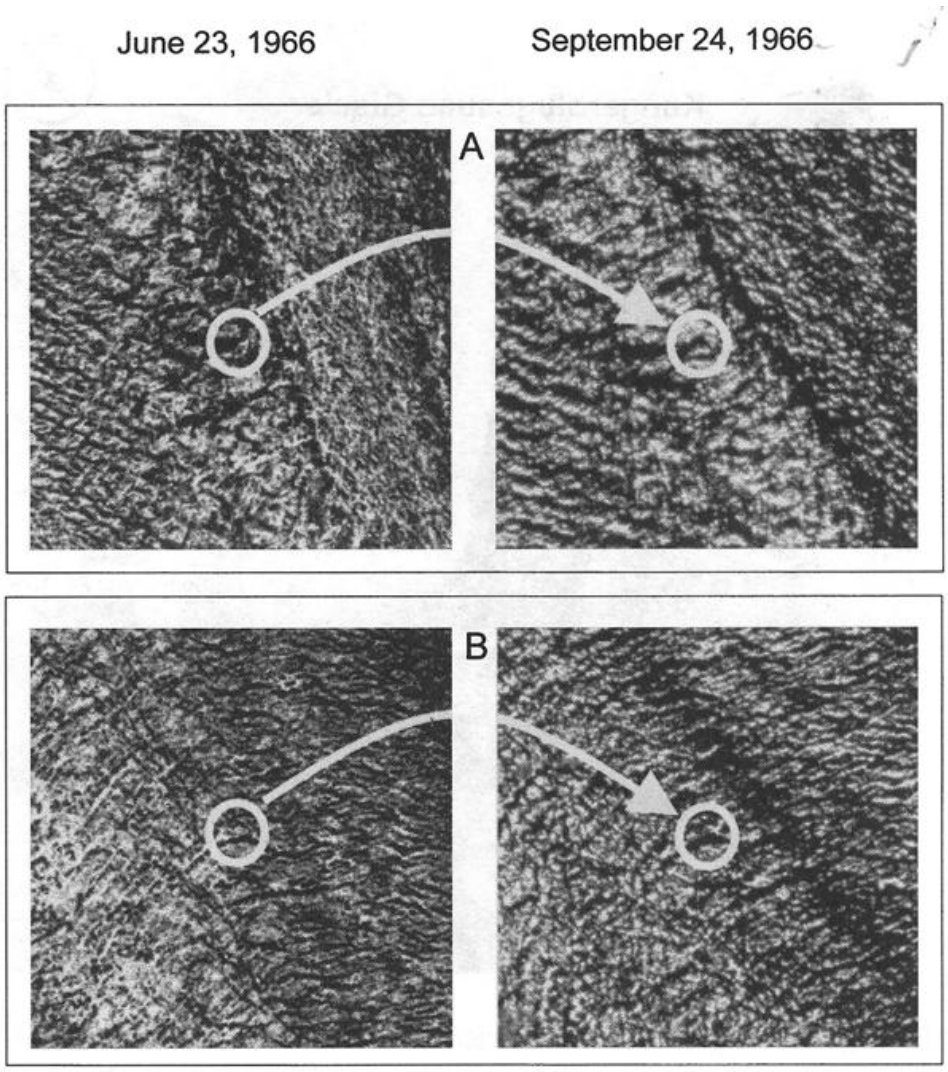

Figure 3.3: DISP images from June 23rd and September 24th 1966, showing two features on the surface of Kangerdlugssuaq Glacier, East Greenland used in feature tracking. Taken from Csatho *et al.*, (1999).

This technique has been applied to acquire the ice velocities of a number of outlet glaciers in Greenland, using a range of image types (e.g. Carbonell and Bauer, 1968; Dwyer, 1995; Csatho *et al.*, 2002; Joughin *et al.*, 2004; Stearns *et al.*, 2005; Howat *et al.*, 2007). The use of declassified intelligence satellite photographs has allowed ice velocity estimates to be made dating back to the 1960's (e.g. Csatho *et al.*, 1999). However, ice velocity measurements from visible imagery are ultimately restricted by the constraints of the sensors. The archive of suitable visible images is limited by cloud conditions and the availability of visible light (i.e. estimates can't be acquired

throughout the winter in the Arctic and Antarctic). These problems can be overcome with SAR images as the wavelengths employed are able to penetrate cloud cover and, because they emit their own energy source, they are able to image in the darkness of the polar winter (Lillesand and Keifer, 1999).

3.1.3 Offset tracking with SAR images

Offset tracking using SAR imagery can be achieved using both the coherent and incoherent attributes of the SAR image signal (Strozzi *et al.*, 2002). Coherent offset tracking tracks surface displacements by taking a series of small data patches throughout the SAR images, forming small interferograms with changing image offsets and estimating the image coherence of these interferograms (e.g. Derauw, 1999; Pattyn and Derauw, 2002). The surface displacement estimate is taken as the offset with the maximum interferometric coherence subject to surpassing a minimum threshold of coherence so as to ensure reliable matches (e.g. Derauw, 1999; Pattyn and Derauw, 2002). The author is not aware of any current applications of this method in Greenland although this technique has been applied in Antarctica (Figure 3.4) (e.g. Derauw, 1999; Pattyn and Derauw, 2002; Young and Hyland, 2002) and Svalbard (Strozzi *et al.*, 2002). Aside from its use to provide surface displacement measurements for velocity field estimates (Young and Hyland, 2002), coherence tracking has been used in tandem with InSAR to improve local registration and therefore interferogram coherence by forming a 'tracked interferogram' (Derauw, 1999), to provide estimates of surface displacements in the azimuth direction (Strozzi *et al.*,2002) and to provide absolute velocity measurements for linking image areas that are separated by incoherence (Derauw, 1999; Derauw *et al.*, 2002). A key advantage of this technique is that, unlike interferometry, it produces displacement estimates in range and azimuth. However, the technique relies upon coherence between images and is therefore subject to similar limitations with image decorrelation as InSAR. Furthermore, the resolution of this technique is substantially lower than that generated by InSAR (Pattyn and Derauw (2002) obtain a resolution of approximately 25 m on the Shirase Glacier in Antarctica).

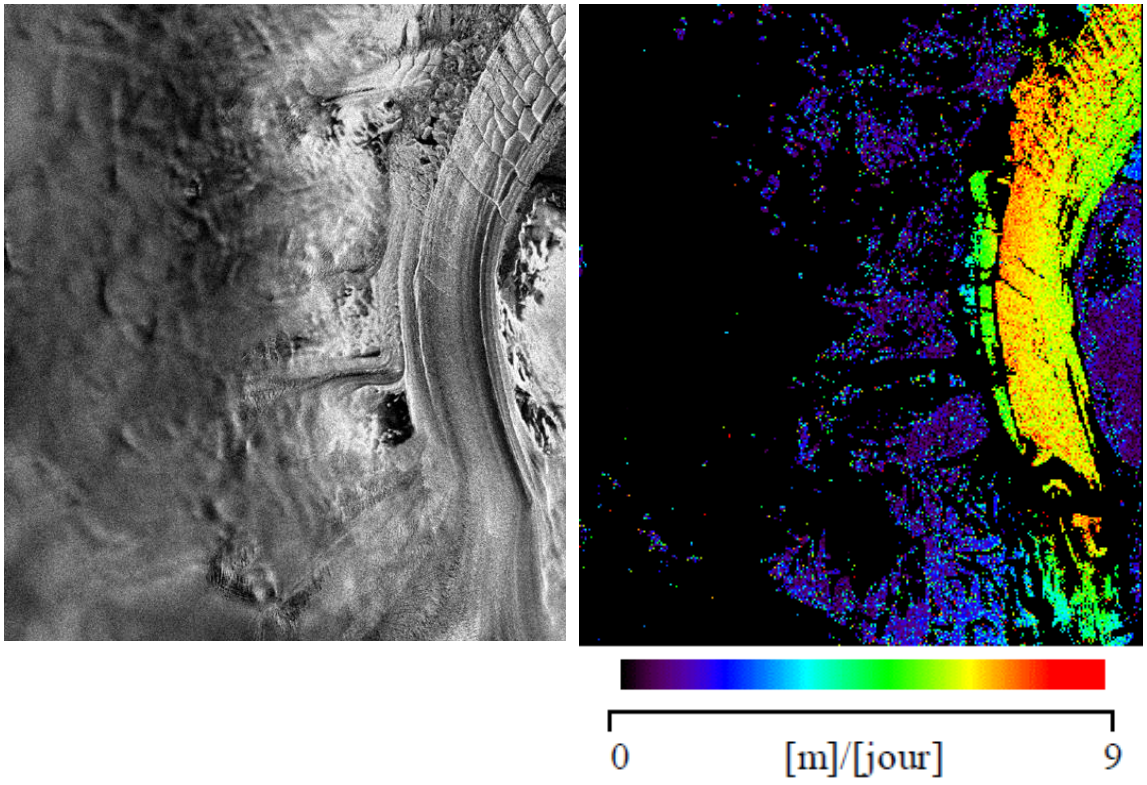

Figure 3.4: ERS-1 scene (left) and surface displacements measured with coherence tracking (right) of the Shirase Glacier, Antarctica. Taken from Derauw (1999).

Intensity tracking is similar to optical image feature tracking although it tracks the speckle pattern in the images as well as the displacement of surface features (e.g. Lucchitta *et al.*, 1995; Rosanova *et al.*, 1998; Rabus and Lang, 2003; Luckman *et al.*, 2003; Luckman and Murray, 2003; Luckman *et al.*, 2006; Luckman *et al.*, 2007). Again, the main disadvantage of this method with respect to InSAR is that it produces velocity measurements at a much lower resolution (between 100m and 2 km according to Pritchard *et al.*, 2005). However, it is a more robust method of mapping surface displacement than coherence tracking and InSAR, as tracking of surface features are not subject to the same problems of image decorrelation. Consequently, this method can be applied to images with larger acquisition intervals (e.g. up to several years in the Himalayas as recorded by Luckman *et al.* 2007) and 35 days in Greenland (e.g. Luckman *et al.*, 2003; Pritchard *et al.*, 2005) and can therefore be applied to a greater portion of the SAR image archive. By comparison to feature tracking, intensity tracking has the potential to provide a greater spatial

coverage as the displacement of speckle may be tracked into the featureless ice sheet interior as long as some coherence between the images is maintained (Joughin *et al.*, 2010b). SAR intensity tracking has been extensively applied in Greenland to acquire seasonal and multi-annual ice velocity measurements at glacier to ice sheet scales using ERS-1 and -2, Radarsat and Envisat images (e.g. Joughin *et al.*, 2004, 2008c, 2010a; Luckman and Murray; 2005; Howat *et al.*, 2005, 2007, 2008; Rignot and Kanagaratnam, 2006; Sundal *et al.*, 2011) with accuracies of ~ ± 20 m/yr (Pritchard *et al.*, 2005). Due to the capability of SAR to image through the polar night and cloud cover, and the greater data availability and robustness of SAR intensity tracking over InSAR, SAR intensity tracking is used to derive the velocity data set in Chapter 4.

3.2 Digital elevation models

To map ice surface depressions in Chapters 5 and 6, surface elevation measurements used to generate continuous high resolution surface models of regions several thousands of km^2, were required. Furthermore, in Chapter 6, high resolution surface topography profiles, covering distances of hundreds of kilometres, were needed to map the distribution of ice surface depressions. A range of ground, airborne and spaceborne methods are available for mapping surface topography.

3.2.1 Ground based DEM acquisition

Ground based methods, including terrestrial laser scanning, triangulation, optical levelling and terrestrial photogrammetry (Figure 3.5), are capable of producing surface topography measurements at resolutions of a few centimetres to millimetres (e.g. Eiken *et al.*, 1997; Koning and Smith, 1999; Paar *et al.*, 2001; Kääb and Weber, 2004; Pitkänen and Kajutti, 2004). These methods are commonly used for precise measurements of surface topography over small regions (e.g. Eiken *et al.*, 1997;

Koning and Smith, 1999; Paar *et al.*, 2001; Kääb and Weber, 2004; Pitkänen and Kajutti, 2004). Therefore, ice surface topography measurements from terrestrial methods are impractical at the scale required for this work.

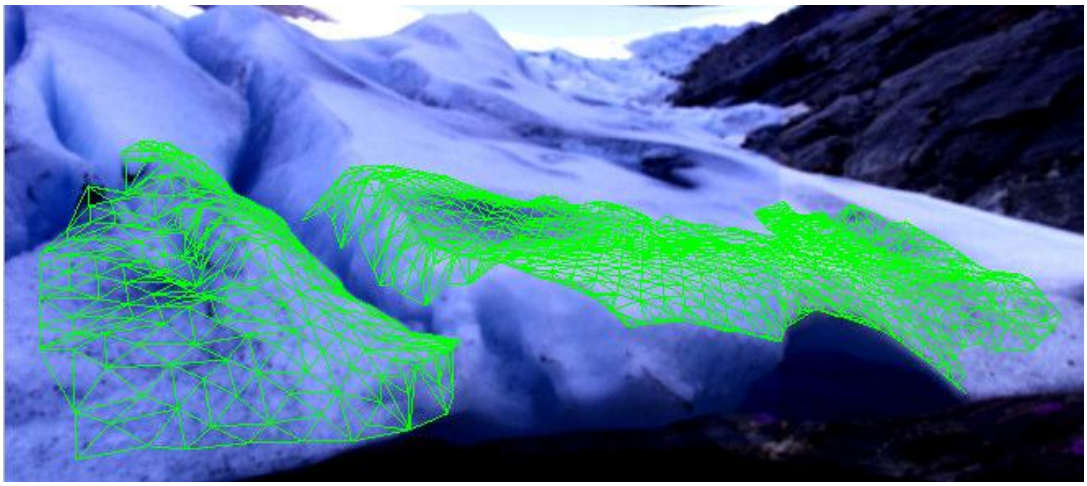

Figure 3.5: DEM of Engabreen, Norway, built using digital photogrammetry from terrestrial photography taken with a digital camera. The point density of the DEM is ~20 cm. Taken from Pitkänen and Kajutti, (2004).

3.2.2 Airborne DEM acquisition

Airborne methods for acquiring surface elevation data of ice sheets include photogrammetry, InSAR and laser altimetry. Photogrammetry can be used to derive surface topography through triangulation between corresponding points in two overlapping images (taken in different places) and the imaging cameras (for further details see Kääb, 2005). One advantage of photogrammetry is that it can be used on image archives, which can date back to as early as the 1930s, in order to acquire retrospective surface height measurements (Barrand *et al.*, 2009). In some cases, height measurements with vertical accuracies of up to a few metres can be achieved (Kääb, 2005). However, the application and accuracy of photogrammetry is often limited by insufficient or poor quality ground-control points (Barrand *et al.*, 2009) that are needed to relate the images to a ground coordinate system (see Kääb, 2005). Furthermore, photogrammetry is severely limited over snow covered areas by the lack of features that are identifiable in both images.

Height measurements from airborne InSAR are derived using similar principals to satellite InSAR, which is dealt with in Section 3.2.3 (for further details see Kääb, 2005). Airborne InSAR DEMs have resolutions of metres or less and their vertical accuracy is on the order of tens of centimetres to metres (e.g. Madson *et al.,* 1995; Hoffman *et al.,* 1999; Wimmer *et al.,* 2000). However, few airborne SAR campaigns focusing on ice and snow have been flown to date (e.g. Vachon *et al.,* 1999; Bindschadler *et al.,* 1999; Stebler *et al.,* 2004).

Laser altimetry is a ranging technique which uses Light Detection And Ranging (LiDAR). Surface heights are measured by estimating the distance between the sensor and the terrain surface. This is done by measuring the travel time of a laser pulse which is sent from an aircraft sensor (of known height and coordinates), reflected at the surface and received again at the aircraft sensor:

$$T_t = \frac{2H}{v} \tag{3.1}$$

Where T_t is the travel time of the pulse, H is the range between the sensor and the surface and v is the travel speed of the pulse (Rees, 2001).

In Greenland, extensive laser altimetry surveys have been flown by NASA using the Airborne Topographic Mapper (ATM) -1 and -2 systems (Figure 3.6) (e.g. Krabill *et al.*, 1995, 2000; Abdalati *et al.*, 2002; Thomas *et al.*, 2008, 2009). The ATM systems combine high pulse rate laser ranging (up to 5000 Hz) with conical scanning capability (Krabill *et al.,* 1995). The scanning capability of the sensor has the advantage of providing a swath of measurements which helps to deliver the principal aim of the mission: to measure ice sheet surface elevation change. The swath width of the scanner is nominally 140 to 250 m and, depending on the aircraft altitude (400-800 m) and the mirror angle, the laser spot has a diameter of the order of 1 m and spots are separated on the ground by approximately 4–7 m (Abdalati *et al.,* 2002). The precision of surface elevation measurements made with the ATM systems have been derived to a root mean square error (RMSE) of better than 10 cm (Krabill *et al.,* 1995). Along with high precision surface elevation estimates, one of the key advantages of using airborne laser surveys for ice surface topography measurements

is that observations can be made in rough and sloping regions of the ice sheet, for example, along outlet glaciers. In such regions, the accuracy of satellite radar altimeters is severely degraded (Section 3.2.3). A limitation of ATM measurements, seen in Figure 3.6, is that there are large gaps in the spatial sampling of the data. However, due to the high vertical- and along-track precision, data from the NASA ATM is used, in Chapter 6, to map the inland extent of surface depressions along a profile in the Kangerlussuaq region of West Greenland. .

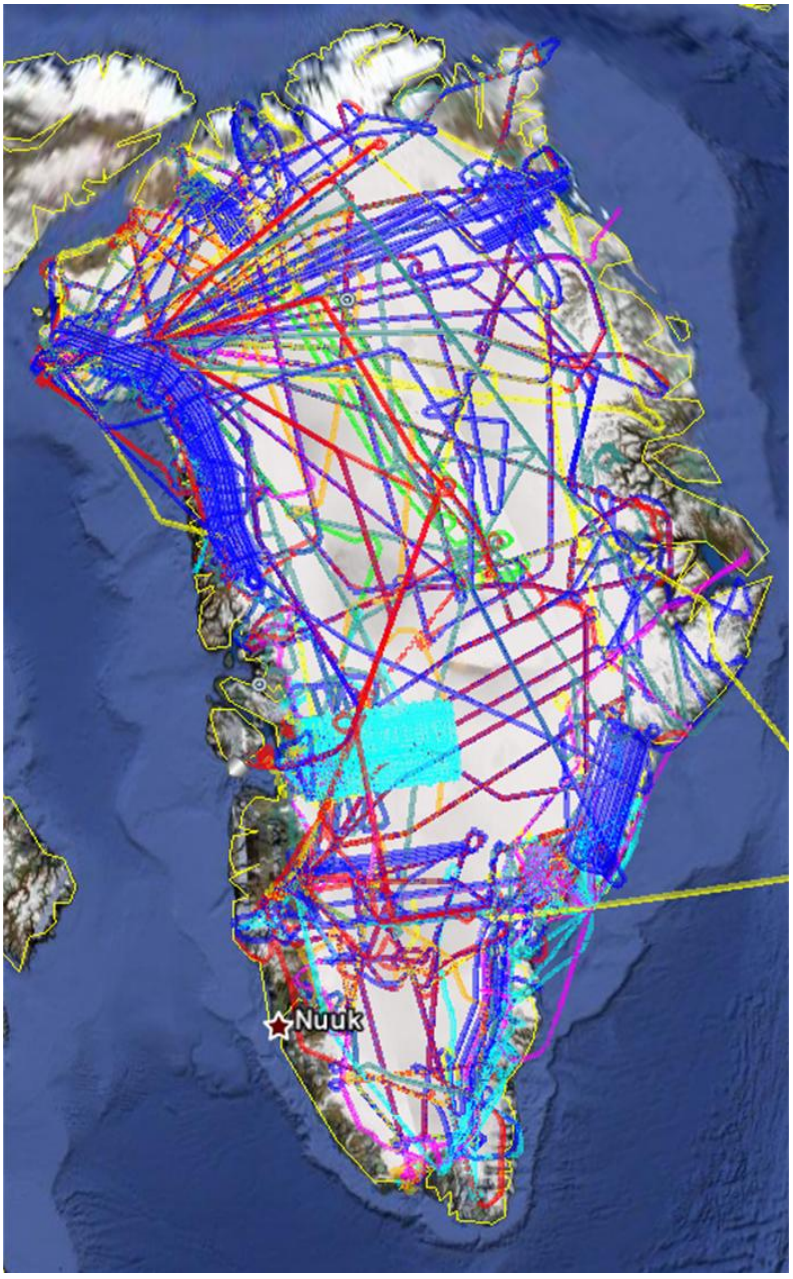

Figure 3.6: NASA ATM flight lines in Greenland from 1993-2010. The different colours represent different years. The data is displayed using Google Earth and downloaded from the NASA ATM trajectory maps website (http://atm.wff.nasa.gov/page/102e5c.html).

3.2.3 Spaceborne DEM acquisition

A key advantage of satellite derived elevation measurements over ground-based and airborne derived measurements is that they can be collected repeatedly over large areas (i.e. at the scale of ice sheets) relatively easily. The following techniques have

been used to measure surface elevation from space: satellite stereo imagery, radar and laser altimetry, and InSAR.

Satellite stereo imagery works on similar principles as ground-based and airborne photogrammetry (Sections 3.2.1 and 3.2.3). Satellite stereo images may be obtained from repeat imaging of the terrain from different viewing angles at different times, i.e. on different satellite tracks (cross-track stereo), or at the same time, i.e. during the same satellite pass of sensors with nadir-, forward- and or aft- looking capabilities (along-track stereo). Cross-track stereo imagery has been conducted using, in particular, multi-temporal SPOT (Systeme probatoire pour l'observation de la terre) 1-4 data (e.g. Al-Rousan and Petrie, 1998; Toutin and Cheng, 2002). SPOT images have ground resolutions of between 10 and 20 m and the DEMs produced by these images have reported accuracies of between 5 and 20 m RMSE depending on the base-to-height ratio (Welch, 1990; Al-Rousan and Petrie, 1998). However, cross-track stereo image coverage is limited by surface changes (e.g. snowfall or snowmelt) between image acquisition dates, thereby reducing image correlation. This problem may be partially overcome with along-track stereo images. Such images have been provided by the SPOT-5, JERS-1 (Japanese Earth Resources Satellite-1) OPS (optical sensor) and the ASTER (Advanced Spaceborne Thermal Emission and Reflection) sensor onboard the NASA Terra satellite (Toutin and Cheng, 2002). In particular, ASTER, with nadir- and aft-looking arrays and ~15m ground resolution, has been used to generate DEMs of glaciated regions (e.g. Kääb *et al.,* 2002; Stearns and Hamilton, 2007). However, as for photogrammetry, on snow surfaces optical satellite stereo imagery suffers from the same lack of identifiable features and is also prone to sensor saturation. Kääb *et al.,* (2002) compared the accuracy of DEMs created using ASTER stereo imagery and aerial photogrammetry and found that the vertical accuracy of the ASTER DEM was low (~ ± 60 m RMS and a maximum of 500 m) in complex high mountain topography (although higher (~ ± 15 m RMS) in smoother terrain). The low accuracy of the DEMs in mountainous regions and restrictions of using optical images (i.e. ASTER and SPOT) in cloudy conditions, limits the utility of this technique in glaciated regions.

Satellite radar and laser altimetry applies similar principles to that of airborne altimetry, as outlined in Section 3.2.2. Surface heights are measured by taking the altitude of the satellite orbit and subtracting the range between the satellite and the reflecting surface, as recorded by the radar or laser pulse. Satellite radar altimetry, using the Seasat, Geosat, ERS-1 and -2, and Envisat RA-2 instruments, has enabled the construction of kilometre scale resolution DEMs (e.g. Bamber *et al.,* 2001a) and the mapping of ice sheet surface elevation changes (e.g. Zwally *et al.,* 1989; Wingham, 1995; Davis *et al.,* 1998; 2000; Johannessen *et al.,* 2005). However, the resolution of satellite radar altimeter measurements is relatively low. ERS-1 and Envisat make observations every 330 m in the along-track direction and the diameter of the radar footprint ranges from 1.2 to 16 km in diameter (depending on surface roughness and slope). The separation between satellite tracks varies depending on the satellite orbital characteristics and latitude; for example, the across track sampling of ERS is ~15 km at 70˚ (Massom and Lubin, 2006). The vertical accuracy of radar altimeters can be on the order of centimetres (e.g. Brenner *et al.,* 2007). However, the accuracy and precision of the elevation estimates degrades over regions of higher and more variable terrain, rough surfaces and steep or abrupt slopes. This is due to the large footprint of the radar and because the measurement is the range to the closest point within the footprint, the location of which, within the footprint, is not known (Massom and Lubin, 2006; Brenner *et al.,* 2007). For ERS and Envisat, accurate elevation measurements on slopes with gradients exceeding 0.5º become difficult (Massom and Lubin, 2006). On slopes exceeding 1˚, van de Wal and Ekholm (1996) estimated vertical accuracies of satellite radar altimeter measurements of 75-100 m. This technique can not, therefore, be applied in the steep coastal areas of Greenland; in fact, it has been estimated that ~23% of the surface of the Greenland Ice Sheet exceeds 1˚ (Phalippou and Wingham, 1999). Additional error is introduced into elevation measurements of satellite radar altimeters through surface penetration of the radar pulse and ionospheric path delays (for further detail see Massom and Lubin, 2006; Brenner *et al.,* 2007).

The first spaceborne, earth-observing laser altimeter - the Geoscience Laser Altimeter System (GLAS) onboard NASA's ICESat (Ice, Cloud and land Elevation Satellite) - was launched in January 2003. The ICESat laser has a surface footprint of

70 m and an along-track measurement spacing of ~172 m; both substantially smaller than those achieved with radar altimeters. This has led to lower slope induced errors. In low slope areas, ICESat GLAS elevation measurements have a vertical accuracy of ~30 cm and, on slopes of 1-2˚, they have an accuracy of ~80 cm (Massom and Lubin, 2006). Thomas *et al.,* (2004) identified that the main sources of error in ICESat elevation measurements are due to forward scattering in thin clouds and errors in the knowledge of laser pointing which have been caused by technical difficulties with the instruments. The major disadvantages of ICESat laser altimetry are its inability to penetrate significant cloud cover (Massom and Lubin, 2006) and the across track spacing (~54 km at a latitude of 50˚) which results in sizeable gaps in data coverage. Nevertheless, ICESat data has produced some valuable results in glaciology. These include the production of a 500 m resolution DEM of Antarctica (Di Marzio *et al.,* 2007a) and a 1 km resolution DEM of Greenland (Di Marzio *et al.,* 2007b), the measurements of ice sheet surface elevation change (e.g. Pritchard *et al.,* 2009) and by providing valuable control points for constraining and validating other DEMs (e.g. Baek *et al.,* 2005; Atwood *et al.,* 2007; Yamanokuchi *et al.,* 2007). In Chapters 5 and 6, ICESat GLAS data is used to constrain InSAR DEMs in the northeast and west of Greenland.

InSAR has been used to derive high resolution and precise ice surface topography measurements (e.g. Kwok and Fahnestock, 1996 and Joughin et al., 1996b). As stated, in Section 3.1.1, InSAR combines two complex SAR images of the same region. The complex SAR image contains both the phase and amplitude of the returned pulse (Mather, 2004). The amplitude of the signal is a measure of the reflectivity of the surface which varies with terrain (Massonnet and Feigl, 1998). The phase signal is recorded as a shift between 0 π and 2 π radians of the electromagnetic wave transmitted by the radar relative to a reference wave (Figure 3.7). The phase signal is directly related to the range from the sensor to the surface, although because it is wrapped between 0 and 2π, it appears random from pixel-to-pixel, hence little meaning can be derived from the phase record of an independent image. However, when the phase signals of two images of the same scene are sufficiently coherent, their phase can be differenced. In such instances, differencing of the phase images derives phase signals which, over an image, or interferogram, are meaningful

because they result from differences in range from the satellite to the surface between the two image acquisitions.

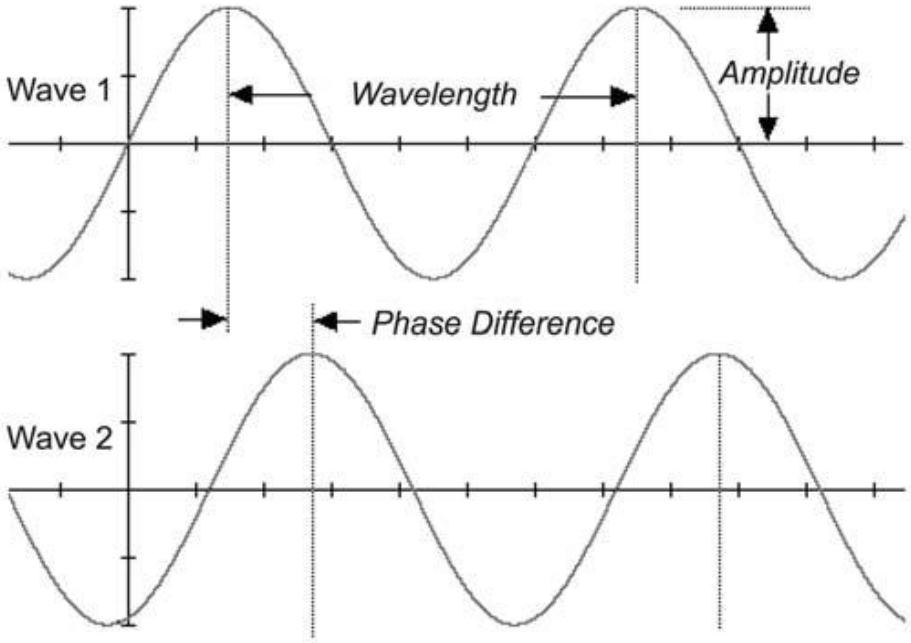

Figure 3.7: The microwave radiation of a SAR can be described by its wavelength, phase and amplitude. The amplitude of the SAR signal corresponds to the image brightness. The phase describes the shift of a wave relative to another, in degrees or radians between 0 and 360° or 2π respectively. The phase is directly related to the distance range between the sensor and the surface. Taken from Massom and Lubin (2006).

The phase signal of an interferogram contains components of topography and surface displacement. This can be expressed very simply in the equation (3.2);

$$\varphi_{\text{unwrap}} = \varphi_{\text{topography}} + \varphi_{\text{displacement}} \quad (3.2)$$

where φ is phase. Joughin *et al.,* (1998) provide expressions for the $\varphi_{\text{topography}}$ and $\varphi_{\text{displacement}}$ components of this equation in terms of sensor wavelength and the geometry of the interferometric SAR (Figure 3.8). They state that the phase due to topography can be solved for using the equation (3.3);

$$\varphi_{\text{topography}} \approx -2k\,(B_n \sin\theta_d + B_p \cos\theta_d - B^2/2r_0) \quad (3.3)$$

where $2k$ is related to the sensor wavelength, r_0 is the distance between the 1st sensor and the ground focus, θ is an angle relating to the look angle of the sensor and

alignment of the two sensors, and B_n, B_p and B are related to the spatial separation of the imaging sensors (the baseline). Expression (3.3) demonstrates how the phase signal due to topography is dependant upon the baseline length: if the baseline terms were to be substituted with 0 (i.e. theoretically there is no spatial separation of the sensors) the phase due to topography would also be 0. The optimum baseline length for deriving DEMs is between 150 and 300 m; if the baseline length becomes too long (>450 m) phase coherence is lost (Ferretti *et al.*, 2007).

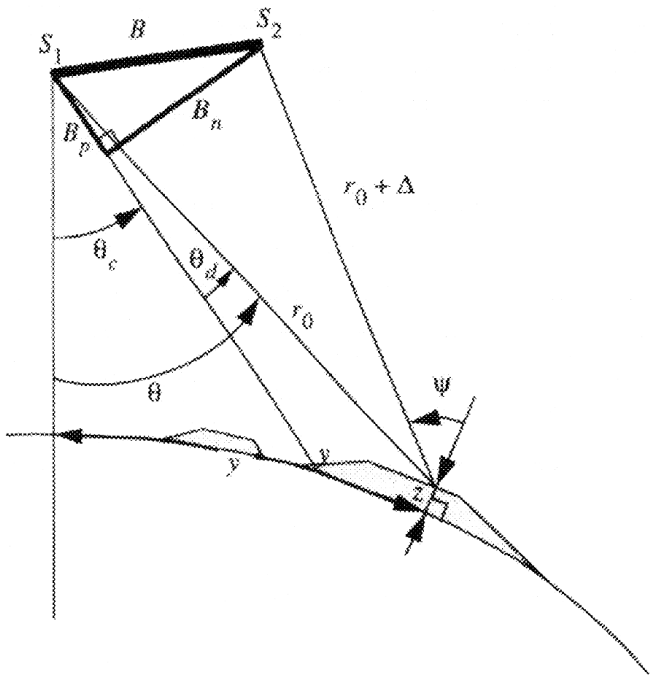

Figure 3.8: InSAR geometry. Taken from Joughin *et al.*, (1996b).

The expression for phase due to displacement is given by Joughin *et al.*, (1998) as;

$$\varphi_{\text{displacement}} = 2k\delta T\,(v_x \sin\psi - v_z \cos\psi) \qquad (3.4)$$

where v_x and v_z are velocity measurements, ψ is the local incidence angle and δT is the temporal separation of the images. This equation (3.4) demonstrates the dependence of $\varphi_{\text{displacement}}$ on δT: if the images used to derive an interferogram were acquired at the same time (i.e. δT =0) there would be no phase signal due to displacement. Equations 3.3 and 3.4 also show the independence of $\varphi_{\text{topography}}$ and $\varphi_{\text{displacement}}$ from temporal and spatial separation respectively.

As topography is dependent upon baseline length and independent of the temporal separation between images, it is most effectively derived using 'single-pass interferometry'. Single pass interferometry is achieved using images derived from two antennas carried on a single platform and separated by a precisely known distance (Rosen *et al.,* 2000). The platform's two antennas receive the phase signal at the same time, and thus in single pass interferometry there is no displacement component in the phase signal (see equation 3.4). However, limited data exists for single-pass interferometry and so repeat-pass interferometry, which utilises images taken from the same flight path but on successive orbits, is often used (Massom and Lubin, 2006). Repeat-pass interferometry rarely achieves repetition of an exact path (Rosen *et al.,* 2000) and so the resultant images are separated both spatially and temporally. Consequently, the phase signal has both topographic and displacement components. Therefore, in order to derive data for topography of a given scene using repeat pass interferometry, the two phase signals must be separated. This is achieved by using 'differential interferometric SAR' (DInSAR) (Kwok and Fahnestock, 1996).

Differential interferometry requires two interferograms derived from three or four images of a given area, or one interferogram and an external DEM (digital elevation model). If a difference in the temporal baseline of the two interferograms exists, the phase signals are scaled in order to account for this. In doing so, the assumption of constant motion is made, meaning that the phase due to motion is equal in both interferograms (Kwok and Fahnestock, 1996). Therefore, by subtracting one interferogram from the other, the phase due to topography can be obtained (see Figure 3.2).

For a DEM to be produced from a topography only interferogram, a number of further processing steps are required; these include flattening, filtering, phase unwrapping, refinement of the baseline and the calculation of topographic heights. The phase signal of a topography only interferogram contains an almost linear phase signal across the image. This is due to the curvature of the Earth's surface and is removed by 'flattening' the interferogram. Next, the component of the phase signal due to noise can be reduced by applying a filter. Doing so reduces the complexity of phase unwrapping (see below) and provides more robust results. However, it can

lead to a loss of fringes (see below) which causes error in phase unwrapping (Wëgmuller *et al.*, 2002).

As mentioned previously, the phase of the SAR signal is recorded between 0 and 2π radians. Therefore, the topography only interferogram contains phase information in fringes, or cycles, of modulo 2π, i.e. if the phase variation exceeds 2π it wraps round again to 0. The fringes in the topography only interferogram can be likened to contour lines, as a phase shift of 2π represents a fixed height difference. This is termed the altitude of ambiguity (h_a) and is inversely proportional to the perpendicular baseline (B_n):

$$h_a = \frac{\lambda R \sin\theta}{2B_n} \tag{3.5}$$

where λ is the radar wavelength, R is the range of the SAR to the surface and θ is the satellite look angle. Therefore, the greater the baseline (to a point, as stated above), the greater the sensitivity and accuracy of the altitude measurement.

To recover the absolute phase differences and the actual elevation at each point, the integer number of phase cycles must be added to each other. This is known as phase unwrapping. Phase unwrapping is based on the assumption that the surface is smooth and that there should be an absence of jumps in the unwrapped phase. More precisely, neighbouring phase values are assumed to be within 1π radian of one another (hence why larger baselines and smaller altitudes of ambiguity produce more accurate results). Although this assumption is often valid, phase unwrapping must account for phase discontinuities which occur due to phase noise and undersampling (in particular in steep terrain such as at ice sheet margins) (see Massom and Lubin (2006) for further detail). If not accounted for, such inconsistencies will propagate error through scenes when unwrapping. A number of phase unwrapping methods aimed at reducing these errors have been developed (including the branch-cut region growing algorithm introduced by Goldstein *et al.*, (1988) and the minimum cost flow networks algorithm developed by Costantini (1998)). The quality of phase unwrapping also relies heavily on the quality of the interferogram and of the human interaction (Massom and Lubin, 2006).

The unwrapped interferogram now contains relative heights in phase radians which must be converted to absolute heights. This requires precision estimates of the satellite orbit positions and the interferometric baselines. Although initial estimates are obtained from the satellite orbits, they are not accurate enough to convert interferometric phase to elevation. Instead, this is achieved by fitting topographic phase to a series of Ground Control Points (GCPs) height measurements using a least squares solution. GCPs should be spread across the image and there should be at least four; however, a greater number will reduce the error in the baseline estimate (Zebker *et al.,* 1994). GCPs from external DEMs, in situ GPS and altimetry can be used (Massom and Lubin, 2006). Phase measurements are then converted to heights by, again, linking GCP height measurements to topographic phase. Finally, the DEM can be converted from SAR image geometry into orthorectified coordinates.

Uncertainty in an InSAR DEM is related to the baseline length and error, image coherence, failure of/maintaining the constant velocity assumption, accuracy and number of the GCPs, penetration of the radar signal below the surface, ionospheric signal disturbance, and unwrapping errors (see Massom and Lubin, 2006, and Zebker *et al.,* 1994, for more in depth discussions of uncertainty of InSAR DEMs). These sources of error will, in some cases, (e.g. low image coherence) lead to a loss of precision in the DEM (i.e. uncertainty in the pixel-to-pixel heights), while others (e.g. baseline errors, changes in velocity and unwrapping errors) will degrade the absolute accuracy of the heights (i.e. will introduce height offsets or ramps).

To give examples, the magnitudes of inaccuracy and imprecision introduced by the various error sources to an InSAR DEM may be quantified as follows. An interferogram made from a pair of images with a baseline of 100 m will, according to equation 3.5, have an altitude of ambiguity of 93 m (i.e. one phase cycle represents 93 m of height change). If the average coherence of the image is 0.95, the phase noise will limit the detection of phase differences to ~5º (from Zebker *et al.,* 1994), which in this scenario represents a vertical precision of 1.3 m. A failure of the constant velocity assumption (i.e. a change in velocity) of 5 m/yr would introduce an apparent topographic signal of 17.5 m. Penetration depths of up to 35 m have been computed for C-Band radar in Greenland (Hoen and Zebker, 2000).

Joughin *et al.,* (1996b) used InSAR to derive surface topography measurements of an area of the West Greenland Ice Sheet. They were able to produce maps of continuous topography with 80 m horizontal resolution, which is substantially higher than DEMs derived with techniques such as radar altimetry (c.f. ~500 m- Wingham, 1995) (Figure 3.9). The vertical precision achievable with InSAR DEMs has ranged between 2 m and 20 m (e.g. Joughin *et al.,* 1996b; Forsberg *et al.,* 2000; Rignot *et al.,* 2001; Atwood *et al,*. 2007) and depends on the topography, baseline, coherence and GCPs. The high resolution and precision of topography measurements using InSAR, achieved continuously and over large regions, provide the DEMs required to fulfil the objectives of Chapters 5 and 6 of this thesis.

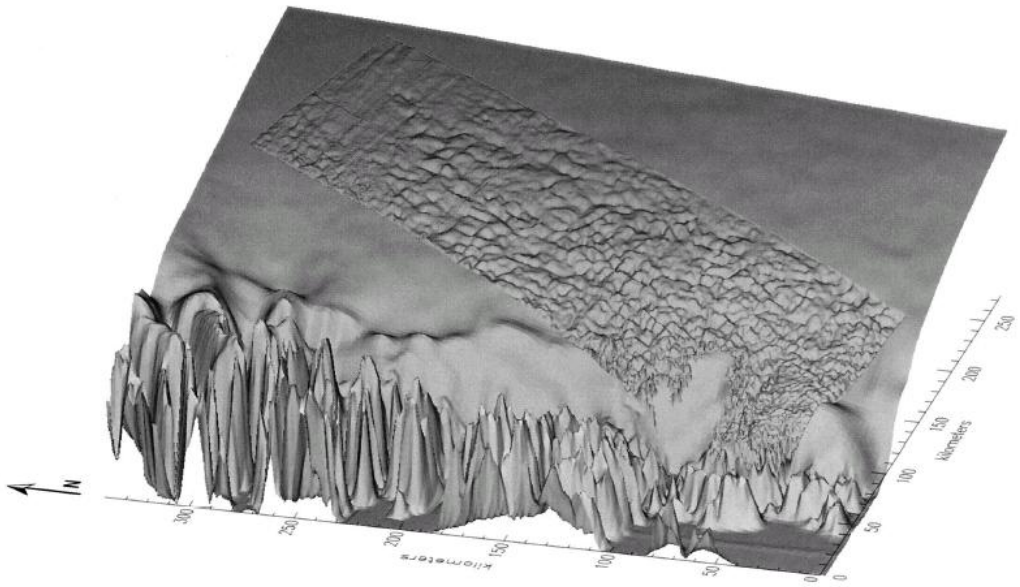

Figure 3.9: Shaded surface elevation model of an area of the West GrIS. The strip with greater detail was derived from InSAR and the smoother surface data was derived from radar altimetry. Taken from Joughin *et al.,* (1996b).

3.3 Supraglacial lake analysis

In Chapters 5 and 6, the distribution of supraglacial lakes is mapped in regions covering thousands of square kilometres. Supraglacial lakes have previously been monitored using a combination of *in-situ* and remote sensing data. *In-situ* measurements have provided detailed data on lake dimensions and drainage events

from individual lakes (e.g. Boon and Sharp, 2003; Box and Ski, 2007; Das *et al.,* 2008). For example, using *in-situ* measurements from pressure transducers, GPS, seismometers and sonar surveys, in combination with remote sensing images, Das *et al.,* (2008) were able to record the volume and rate of water released during a lake drainage event and provide important insights into the ice dynamic response. However, due to the intensive nature of *in-situ* studies, such measurements have been limited to a small number of lakes.

During the melt season, thousands of lakes cover vast areas of the GrIS (Figure 3.11). In order to monitor lakes at this scale, remote sensing data has been employed (e.g. Box and Ski, 2007, McMillan *et al.,* 2007; Sundal *et al.,* 2009). A range of remote sensing image types have been used to map lake areas (e.g. McMillan *et al.,* 2007; Sundal *et al.,* 2009), depths and therefore volumes (e.g. Box and Ski, 2007; Sneed and Hamilton, 2007, Georgoiu *et al.,* 2009), over areas of tens of thousands of km^2 (e.g. Box and Ski, 20007; McMillan *et al.,* 2007; Sundal *et al.,* 2009) and on intra- and interannual timescales (e.g. Box and Ski, 2007; Sundal *et al.,* 2009).

To address objectives 2 and 3 in Chapters 5 and 6, lake area data from a large number of lakes in the northeast and west of the GrIS was required. Remote sensing methods were therefore employed. The remainder of this section will focus on, and discuss, the remote sensing data and methods that have previously been used to measure supraglacial lake areas.

3.3.1 Data

A range of image types have been used to measure the areas of supraglacial lakes, including data from the Marine Observation Satellite –1 (MOS-1; Echelmeyer *et al.,* 1991), Advanced Spaceborne Thermal Emission and Reflectance Radiometer (ASTER; McMillan *et al.,* 2007; Sneed and Hamilton, 2007; Georgiou *et al.,* 2009; Sundal *et al.,* 2009), Landsat program (Luthje *et al.,* 2006; McMillan *et al.,* 2007) and Moderate Resolution Imaging Spectroradiometer (MODIS; Box and Ski, 2007;

Sundal *et al.*, 2009). The attributes of the different image types present different advantages for analysing supraglacial lakes.

The relatively high resolution of ASTER and Landsat images (15 m and 30 m respectively) in comparison to MODIS images (250 m) makes them advantageous for gaining more precise measurements of lake dimensions (Figure 3.10). The uncertainties associated with lake area measurements from ASTER and Landsat images are between 4% and 8% (McMillan *et al.*, 2007; Sundal *et al.*, 2009; Johansson *et al.* 2010) and are caused by the loss of precision at lake margins due to the pixel size. Consequently, the error associated with large, round lakes is proportionally less than for small lakes with tortuous perimeters (McMillan *et al.*, 2007). Sundal *et al.*, (2009) quantified the level of uncertainty in lake area measurements from MODIS images by comparing the areas of lakes identified in both the MODIS and ASTER images acquired on the same day. They found that the lake area estimate from the MODIS image exceeded that from the ASTER image by 1.6%.

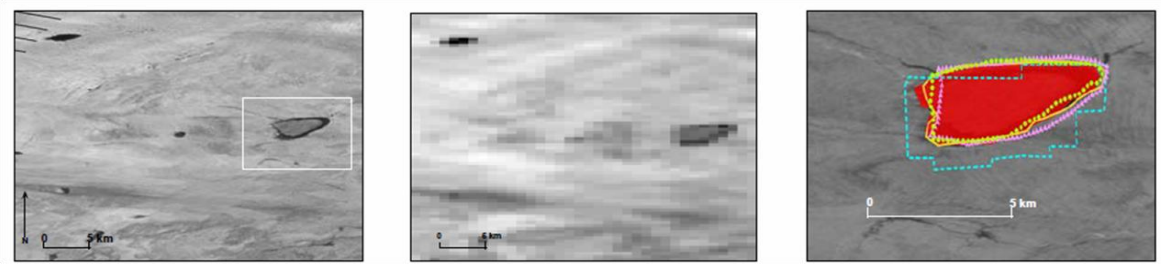

Figure 3.10: A lake identified in a 15 m resolution Landsat image (left) and the same lake identified in a 250 m resolution MODIS image (middle). The right hand image is zoomed into the lake in the white box in the left hand image and shows the difference between the lake area classified in the Landsat image (red) and the MODIS image (blue). Taken from Johansson *et al.*, (2010).

To capture the temporal dynamics of the rapid developments of supraglacial lakes (e.g. Box and Ski 2007; McMillan *et al.*, 2007), high temporal resolution sampling is required. The repeat period of ASTER and Landsat images is 4-16 days, whereas the repeat period of MODIS images is just 1 day, making MODIS images preferable for monitoring temporal changes in supraglacial lakes. However, because the MODIS satellite is an optical imaging sensor, it is unable to derive surface measurements

when there is cloud cover. In Greenland, there is frequent cloud cover (Hatzianastassiou *et al.,* 2001) and so the achievable temporal resolution of surface images with MODIS is lower than 1 day. Johansson *et al.,* (2010) showed that, when available, SAR data from Radarsat, Envisat and ERS can be used to compliment optical images and improve the temporal coverage of lakes from optical images. However, the repeat period of these sensors is 24, 35 and 35 days respectively, and so the availability of these images is limited to a few days a month.

3.3.2 Classification of lake areas

The areas of lakes have been mapped using both manual digitisation (McMillan *et al.,* 2007; Johansson *et al.,* 2010) and automated classifications (Box and Ski, 2007; Sundal *et al.,* 2009). Lakes can be readily identified in optical imagery (Figure 3.11) because water lowers the reflectance of the surface making lakes appear as dark, rounded shapes. The difference in reflectance values between lakes and the ice/snow surface also provides the basis for automated image classification. Box and Ski (2007) classified lakes in 170 MODIS images from the western margin of the GrIS using thresholds of reflectance values. The thresholds were determined experimentally from the satellite data and by using *in-situ* data of 2 lakes in the study region. They found that in band 1 (red wavelengths) there is good contrast in the reflectance values of lakes and snow. However, over bare ice with large amounts of impurities there is an overlap in the reflectance values with those of lake areas. In addition to using band 1, pixel values derived from a ratio of band 1 to band 3 (blue wavelengths) was used. The ratio clearly distinguished between lakes and ice surfaces as it was less sensitive to changes in ice colour. Lakes were therefore classified using a combination of thresholds of the reflectance values from band 1 and from the ratio of band 3/band 1 (Box and Ski, 2007). Using the same band 1 and 3/1 ratio combination, Sundal *et al.,* (2009) presented an alternative classification system which used a fuzzy logic membership function, enabling pixels to be assigned according to the degree of membership to a given class rather than a crisp threshold value.

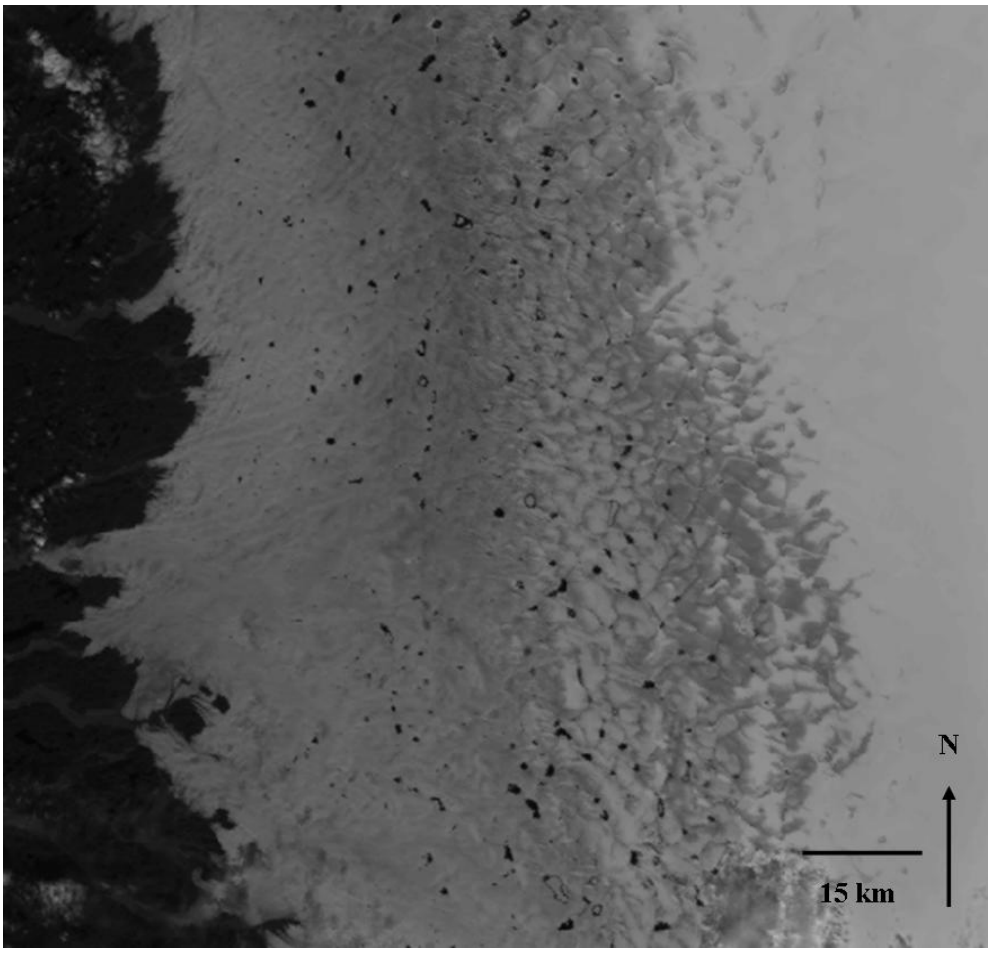

Figure 3.11: A MODIS image from West Greenland showing supraglacial lakes.

There are relative advantages and disadvantages of mapping lakes manually and automatically. The main advantage of automated classification of lake areas is the provision of an efficient means of mapping lakes over large areas and long time periods. However, automated classification is subject to a number of limitations. As a result of the resolution of the images used in classification, a proportion of small lakes are often not identified. Using high resolution ASTER and Landsat images, only lakes larger than 0.01 km^2 may be confidently classified (McMillan *et al.*, 2007). The percentage of lakes this excludes has been calculated to be between 1 and 5% (McMillan *et al.* 2007; Johansson *et al.*, 2010). In lower resolution MODIS imagery, only lakes larger than ~0.1 km^2 are identified (Figure 3.12 - Sundal *et al.*, 2009). Using an ASTER image from the west of Greenland, Sundal *et al.*, (2009)

estimated the total area of lakes smaller than 0.1 km^2. They found that these lakes accounted for ~12% of the total area of lakes in an image acquired late in the melt season (August). At the beginning of the melt season, when lakes are developing and their sizes are relatively small, this percentage would be higher (Sundal *et al.,* 2009; Johansson *et al.,* 2010).

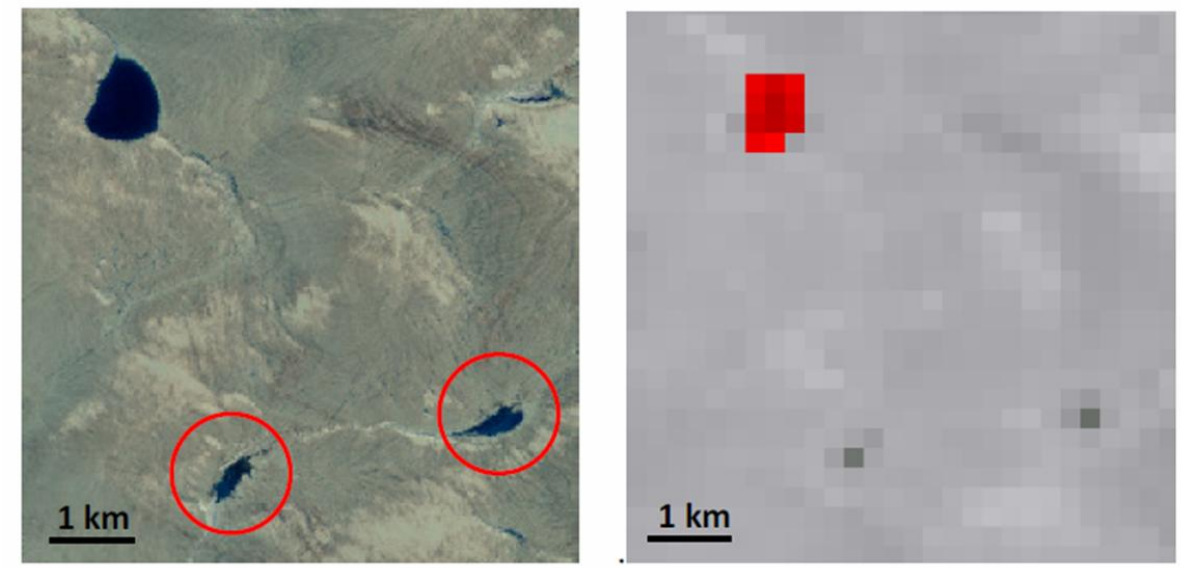

Figure 3.12: The influence of lake size on lake identification. The image on the left is 15 m resolution ASTER and the image on the right is 250 m resolution MODIS. The circled lakes are less than 0.1 km^2 and not classified (red) in the MODIS image. Taken from Sundal (2008).

Lake ice forms on the surface of supraglacial lakes in Greenland (Figure 3.13) and since the reflectance values of lake ice are the same as the surrounding ice, these pixels are misclassified. Sundal *et al.,* (2008) estimated that, on average, ~12% of the total lake area at the peak of the melt season is ice covered. This percentage will be greater early in the melt season and again towards the end, when lake surfaces begin to refreeze (Figure 3.13).

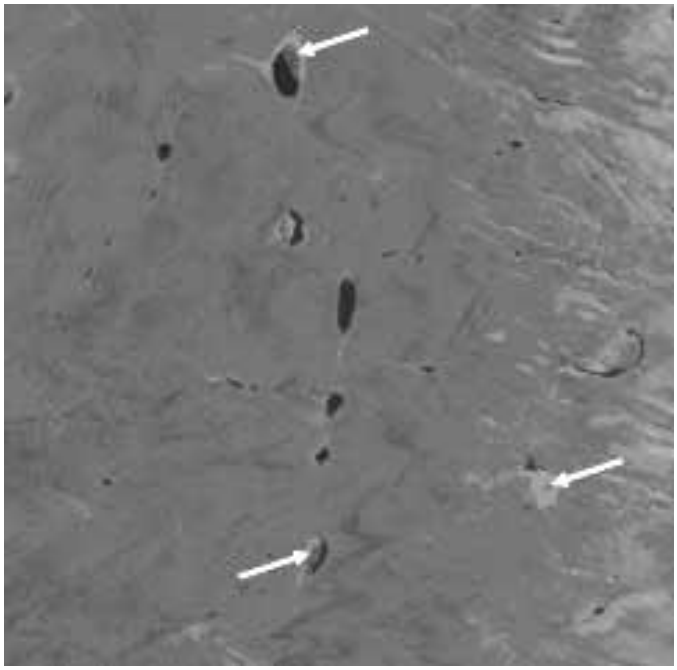

Figure 3.13: Landsat 7 scene from late summer (23/08/2000) from West Greenland. Arrows indicate some of the locations where the surfaces of supraglacial lakes have started to refreeze. Taken from Luthje *et al.*, (2006).

Manual digitisation has been shown to overcome the limitations of classification associated with lake ice and small lakes (e.g. Sundal *et al.*, 2008; Johansson *et al.*, 2010). However, the process is time consuming when dealing with large datasets and subject to some uncertainty related to user subjectivity. Studies on manual digitisation have shown differences between interpreters of ±2.5 pixels from the mean for distinct boundaries and ±3 pixels for diffuse boundaries (Sannel *et al.*, 2010).

In order to achieve objective 2 (an assessment of using high resolution DEMs to map potential supra-glacial lake locations) reported in Chapters 5 and 6, automated classification of lakes in both high spatial resolution Landsat images and high temporal resolution MODIS images enabled supraglacial lake area coverage to be mapped over thousands of square kilometres in the northeast and west of Greenland. In addition, to achieve objective 3 in Chapter 6, manual classification of lakes in MODIS images enabled the timing of lake formation and drainage to be accurately identified.

3.4 Summary

This chapter has reviewed the current methods in glaciology for acquiring measurements of ice velocity, ice surface elevation and supraglacial lake extent. Due to the inaccessibility of the regions studied in this thesis, and the large spatial scales over which measurements are required, remote sensing techniques are employed as follows:

- SAR intensity tracking is used in Chapter 4 to derive seasonal velocity measurements of glaciers in the northeast of Greenland. SAR sensors are able to image through cloud cover and throughout the polar night, and intensity tracking is relatively robust to surface changes, and therefore has the potential to provide continuous, year-round records of velocity.

- InSAR is used to derive ice surface elevation measurements for mapping ice surface depressions, in Chapters 5 and 6, as it is capable of generating continuous, high resolution ice surface DEMs. The DEMs are constrained using ICESat GLAS data due to the high precision and accuracy of the elevation measurements, and the good spatial coverage of data points. Surface elevation measurements from ATM flight lines in the west of Greenland, where available, are also used in Chapter 6 to map the altitudinal extent of ice surface depressions; again, this data is used due to its high precision and accuracy.

- Landsat and MODIS data are used to map the area of supraglacial lakes in the northeast and west of Greenland in Chapters 5 and 6, respectively. The relatively high spatial resolution of Landsat images provide accurate classifications of lake areas in a given image, whereas the high temporal resolution of the MODIS images provide more accurate estimates of evolving lake area over the course of a melt season. A combination of automated and manual classification techniques is employed. Automated classification is used to map lake areas over large regions for ease of computation while manual classification of the lakes is used to enable

precise estimates of the timing of both lake formation and lake drainage events of a smaller sample.

Chapter 4: Seasonal flow variability of outlet glaciers in Northeast Greenland

This chapter describes seasonal velocity measurements of land- and marine-terminating outlet glaciers in the Northeast of Greenland acquired using SAR intensity tracking. This chapter has been prepared for submission to the Journal of Glaciology:

Briggs, K., Shepherd, A. and Nienow, P. (in prep.) Seasonal flow variability of outlet glaciers in the Northeast of Greenland. *Journal of Glaciology*

The majority of the work for this chapter was carried out by myself. A Shepherd and P Nienow developed the original ideas for this chapter and provided comments on the manuscript.

The chapter ends with a section on limitations of the work presented herein (section 4.7) and additional information relevant to this chapter is included in an appendix (section 4.8).

4.1 Abstract

We have determined seasonal velocity measurements at one land- and two marine-terminating glaciers of adjacent positions in a region of the Northeast of Greenland for which little glaciological knowledge exists. Flow rates were determined using Synthetic Aperture Radar (SAR) intensity tracking of 18 ERS-1 and -2 images acquired between March 1995 and March 1996. We calculated along glacier profiles of average winter and summer flow rates for the Wordie (land), Waltershausen (marine) and Adolf Hoel (marine) Gletschers respectively. We identify seasonal velocity trends at all three glaciers. Early summer accelerations of 26%, 34% and 16% were recorded at Wordie, Waltershausen and Adolf Hoel Gletschers respectively, and these were followed by decelerations which occurred during the melt season. Accelerating flow began with the onset of surface melting and peak velocities, followed by progressive deceleration, which coincided with the drainage of supraglacial lakes at all three glaciers. We suggest that this indicates a hydrological control on basal sliding rates similar to that observed in other regions of the Greenland Ice Sheet and Arctic and Alpine areas. Large interannual variability in winter flow rates at Adolf Hoel Gletscher was observed, which exemplifies the complexity of tidewater glacier behaviour. It serves to highlight the limits to our current understanding of the mechanisms that control tidewater glacier dynamics on a seasonal and interannual basis and furthermore, it demonstrates that longer-term records of velocity are essential to isolate seasonal and secular trends in flow.

4.2 Introduction

The Greenland Ice Sheet is losing mass (e.g. Krabill *et al.*, 2000; Luthcke *et al.*, 2006; Rignot and Kanagaratnam, 2006; Rignot *et al.*, 2008; Zwally *et al.*, 2011). Mass loss is occurring by two principal mechanisms, ice discharge into the oceans and surface melting; the rate at which mass loss is occurring via these mechanisms, is linked to ice flow rates (e.g. Parizek and Alley, 2004; Rignot and Kanagaratnam, 2006; van den Broeke *et al.*, 2009). Measurements of Greenland ice flow rates have

shown that they vary on hourly to seasonal and interannual timescales and that they respond rapidly to climate forcing (e.g. Rignot and Kanagaratnam, 2006; Joughin *et al.,* 2008b; Rignot *et al.,* 2008; Shepherd *et al.,* 2009). This is significant for predictions of the future mass balance of the Greenland ice sheet as models do not currently account for the processes linking climate to ice velocity (Meehl *et al.,* 2007).

Climate has been found to regulate Greenland ice velocities in two ways: through surface meltwater supply to the glacier bed (e.g. Das *et al.,* 2008; Joughin *et al.,* 2008c; van de Val *et al.,* 2008; Shepherd *et al.,* 2009; Bartholomew *et al.,* 2010) and through ice-ocean interactions at the ice sheet's marine margins (e.g. Holland *et al.,* 2008; Rignot *et al.,* 2010; Nick *et al.,* 2010). Fluctuations in Greenland ice sheet flow have been linked to the drainage of surface lakes (e.g. Joughin *et al.,* 1996a; Das *et al.,* 2008) and changes in surface melting (e.g. Zwally *et al.,* 2002; van de Wal *et al.,* 2008; Shepherd *et al.,* 2009). The influx of surface meltwater to the bed of a glacier acts to increase surface velocity by increasing water pressures in the basal drainage system (e.g. Iken *et al.,* 1983; Iken and Bindschadler, 1986) which causes 'cavitation' or 'hydraulic jacking' (Iken, 1981) and, in turn, enhances basal sliding; a mechanism well recognised at Alpine and polythermal Arctic glaciers (e.g. Iken *et al.,* 1983; Iken and Bindschadler, 1986; Bingham *et al.,* 2003). However, theoretical and field based studies suggest that on seasonal timescales, continued input of meltwater to the bed forces the drainage system to evolve to a more efficient state which lowers basal water pressures and causes ice flow deceleration (e.g. Kamb, 1987; Hock and Hooke, 1993; Fountain and Walder, 1998; Nienow *et al.,* 1998; Mair *et al.,* 2002). Over interannual timescales the response of ice velocities to variable amounts of surface melting remains uncertain (e.g. Zwally *et al.,* 2002; van de Wal *et al.,* 2008; Schoof, 2010, Sundal *et al.,* 2011) due to our limited understanding of this process.

The dynamics of marine-terminating glaciers have been found to be sensitive to changes at their termini (e.g. Vieli *et al.,* 2001; Holland *et al.,* 2008; Nick *et al.,* 2009; Murray *et al.,* 2010; Straneo *et al.,* 2010). Changing ice velocities as a result of

ice-ocean interaction have been subject to focussed study in recent years as observations have revealed that almost all of the dynamic thinning of the ice sheet is currently occurring at marine-terminating glaciers and with high-levels of interannual variability (Sole *et al.,* 2008; Pritchard *et al.,* 2009). Glacier accelerations of marine-terminating glaciers in Greenland have been linked to a number of possible causes including warming ocean temperatures (e.g. Holland *et al.,* 2008; Straneo *et al.,* 2010), decreased sea ice concentrations (e.g. Joughin *et al.,* 2008a; Amundson *et al.,* 2010) and increasing surface temperatures (e.g. Sohn *et al.,* 1998; Rignot *et al.,* 2010) which, in turn, cause ice thinning, increased calving rates, ice front retreat and reduced backstress at the glacier terminus all resulting in higher rates of basal sliding. Furthermore, understanding the climate response signal of tidewater glaciers is complicated by characteristic cycles of advance and retreat which are regulated by factors external to the climate system, such as subglacial topography (Meier and Post, 1987).

On seasonal timescales two key forcing mechanisms have been identified in driving velocities of tidewater glaciers; 1) those in multi-year retreat are observed to undergo summer velocity increases which correlate with the retreat of the terminus in summer, persists beyond the end of the melt season, and is thought to be driven by changes in backstress exerted by a floating ice tongue (e.g. Joughin *et al.,* 2008a; Howat *et al.,* 2010). 2) Seasonal velocity variations at glaciers with stable front positions have been observed to respond to hydrological forcings similar to those observed at land-terminating glaciers (e.g. Meier and Post, 1987; Meier *et al.,* 1994; Vieli *et al.,* 2004; Howat *et al.,* 2010; Anderson *et al.,* 2010). Investigations into seasonal velocity variations at tidewater glaciers in Greenland are, to date, limited, and more widespread research is required to broaden our understanding of the dynamic responses of the ice sheet to climate perturbations.

Here we examine seasonal variations in the flow of marine- and land-terminating glaciers of the Greenland ice sheet. The glaciers we investigate are of neighbouring positions, allowing for an assessment of seasonal velocity patterns between the glaciers that is independent of differences in climatic conditions. Our study region is

located in the Northeast of Greenland (Figure 4.1), an area for which seasonal velocity measurements have not previously been reported. It is the aim of this investigation to assess the influence of glacier terminus conditions and associated forcing mechanisms on the seasonal velocity behaviour of Northeast Greenland outlet glaciers. Our investigation focuses on 3 glaciers, the land-terminating Wordie Gletscher and the marine-terminating Waltershausen and Adolf Hoel Gletschers (Figure 4.1). We generate velocity measurements during the course of a year using the technique of Synthetic Aperture Radar (SAR) intensity tracking (e.g. Luchitta *et al.*, 1995; Strozzi *et al.*, 2002; Luckman, *et al.*, 2003), and we compare our findings to aspects of the glaciers' geometry, to air temperatures, to the evolution of supraglacial lakes, and to conditions in the fjords into which they terminate.

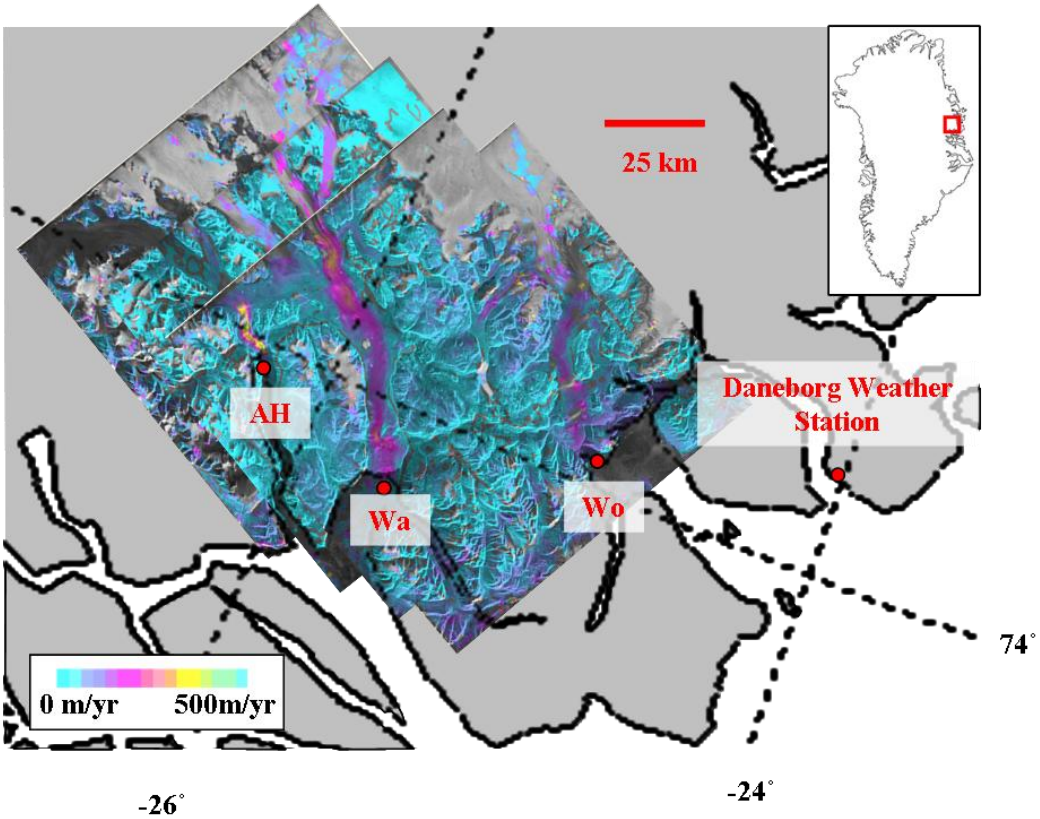

Figure 4.1: Location of the study region in the Northeast of Greenland. The Wordie (Wo), Waltershausen (Wa), and Adolf Hoel (AH) Gletschers are labelled on a map of ice sheet speed determined using a mosaic of 4 35-day SAR image pairs. The location of the Daneborg Meteorological Station is also shown.

4.3 Data and methods

We employed SAR intensity tracking (e.g. Luchitta *et al.,* 1995; Strozzi *et al.,* 2002; Luckman, *et al.,* 2003) to obtain velocity estimates during the period March 1995 to March 1996. From a dataset of 18 ERS-1 and -2 SAR images we formed thirteen 35-day image pairs and one 140-day pair. The data are not uniformly distributed across the whole year as images for the period from 18/09/1995 until 23/11/1995 were not available.

Intensity tracking provides estimates of average ice velocity over the time period between which the pair of SAR images are acquired by tracking the displacement of surface features and/or image speckle from the first to the second image (Strozzi *et al.,* 2002). The broad processing steps involved in intensity tracking include the initial processing of the raw SAR images to a single-look complex (SLC) image, the calculation of global image offsets that result from differences in the orbital configuration of the satellite, the calculation of local image offsets caused by surface displacement, and finally, the filtering of potentially erroneous offset estimates.

Processing the raw data to SLC involved accounting for missing lines, concatenating the consecutive frames, improvement of the orbital state vectors, deriving the range and azimuth spectrums, azimuth auto-focusing, range and azimuth compression radiometric calibration and multi-looking (Wegmüller *et al*., 1998). Bilinear global offset polynomials were then calculated for SLC pairs by first manually estimating initial constant offsets in range and azimuth and then using these estimates to guide more precise estimates calculated using a patch intensity cross correlation (Bindschadler and Scambos, 1991). To acquire the best number of matches and achieve a strong cross correlation, we adjusted the search window size for each application. We found window sizes of either 64 x 256 (~1km^2) or 128 x 512 (2km^2) in the azimuth and range directions, respectively, resulted in the strongest correlations. The confidence level associated with each offset estimate was assessed

with a signal to noise ratio (SNR). The SNR estimates were then used to reject low confidence estimates and thereby limit errors in the global offset polynomial. A SNR threshold of 7 was set, below which offset estimates were rejected. When estimating the global offset, it is important to preferentially track fixed (e.g. rock) points and not include offsets from moving ice surfaces. This was achieved by rejecting offset measurements that were more than 3 standard deviations from the global fit. Producing the final polynomial was an iterative process; the intensity cross correlation procedure and polynomial fit calculations were run iteratively until the accuracy of the registration offset estimation no longer improved.

The local offset (surface displacement) was calculated using an intensity cross-correlation algorithm (Bindschadler and Scambos, 1991). The magnitude of the offset was calculated by identifying the correlation peak of a sample window from the first image moved relative to a larger sample region of a second image at specified intervals. After testing a range of different search window sizes (8 to 192 and 32 to 768 pixels in range and azimuth, respectively) we selected a size of 64 x 256 pixels as this afforded the best combination of areal coverage, high SNR, and resolution of ice velocity signals. Local offsets were estimated at intervals of 12 and 48 range and azimuth pixels, respectively, and, prior to their calculation, we applied an image oversampling factor of 2 as this has been found to increase the accuracy of displacement estimates (Werner *et al.*, 2005). Finally, movement of the surface was calculated as the displacement between the two images at the correlation peak minus the global offset.

We filtered our intensity tracking results for erroneous estimates using a method adapted from that of Luckman *et al.*, (2003). This involved applying a SNR threshold of 4 to local offset estimates, rejecting values which exceed 4 times the average of a 9 x 9 pixel neighbourhood, and removing areas with an image pair coherence of less than 0.6.

The errors associated with our displacement measurements were estimated by calculating the mean difference from 0 of local offsets using samples of up to 500

points taken from static regions (i.e. bedrock) (e.g. Pritchard *et al.,* 2005; de Lange *et al.,* 2007; Luckman *et al.,* 2007). Systematic errors occur in offsets estimates in the range direction as a result of changes in the extent of relief distortion with distance form the sensor (Pritchard and Vaughan, 2007). In mountainous regions this causes inaccuracy in the global offset estimation which then causes inaccuracy in the local offset estimations. For image pairs where the error estimates were initially large (the three image pairs in period 3 - Figure 4.3), we removed this systematic error and improved the accuracy of the local offsets by measuring the mean local offsets in range and azimuth on flat static areas (i.e. rock) near the detailed study areas shown in Figure 4.2. The mean offset in range was then removed from the range component of the local offsets before calculating the displacement vector. Systematic errors of up to 39 m/yr in range were removed.

In order to compare our velocity estimates to external forcing factors, we assembled datasets of air temperature, supraglacial lake evolution, ice front conditions, and ice surface geometry. Maximum air temperature data collected at the Daneborg meteorological station (No. 043300; 74º 18’ N 20º 13’ W) (Figure 4.1) between 01/01/1995 and 31/03/1996 were used to quantify positive degree days to establish when surface melting occurred. The seasonal evolution of supraglacial lakes and the calving front positions of Waltershausen and Adolf Hoel Gletschers (Figure 4.4) were recorded using the same SAR amplitude imagery which we used to estimate ice velocities (section 4.8). The ice surface topography of the three glaciers was derived from an InSAR DEM of ~30 m horizontal resolution created by the authors for another study (Chapter 4).

4.4 Results

4.4.1 Along glacier velocity profiles

Average winter and summer velocities at transects along centre flow lines of the Wordie, Waltershausen and Adolf Hoel Gletschers are shown in Figure 4.2. Due to the limited spatial distribution of summer velocity estimates which we were able to

acquire along the transects relative to the winter (Figure 4.2), we are unable to provide reliable estimates of annual average velocities for the glaciers. However, we were able to assess differences in the average wintertime flow rates of the 3 glaciers; the mean along-transect velocities of the Wordie, Waltershausen and Adolf Hoel Gletschers were 140 ± 42 myr^{-1}, 171 ± 42 myr^{-1} and 248 ± 42 myr^{-1}, respectively. Where summertime velocity measurements were available, it is found that, in general, they exceed average wintertime velocities. On average, summertime velocities were 16%, 2% and 63% greater, and the maximum increases were 27%, 36% and 146% at the Wordie, Waltershausen and Adolf Hoel Gletschers respectively. Although limited data coverage prevents an assessment of spatial variations in seasonal velocity differences at the Wordie and Waltershausen Gletschers, at Adolf Hoel Gletscher we observe a general increase in summertime velocity towards the terminus (Figure 4.2c) which occurs at an average rate of 11.3% m^{-1}.

We examined the along-transect winter velocity profiles of Wordie, Waltershausen and Adolf Hoel Gletschers to investigate the extent to which changes in flow are correlated with fluctuations in ice surface topography and glacier width. At Wordie and Waltershausen Gletschers we observe no distinct trends in velocity with distance from the terminus over the respective 30 and 60 km sections surveyed. However, we do observe local increases in velocity that are coincident with narrowing of the flow band width and increases in surface slope (Figure 4.2). For example, at 12 km along Waltershausen Gletscher (Figure 4.2b), wintertime velocities are 55% greater than the along-transect average at a location where the flow unit is less than half the average width. Similarly, at 3 km along Wordie Gletscher (Figure 4.2a), wintertime velocities are 56% greater than the along-transect average at a location where the surface gradient (~86 m km^{-1}) is five times greater than glacier average. At Adolf Hoel Gletscher there are two regions of markedly different flow; the section above 16 km exhibits low surface slopes, spreads into the tributary of Waltershausen Gletscher (Figure 4.2c), and flows slowly (63 ± 42 m yr^{-1} during winter), whereas the section below 16 km which follows a sharp drop in elevation and is confined within a narrow valley flows at a much faster speed (261 ± 42 m yr^{-1} winter average).

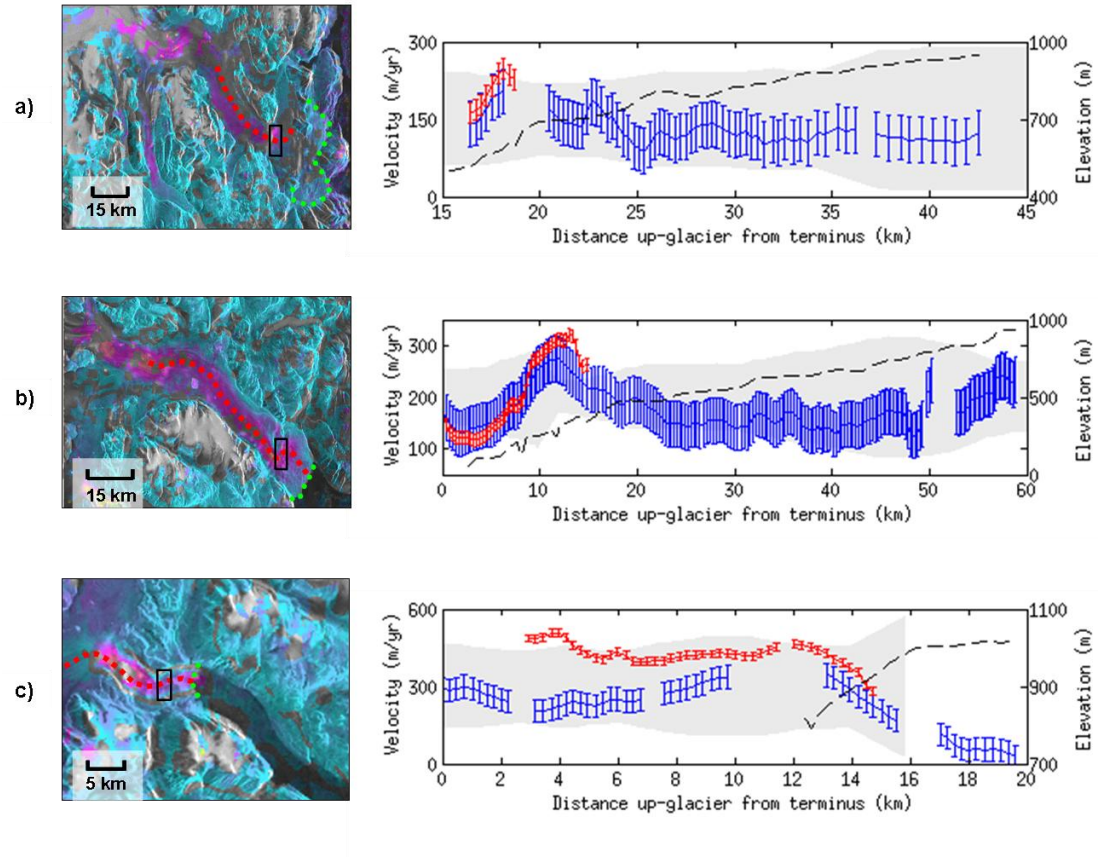

Figure 4.2: Velocity and geometry of the Wordie, Waltershausen, and Adolf Hoel glaciers between 1995 and 1996. A, B and C show the velocity distributions (left) and the along glacier profiles (right) from the termini (green dotted lines) of Wordie, Waltershausen and Adolf Hoel Gletschers, respectively. The profiles include average summer (May, June and July) and winter (December, January, February and March) along glacier velocities (red and blue lines respectively), surface topography (black dashed line) and relative changes in glacier width (grey boxes). The velocity profiles have been smoothed using a moving average filter over subsets of 2 points to reduce variance introduced from inconsistent coverage between image pairs at corresponding positions along the transect. The black boxes in the left hand images delineate the portion of the transects (red dotted lines) over which the velocity time series in Figure 4.3 were taken.

4.4.2 Time series observations

The temporal evolution of ice velocity at locations along the Wordie, Waltershausen, and Adolf Hoel Gletschers (Figure 4.2) where data are consistently available is shown in Figure 4.3. These data reveal seasonal patterns in flow at all 3 glaciers and, based on the broad patterns of change, we divide the time-series into 3 discrete periods. Periods 1 and 2 are identified as the times during which the glaciers are

accelerating and decelerating, respectively. Due to the relatively coarse temporal resolution and sampling of the velocity data, we are unable to identify the precise limits of these periods from the data themselves. Instead, we estimate the approximate timing of the transition between accelerating and decelerating flow by fitting a quadratic polynomial through the velocity data; the period of transition is defined by the switch from positive to negative slope gradients. Period 3 includes data from the winter of 1995/1996 when, on average, flow velocities are relatively low; it is separated from periods 1 and 2 by a gap in data coverage. There are large uncertainties associated with the velocity estimates during period 3 (related to inaccuracy in the global offset estimates, possibly arising from surface changes, e.g. snowfall events), and so we additionally compute the average flow speed of each glacier across this time interval. Descriptive statistics for each period are given in Table 4.1.

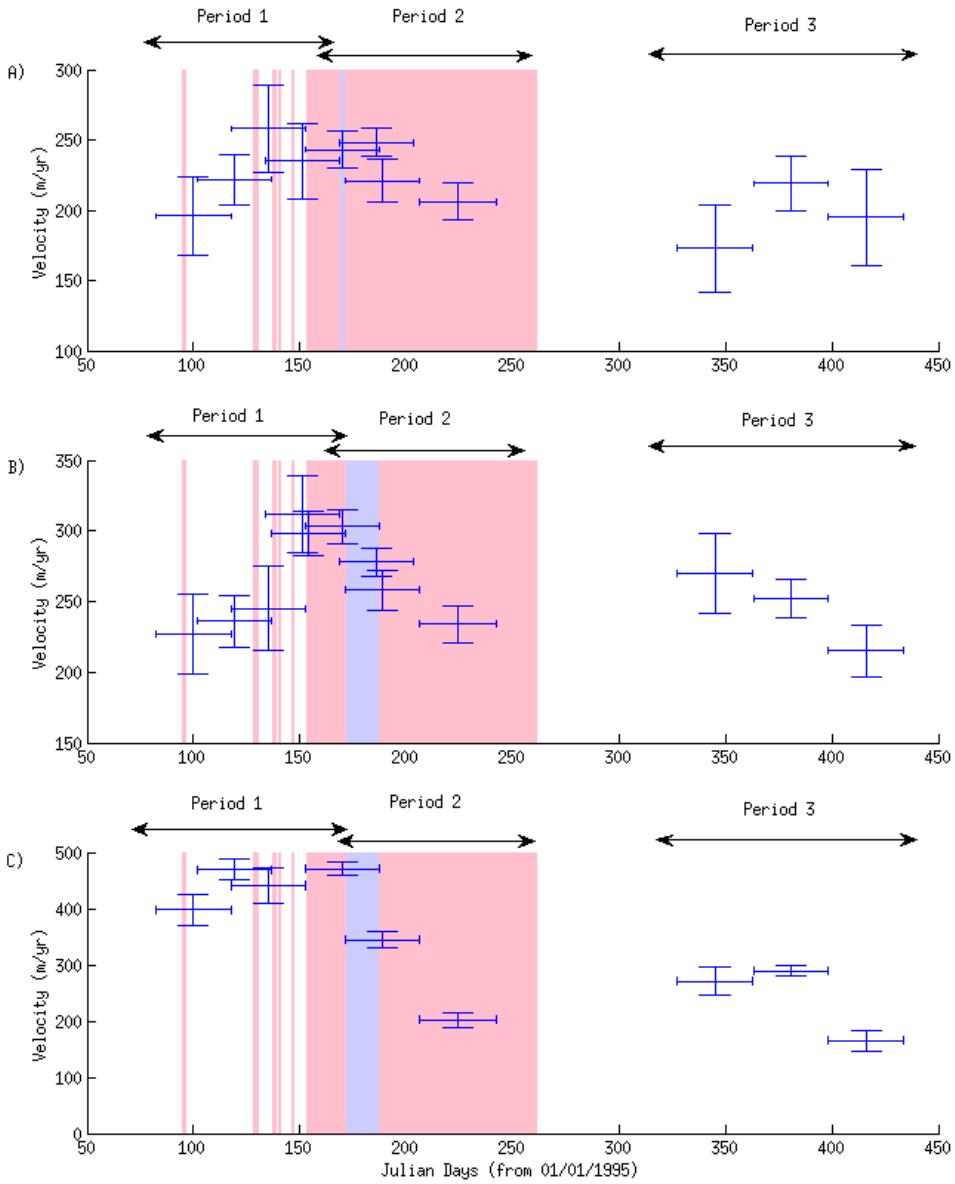

Figure 4.3: Time series of velocity at the Wordie (a), Waltershausen (b), and Adolf Hoel (c) Gletschers determined at the locations shown in Figure 4.2. Blue points show velocity measurements with horizontal bars representing the period across which they are calculated and vertical bars showing the estimated error. Averages of velocities during the winter of 1995/1996 are shown in red. Pink shaded areas represent the days where air temperatures exceeded 0ºC at Daneborg meteorological station; blue shaded areas indicate the approximate timing of the first lake drainage events on each glacier. The three periods of velocity described in the text are delimited with black horizontal arrows.

Table 4.1: Minimum (V_{min}), maximum (V_{max}) and mean (V_{mean}) velocities (m yr^{-1}) of the 3 periods shown in Figure 4.3 for the portions of Wordie, Waltershausen and Adolf Hoel Gletschers used in Figure 4.3.

	Period 1			Period 2			Period 3		
Glacier	V_{min}	V_{max}	V_{mean}	V_{min}	V_{max}	V_{mean}	V_{min}	V_{max}	V_{mean}
Wordie	196±28	258±31	228±26	206±13	248±10	230±13	173±31	219±19	195±28
Waltershausen	227±28	312±27	264±24	234±13	303±13	269±13	215±18	270±28	245±20
Adolf Hoel	398±28	471±13	445±22	202±13	344±15	273±14	165±19	289±10	241±18

During period 1 (approximately days 82 to 160, spring) velocities increase at all three glaciers; we calculate average velocity increases from the beginning of the period to peak velocities, of 26%, 34% and 16% at Wordie, Waltershausen and Adolf Hoel Gletschers respectively. According to the temperature data, peak velocities occurred early in the melt season (within 2-3 weeks of the onset of positive temperatures). We find no evidence of lake drainage events prior to the period of peak velocities; the first observed lake drainage events occurred between days 168 and 171 at Wordie Gletscher and between days 171 and 187 at Waltershausen and Adolf Hoel Gletschers (see Figure 4.7 in section 4.8). Lake drainage therefore began towards the end of period 1 when velocities were peaking. Sea ice began to clear at the terminus of Waltershausen Gletscher towards the end of period 1 (between days 171 and 187) (see section 4.8). At Adolf Hoel Gletscher, clearing of sea ice and trapped icebergs (between days 117 and 171) occurs during period 1. We also observed retreat of the ice front of Adolf Hoel Gletscher during period 1, beginning between days 135 and 170 (Figure 4.4) at a rate of 2.1 md^{-1}. In contrast, the terminus position of Waltershausen Gletscher did not exhibit substantial change.

During period 2 (approximately days 160 to 242, early summer) ice speeds progressively decrease at all three glaciers. At both Wordie and Waltershausen Gletschers, velocities slowed to values close to those at the beginning of period 1 by the end of the period 2 (between days 206 to 242). At Adolf Hoel Gletscher, the magnitude of deceleration far exceeded the acceleration observed in period 1. The final velocity estimate during period 2 (days 206-242) was half that of the slowest

velocity estimate from period 1; this explains the large differences in winter and summer velocities seen in Figure 4.2. Note that, due to a gap in the availability of SAR data immediately following this period, we are unable to assess to what extent the entire deceleration in flow is captured in our dataset. Throughout period 2, air temperatures remain positive and lakes on the surfaces of all three glaciers continue to drain. In addition, the fjords in front of Adolf Hoel and Waltershausen Gletscher clear of sea ice and the terminus of Adolf Hoel Gletscher retreats to a position several hundred metres behind average (Figure 4.4).

During period 3 (days 327 to 433, winter) ice speeds exhibit high variability and high measurement uncertainty; both of these aspects of the data limit our ability to analyse trends in flow during this interval. On average, the Wordie Gletscher velocity during period 3 (206 ± 44 m yr^{-1}) is close (within 5%) to that recorded at the beginning of period 1 and the end of period 2. At Waltershausen, the average velocity during period 3 (255 ± 44 m yr^{-1}) is ~10% greater than at the beginning of period 1 and the end of period 2. At Adolf Hoel Gletscher, the average velocity during period 3 is comparable to the velocity measurements from the end of period 2 but 42% lower than that estimated at the beginning of period 1. During period 3, air temperatures were negative and supraglacial lakes appeared to be frozen. In addition, the proglacial fjords of Adolf Hoel and Waltershausen Gletschers were completely covered in sea ice, and the terminus of Adolf Hoel Gletscher advanced at an average rate of 0.4 md^{-1}.

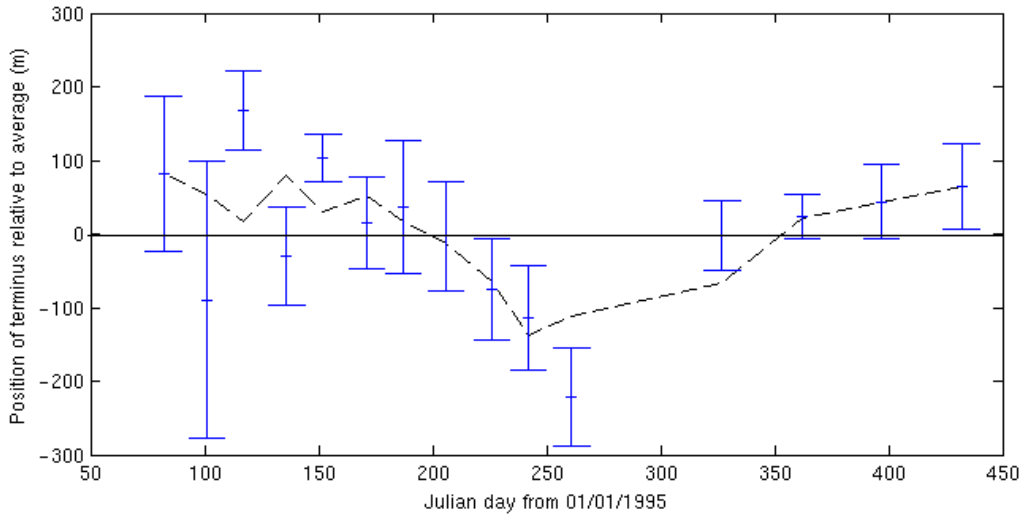

Figure 4.4: Time series of the mean difference in terminus positions of Adolf Hoel Gletscher relative to the average position. The blue points are the mean relative position measurements; vertical bars represent the standard deviation of position differences along the length of the terminus; the dashed black line is the moving average of these points.

4.5 Discussion

4.5.1 Spatial flow patterns

The differences in winter average velocities between the glaciers can be explained by differences in basal sliding rates as a result of differences in effective pressure at the glacier bed (Paterson, 1994). According to Budd *et al.* (1979), the effective pressure (P_{eff}) at the bed of a glacier can be defined as:

$$P_{eff} = p_i - p_w \qquad (4.1)$$

where p_i and p_w are the ice overburden and water pressures, respectively. In the case of tidewater glaciers, the pressures can be written in terms of the densities of ice (ρ_i) and sea water (ρ_w), gravity (g), the thickness of ice (h), the depth of the glacier bed below sea level (h_w), and the additional hydraulic head above sea level (Δp):

$$p_i = \rho_i g h$$
$$p_w = \rho_w g h_w + \Delta p \quad (4.2)$$

so that

$$P_{eff} = \rho_i g h - (\rho_w g h_w + \Delta p) \quad (4.3)$$

The subglacial effective pressure at the bed of a glacier will decrease if h decreases and/or, h_w and Δp increases, resulting in increased sliding velocities. The relatively fast flow observed at Adolf Hoel Gletscher can therefore be explained by its configuration as a marine-terminating glacier (i.e. h_w decreases P_{eff}) and the slower flow recorded at Waltershausen Gletscher may be explained by a number of factors, including it having a relatively shallow bed geometry which leads to lower values of h_w and/or it being a relatively large, thick glacier (i.e. with higher values of h). Although the higher flow rates of Adolf Hoel Gletscher could be explained by episodic surge-type behaviour typical of tidewater glaciers (Meier and Post, 1987), we discount this possibility for two reasons; first, the position of the ice front returned to the same position in March 1996 as it was at in March 1995 and, second, comparable speeds have been recorded in subsequent years (~450 m/yr in 2000/2001 and ~350 m/yr in 2005/2006, Joughin *et al*., 2010a).

The along flow changes in velocity observed at Adolf Hoel Gletscher may also be explained by fluctuations in effective pressure (Equation 4.3). The abrupt drop in glacier surface elevation at ~16 km along glacier may, for example, reflect a drop in the elevation of the glacier bed below sea-level that would lower the effective pressure and lead to increased rates of sliding. Bed topography data, which are currently unavailable for this glacier, are required to confirm this hypothesis. Local velocity increases at Waltershausen and Wordie Gletschers that are linked to increases in their surface slopes and narrowing of their flow widths may be explained by local variations in stress regimes. Increased ice surface slopes result in higher driving stresses and flow band narrowing causes transverse compression which is compensated for by longitudinal extension (Paterson, 1994).

4.5.2 Seasonal flow patterns

The seasonal evolution of velocities recorded at all three glaciers is similar to that observed at other land- and marine-terminating glaciers in Greenland and other Arctic and Alpine regions where it has been linked to a hydrological forcing mechanism (e.g. Iken and Bindschadler, 1986; Mair *et al.,* 2002; Zwally *et al.,* 2002; Bingham *et al.,* 2004; Howat *et al.,* 2010). The summertime speedup of the glaciers in our study, which are correlated with the onset of positive surface temperatures and surface melting, suggests that surface meltwater may be routed to these glacier beds too, raising subglacial water pressure and increasing basal sliding. Peak velocities, and the subsequent slowdown in flow, occur part-way through the melting season, and coincide with the first supraglacial lake drainage events. It is possible that water released during lake drainage events may have triggered a switch in the efficiency of subglacial water drainage (Schoof, 2010) which is understood to lead to reduced rates of ice sliding and flow.

We consider the possible influence of frontal forcing on early summer acceleration at marine-terminating Waltershausen and Adolf Hoel Gletschers. We report some correlation between the timing of early summer accelerations and sea ice clearing at both glaciers and ice front retreat at Adolf Hoel Gletscher. It has previously been proposed that seasonal acceleration may occur at tidewater glaciers due to changes in backstresses exerted on the front of the glacier (e.g. Joughin *et al.,* 2008a; Howat *et al.,* 2010). However, such a mechanism has only been linked to seasonal velocity fluctuations at marine-terminating glaciers which are undergoing multi-year retreat (e.g. Joughin *et al.,* 2008a; Howat *et al.,* 2010). Furthermore, the seasonal velocity patterns of such glaciers have been found to correlate with the changing position of the calving front (i.e. the frontal retreat persists throughout the melt season and so too do the acceleration velocities) (e.g. Joughin *et al.,* 2008a; Howat *et al.,* 2010). At Waltershausen and Adolf Hoel Gletschers we have found the positions of the fronts to be stable on an interannual basis, and where we observe a seasonal fluctuation in the position of the front of Adolf Hoel Gletscher, we find that the retreat does not correlate with increasing ice flow throughout the whole season (i.e. ice velocity

decelerates in the summer whilst the front continues to retreat). This suggests that the impacts of frontal forcing on seasonal variations in the flow of Waltershausen and Adolf Hoel Gletschers may be small in comparison to the impact of changes in their inland hydrology. Instead of forcing velocity changes at these glaciers, the correlation in timing between the break-up of sea ice and ice front retreat with accelerated flow, may indicate that they are responding to the same forcing or, in the case of ice front retreat, it is occurring as a consequence of increased ice velocity.

Consideration of the influence of the force balance on ice flow at the 3 glaciers is also suggestive of a lack of influence on seasonal flow variability from longitudinal stress changes and therefore lends support to the implied importance of seasonal meltwater forcing on seasonal flow variability. At Wordie Gletscher, the ~50 ma^{-1} summer speed up observed at 550 m elevation (Figure 4.2a) occurs over a presumed ice fall where the influence of lower glacier longitudinal stresses will be negligible. At Waltershausen Gletscher a ~50 ma^{-1} summer speed up at 300 m elevation (Figure 4.2b) occurs where the ice passes through a constriction and lateral drag is likely to dominate flow conditions over longitudinal stresses. Furthermore at Waltershausen Gletscher, the absence of seasonal flow variability near the front of the glacier may be explained by the directing of flow into the valley side which results in a greater importance of lateral drag than basal drag on the glacier flow and a limited impact of seasonal variability in basal lubrication on flow. At Adolf Hoel Gletscher, summertime speed ups are observed at up to at least 900m elevation and 12 km upglacier of the calving front and the lower glacier is steeply sloping (~4º) elevation (Figure 4.2c). Thus local basal drag is likely to dominate resistance to flow with little sensitivity to longitudinal stress from the front.

We compare the magnitude of seasonal variations in ice flow observed in our study to those observed at other land- and marine-terminating glaciers. The magnitude of accelerations calculated at Wordie and Waltershausen Gletschers (26 and 34% respectively) are low, although comparable, to average summer speed ups recorded at land-terminating glaciers in the west of Greenland which typically lie between 50 and 125% (Joughin *et al.,* 2008c; Bartholomew *et al.,*2010; Sundal *et al.,* 2011).

Palmer *et al.,* (2011) observe large spatial variations in the magnitude of summer speed ups for a region in the West of Greenland with values ranging between 0 and 360%; thus the relatively low values observed at Wordie and Waltershausen may be attributable to the limited spatial extent over which we were able to obtain velocity measurements. The magnitude of summertime speedup at Adolf Hoel Gletscher (16%) is comparable to findings at other marine-terminating glaciers (i.e. <50% - Vieli *et al.,* 2004; Joughin *et al.,* 2008c; Howat *et al.,* 2010). Furthermore, the lower magnitude of summer speed up on Adolf Hoel Gletscher relative to Wordie Gletscher is consistent with observations elsewhere in Greenland that report greater proportional summer speed ups at land- than marine-terminating margins (Joughin *et al.,* 2008c). Joughin *et al.,* (2008c) suggest that there may be a number of reasons for this, including differences in bed smoothness, basal shear heating and lateral or basal drag between land- and marine-terminating outlets.

Of further interest is the large deceleration (57%) observed at Adolf Hoel Gletscher during period 2 (summer) relative to the magnitude of acceleration observed during period 1 (spring) at the start of the melt season, and the large difference in winter velocities recorded between the two years of our survey (Figure 4.3). Although such changes could be attributed to interannual variations in the degree of surface melting, just 1 positive degree day (PDD) of melting was recorded during the first measurement period, and so the early speedup in March 1995 is unlikely to be associated with this effect. There is also no evidence of fluctuations in the extent of sea ice or the position of the glacier front during either period 1 or 2, and we have already discounted the possibility of surging (section 4.5.1). We do notice, however, that the magnitude of seasonal flow variability increases towards the glacier terminus (Figure 4.2) and that these increases are dominated by differences between period 2 and 3 (no trend is identified when looking at differences between March and summer 1995 velocities). This may suggest a frontal forcing mechanism. Given the interannual stability observed in the terminus position, a possible alternative cause may be differences in the volume/thickness of sea ice (not detectable in the SAR images) and therefore the degree of back stress acting on the terminus (e.g. Sohn *et al.,* 1998; Amundson *et al.,* 2010). Further data is required to validate this statement.

4.6 Conclusions

We have quantified seasonal flow variations at three glaciers situated in a region of Northeast Greenland which has received little previous glaciological investigation. The glaciers have a mixture of terminus conditions; one (Wordie Gletscher) is land-terminating, and two (Waltershausen and Adolf Hoel Gletschers) are marine-terminating. According to our velocity data, there is little evidence to suggest that marine conditions exert a strong influence on Waltershausen Gletscher. We identify evolution of seasonal ice flow similar to that observed in other regions of the GrIS (e.g. Zwally *et al*., 2002; van de Wal *et al.,* 2008; Bartholomew *et al.,* 2010; Howat *et al*., 2010; Sundal *et al*., 2011) and Arctic and Alpine regions (e.g. Iken and Bindschadler, 1986; Mair *et al*., 2002; Bingham *et al*., 2003). Much of the seasonal evolution of flow at both the land- and marine-terminating glaciers appears to be correlated with seasonal changes in surface hydrology. In contrast to the sensitive relationship between acceleration and frontal retreat or ice melange conditions of rapidly retreating tidewater glaciers elsewhere, fluctuations in terminus conditions appear to have little impact on flow variability. We also observe a large unexplained difference in winter velocities recorded on different years (by almost a factor of 2) at Adolf Hoel Gletscher which could be driven by winter sea ice conditions.

Our findings indicate that the surface melt driven processes which have been inferred to govern seasonal flow variations at land- and stable marine-terminating glaciers in the west and southeast of Greenland (e.g. Zwally *et al.,* 2002; Shepherd *et al.,* 2009; Bartholomew *et al.,* 2010; Howat *et al.,* 2010; Anderson *et al.,* 2010) and other glaciated areas may also be inferred in the northeast of Greenland. However, we see that flow is modulated by local factors that affect the force balance, such as the role of lateral drag and perhaps resistance from winter sea ice. Furthermore, our findings highlight the complexity of ice flow at marine-terminating glaciers. The interannual and inter-glacier variability in flow that exists emphasises the need for multi-annual observations of glacier flow and surface melt at fine spatial and temporal resolutions, and ice dynamical models that account for the temporal variability in meltwater supply to the glacier bed.

4.7 Limitations

The results presented in this chapter were subject to the following limitations:

- A limited spatial coverage of the SAR intensity tracking velocity estimates. In particular the coverage of velocity estimates during the summer on Waltershausen and Wordie Gletschers was restricted (Figure 4.5). This may have occurred as a result of excessive surface changes (e.g. surface melting) between image acquisitions which meant the features on the surface could no longer be matched reliably. The limited summer coverage prevented the estimation of average annual velocities at the glaciers (a common velocity statistic which would have allowed comparison to other Greenland outlet glaciers) and an investigation of spatial and temporal differences of along transect seasonal flow variability (cf. Sundal *et al.*, 2011).

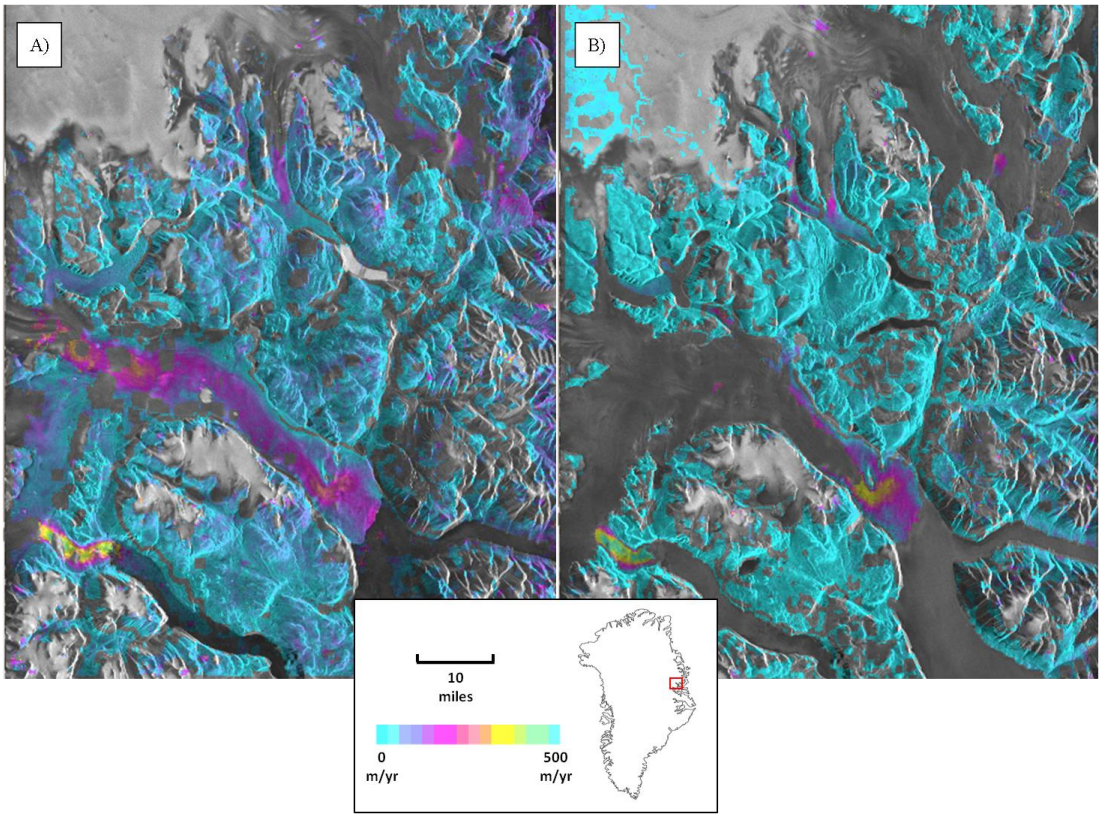

Figure 4.5: SAR intensity tracking results from the Zakenberg region of the northeast Greenland Ice Sheet from a) January 1996 and b) June 1995. The regions in grey represent areas where velocity estimates were not obtained; note the difference in coverage of velocity results on the outlet glaciers between a) and b).

- The low temporal resolution of SAR intensity tracking velocity estimates. The velocity estimates which were derived were averaged over 35 days (i.e. the repeat pass time of the ERS satellites). The loss of detail in the timing of velocity changes limits confidence in the links that can be made between the velocity records and the potential forcing mechanisms as in inferred from other data such as air temperatures and supraglacial lake drainage (c.f. Bartholomew *et al.,* 2010).

- The lack of available ERS- 1 and -2 data for September, October and November 1995 meant that velocity estimates for these months could not be calculated. This prevented us from gaining a full annual dataset of velocities for these glaciers.

- The method used to estimate the errors of the intensity tracking results relied on the assumption that the errors associated with velocity estimates over land surfaces would be the same as ice. The errors associated with intensity tracking velocity estimates have been found to be strongly correlated with errors in the global offset estimation (Figure 4.5 & de Lange *et al.,* 2007) which is constant over ice and land surfaces. Furthermore, Pritchard *et al.,* (2005) compared velocity estimates from intensity tracking and InSAR over slow flowing ice and derived an error estimate of the intensity tracking results similar to that calculated by measuring velocity on static regions, suggesting that this is a suitable method for calculating error. Nonetheless it is recognised that there may be some differences in the errors of velocity measurements derived on ice in comparison to those on land due to differences in the nature of the features being tracked.

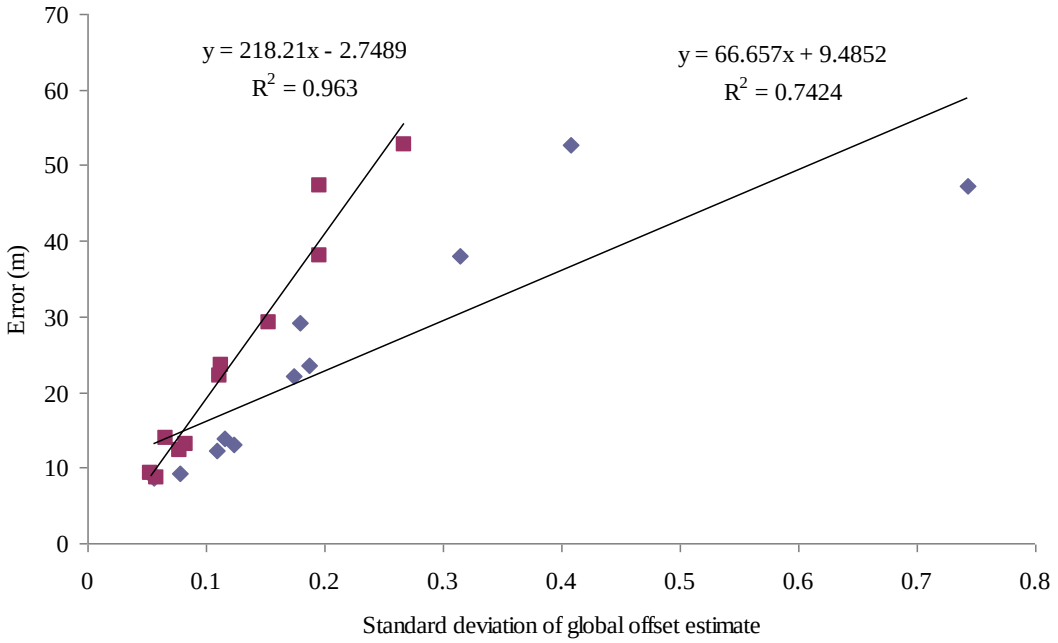

Figure 4.6: Regression of the error estimates associated with local offset and global offset estimations in range (red) and azimuth (blue) of pairs used in intensity tracking velocity estimates.

- Since no other velocity data exists for these glaciers at this time it is not possible to provide any validation of our velocity measurements.

- The meteorological station at Daneborg, where the temperature data was recorded, is situated by a fjord 75 km from the ice sheet margin and up to 200 km from the glaciers measured in this work. It is clear that there may be significant differences in meteorological conditions between these locations due to regional differences in weather patterns and lapse rates which exist between the coast and the ice sheet (e.g. Holzapfel *et al.*, 1939; Cappelen *et al.*, 2001). Furthermore, surface temperature lapse rates will apply on the ice sheet surface relating to both distance inland and elevation (e.g. Steffen and Box, 2001; Hanna *et al.*, 2005) which will affect the timing of the seasonal onset of positive temperatures and surface melting.

4.8 Appendix

This appendix contains additional data referred to in this chapter and in support of the results presented therein.

Supra-glacial lake evolution

We observe seasonal evolution of the supra-glacial lakes on Wordie, Waltershausen and Adolf Hoel Gletschers in the SAR MLI amplitude images (Figure 4.7). We find that water was present in small supra-glacial lakes (< 1 km^2) at altitudes up to 1000 m asl at Waltershausen Gletscher by day 152 and by day 168 small lakes (<1 km^2) were visible at low elevations (<600 m a.s.l.) on Wordie Gletscher. On day 171 the low elevation lakes at Wordie Gletscher had drained and lakes at higher elevations on all 3 glaciers had begun to fill (Figure 4.7). By day 187, several substantial lakes (1-2 km^2) on Waltershausen Gletscher and at the top of Adolf Hoel Gletscher had drained. By day 206, a large proportion of the lakes on the ice surface of all three glaciers had drained.

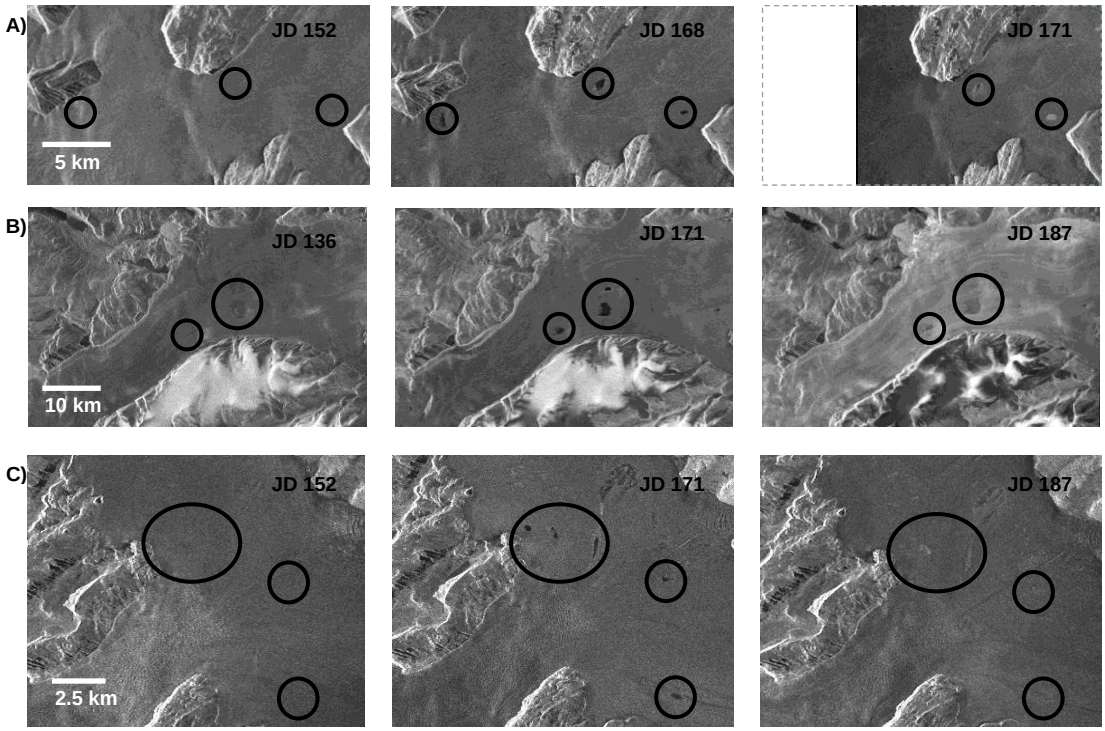

Figure 4.7: SAR MLI amplitude images depicting the seasonal evolution of supra-glacial lakes (black circles) on the surface of Waltershausen Gletscher, Wordie and Adolf Hoel.

Proglacial sea ice conditions.

The break-up of the sea ice mélange in front of Adolf Hoel Gletscher is shown in Figure 4.8. The image from day 117 and the preceding images show that the extent and position of visible icebergs are consistent. The image from day 171 shows that the extent of the mélange is far greater and the position of the visible icebergs is changed indicating a break-up of the mélange. However, due to unfavourable contrast of this region in the MLI images between days 117 and 171, (Figure 4.8) we are unable to determine with greater accuracy the timing of the break-up. MLI imagery of the terminus of Waltershausen Gletscher shows that, unlike Adolf Hoel Gletscher, an ice mélange is absent from the terminus in winter and that open water develops between days 171 and 187.

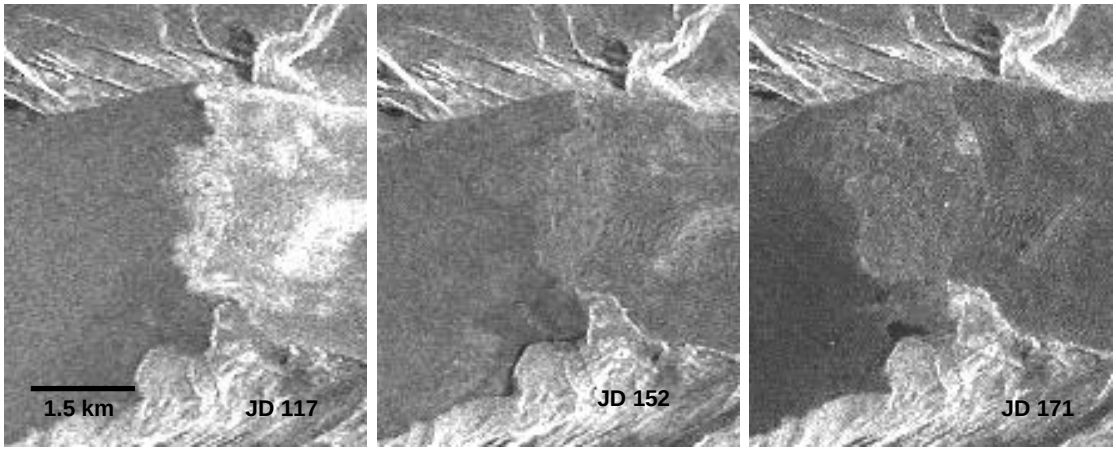

Figure 4.8: SAR MLI amplitude images of the front of Adolf Hoel Gletscher showing the break up of the sea ice mélange.

Chapter 5: Coincidence of supraglacial lakes and topographic depressions in Northeast Greenland

In the previous chapter (and in the work of several other authors e.g. Zwally *et al.*, 2002; Das *et al.*, 2008; Bartholomew *et al.*, 2010), the seasonal filling and draining of supraglacial lakes is identified as an important factor in the seasonal regulation of glacier ice flow. For this reason, one of the key conclusions of Chapter 4 was that the temporal variability of meltwater supply to the glacier bed must be able to be included in ice sheet models. Doing so relies on accurate parameterisation of supraglacial lakes. This chapter describes an assessment of using a high resolution InSAR DEM to identify the locations of supraglacial lakes for the same region of the northeast GrIS as in Chapter 4. This chapter is in preparation for submission to Remote Sensing of the Environment:

Briggs, K., Shepherd, A. and Nienow, P. (in prep.). Coincidence of supraglacial lakes and topographic depressions in Northeast Greenland. *Ready for Submission to Remote Sensing of Environment*

The majority of the work for this chapter was carried out by myself. A Shepherd and P Nienow developed the original ideas for this chapter and provided comments on the manuscript. E Rinne extracted and helped with processing of the ICESat data.

Limitations of the work presented in Chapter 5 are discussed in Section 5.7 and additional information for this chapter is included in Section 5.8.

5.1 Abstract

Supraglacial lakes, which form annually on the surface of the GrIS, are identified as a factor in the interaction between ice sheets and climate (e.g. Joughin *et al.,* 1996a; Boon and Sharp, 2003), and their drainage has been linked to fluctuations in glacier discharge (Das *et al.,* 2008). Here we investigate the extent to which the locations and area of supraglacial lakes may be identified using digital elevation models (DEMs) of the ice sheet surface. We generate a 150 m ground-resolution DEM of a 10,500 km^2 coastal region of the northeast GrIS using differential interferometric synthetic aperture radar (InSAR) observations. We identify the number, location and area of topographic depressions (sinks) in this DEM, and draw comparisons with the distribution of supraglacial lakes we observe in 30 m ground-resolution Landsat imagery. The agreement between sinks and lakes is improved by limiting the maximum altitudinal extent of the comparison and the minimum size of features included in the analysis. In this dataset we identify 428 individual sinks and 199 lakes that are greater than 0.0125 km^2 and which cover total areas of 81.4 km^2 and 29.7 km^2 respectively. We find that 13% of the total area of sinks coincide with lakes, and that 36% of the total area of lakes coincide with sinks, showing that the DEM identifies lake locations more reliably than it is able to predict them. We interpret the differences in the distribution of sinks and lakes to reflect both limitations in the spatial and temporal sampling of the satellite data used in the analysis, and the physical differences between lakes and sinks. We conclude that, in Northeast Greenland, the accuracy of using sinks as a proxy for lake location and area is generally poor.

5.2 Introduction

At the Western margin of the Greenland Ice Sheet, rapid drainage events of supraglacial lakes are coincident with accelerations in glacier flow (Das *et al.*, 2008). These lakes form in depressions on the ice sheet surface and fill during the melt season (Sundal *et al.*, 2009). It is thought that when lakes reach a certain depth, the pressure exerted by the water on the ice below is capable of fracturing the ice (hydrofracture) (van der Veen, 1998) and, if there is a sufficient volume of water available, the fracture can propagate to the ice sheet base (Das *et al.*, 2008). The coincidence of lake drainage events with increases in ice motion is indicative of the transit of water to the ice sheet base, where it can enhance basal sliding – a process that could lead to ice flow acceleration and increased ice discharge (e.g. Zwally *et al.*, 2002; Alley *et al.*, 2005b; Das *et al.*, 2008; Bartholomew *et al.*, 2010). At present it is estimated that the contribution to annual ice sheet mass loss due to seasonal fluctuations in ice flow is small (Joughin *et al.*, 2008c). However, it is possible that expected increases in surface temperatures in Greenland over the coming century (Meehl *et al.*, 2007) may lead to an expansion of the area of seasonal surface melting and lake formation, and so the impacts of lake drainage events on long-term trends in ice sheet flow may increase.

Lake locations, surface areas, volumes and seasonal evolution have been observed in optical imagery (e.g. Box and Ski, 2007; McMillan *et al.*, 2007; Sneed and Hamilton, 2007; Georgiou *et al.*, 2009; Sundal *et al.*, 2009). Here we assess an alternative method to obtain lake locations and areas through the analysis of a digital elevation model (DEM) of the ice sheet surface. Because water flowing on the ice sheet surface will pond in topographic depressions, DEMs may provide a means of predicting the locations of lakes. Furthermore, this method may provide a means of identifying sites at which lakes may form at higher (colder) elevations in the future which is valuable for modelling forecasted warmer ice sheet scenarios. Luthje *et al.*, (2006) modelled the seasonal evolution of lakes in a 400 km^2 region at the western margin of the ice sheet using a DEM. Lake sites were predicted using a drainage model and local estimates of ablation. The positions of the modelled lakes compared

favourably with those observed in optical imagery although the area covered by model lakes was 3 to 4 times larger than that of the observed lakes. In this study, we investigate the use of DEMs to identify and predict locations of supraglacial lakes in the northeast of the GrIS and, we assess the utility of DEMs to predict where lakes may form in future. We generate a new, high resolution InSAR DEM and use it to identify topographic depressions (water sinks) where lakes could form on the ice surface. We use optical images to map the supraglacial lakes in the same region. We then compare the coincidence of the sinks identified in the DEM to the lakes identified in the optical imagery. Finally, we use our data to consider the potential reasons for the observed similarities and differences in the locations of lakes and sinks.

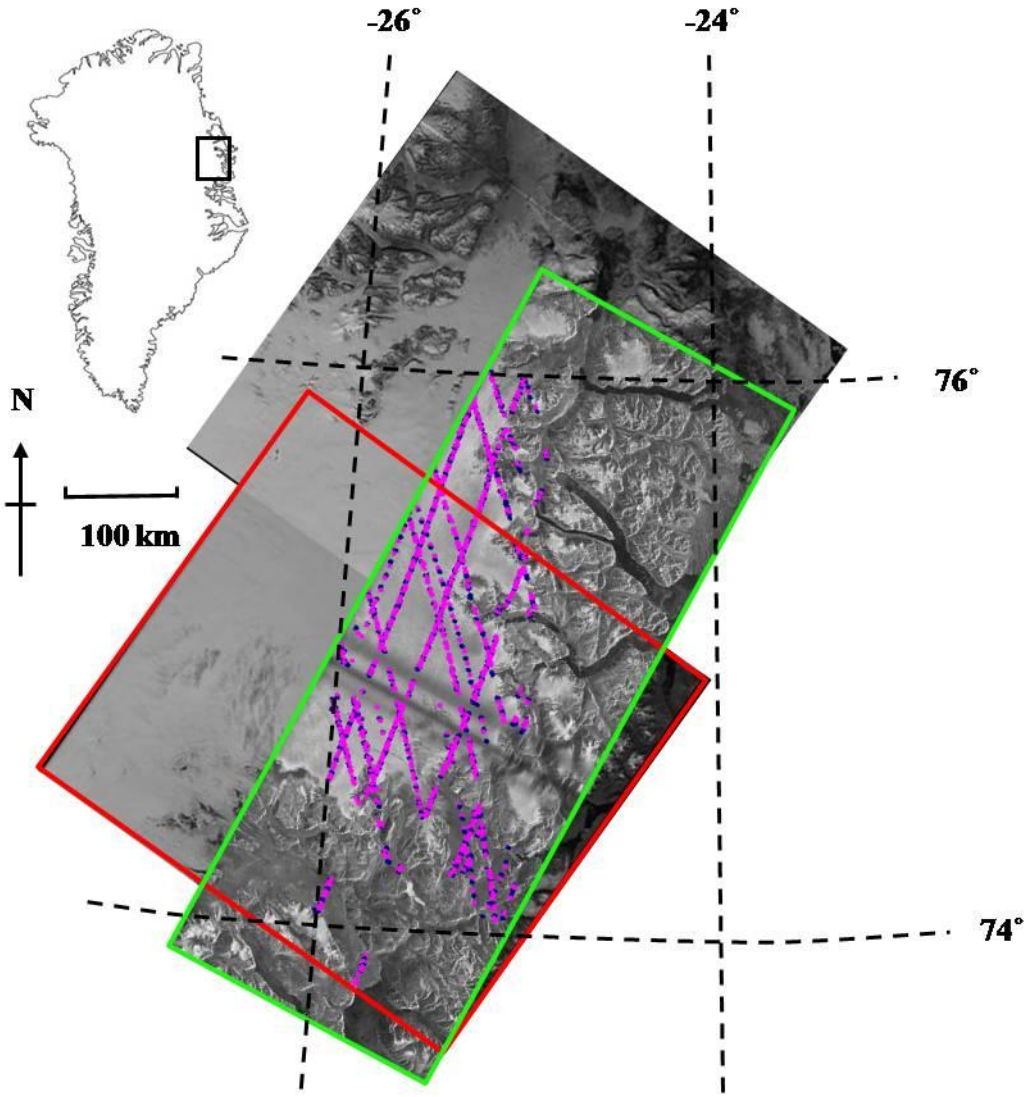

Figure 5.1: Study area in Northeast Greenland. Greyscale images of two Landsat ETM+ scenes of the region are overlain by the SAR data from which a DEM is formed (green box). The red box highlights the Landsat scene used. The area of overlap was used in the analysis. Location of the ICESat GLAS track data used to constrain the precision baseline of the InSAR DEM and to assess the accuracy of the InSAR DEM are shown with blue and pink dots respectively.

5.3 Methods

5.3.1 InSAR DEM

We used European Remote Sensing (ERS) satellite SAR data to form an InSAR DEM, and ICESat (Ice, Cloud and land Elevation Satellite) GLAS (Geoscience Laser Altimeter System) elevation data to constrain the interferometric baseline. Two descending pass ERS-1 and ERS-2 SAR tandem phase image pairs from the winter

of 1995 (Table 5.1) were used to generate a DEM. The images span 3 consecutive frames (Figure 5.1) and cover an approximate ice sheet area of 10,500 km^2 centred at 74˚N 24˚W in the northeast of Greenland (Figure 5.1). The perpendicular baselines of the image pairs were 149.7 m and -67.7 m. We used SAR image pairs acquired during the winter to minimise errors in the DEM due to changes in flow rates between image pairs (see below) and to maximise the possibility of surveying the elevation of lake beds (in the summer, the microwaves, which are not able to penetrate the liquid water, are reflected from the surface of the water-filled lakes).

Table 5.1: ERS-1/-2 descending pass data used in this study.

Track	Orbit (ERS-1/-2)	Frames	Acquisition dates	Perpendicular Baseline
253	22786/3113	2061, 2079, 2097	23/24 Nov 1995	149.7 m
	23287/3614		28/29 Dec 1995	-67.7 m

A random subset of the available ICESat GLAS track data was used to constrain and validate the InSAR DEM. The ICESat mission provides surface elevation data from 65 m diameter ground-footprints every 172 m along the satellite ground track with high vertical precision (~2.1 cm) (Shuman *et al.,* 2006) and the absolute accuracy of the measurements in Greenland are estimated to fall in the range of 16-20 cm for surfaces with slopes of 0.6˚ increasing to 50 cm for surfaces with slopes of 1.15˚ (Brenner *et al.*, 2007). In this study we used ICESat GLAS product number GLA-06 from release 28 (Zwally *et al.,* 2003) and we applied corrections for the geoid and to compensate for saturated signal returns. The ICESat data were acquired in 2003, 2006 and 2007.

We formed the InSAR DEM using differential interferometry (e.g. Zebker and Goldstein, 1986; Kwok and Fahnestock, 1996; Joughin *et al.*, 1996b; Wegmuller *et al.,* 1998). Forming the DEM involved processing the raw SAR data to single-look complex (SLC) images, co-registering the SAR image pairs, generation of interferograms, co-registration of interferograms, generation of differential interferograms, filtering to reduce phase-noise, phase unwrapping, baseline

refinement, and calculation of topographic heights from the differential interferometric phase. Processing the raw data to SLC involved accounting for missing lines, concatenating the consecutive frames, improvement of the orbital state vectors, deriving the range and azimuth spectrums, azimuth auto-focusing, range and azimuth compression, radiometric calibration and multi-looking. The image pairs were co-registered to sub-pixel accuracy using a cross-correlation optimization of the SLC detected images. Single-difference interferograms were computed with multi-look factors in range and azimuth of 2 and 10 respectively, resulting in approximate ground-range and azimuth resolutions of 40 m. Co-registration of the two repeat-pass interferograms was performed to sub-pixel accuracy and, assuming a constant rate of ice flow during the period of the SAR data, the interferograms were differenced to cancel the phase signal due to motion (Kwok and Fahnestock, 1996). The perpendicular baseline of the resulting differential interferogram was 231 m, and provides sensitivity to topography that is well suited to generating a DEM (Massom and Lubin, 2006). We accounted for the Earth's curvature in the interferogram and applied an adaptive filter based on the local fringe pattern (Goldstein and Werner, 1998) with an exponent for non-linear filtering of 0.5.

The topographic phase signal was unwrapped using a branch-cut region growing algorithm (Goldstein *et al.,* 1988; Rosen *et al.,* 1994) and with the manual identification of correlation thresholds of coherence, inspection for unwrapping errors, drawing and deletion of branches and construction of bridges, so as to limit the propagation of errors. We tested a range of correlation thresholds (0.1 to 0.9) to establish the best cutoff to employ when masking areas of low-coherence in unwrapping. The unwrapped topographic phase was then compared to 500-1000 ICESat GLAS elevation measurements (depending on the size of the area masked due to low-coherence) distributed across the region of the SAR data to ensure that phase unwrapping errors did not occur. Branches were manually drawn to prevent the phase unwrapping algorithm entering regions of steeply sloping terrain and 3 branches were deleted to enable unwrapping of 3 glaciers. We also introduced bridges to connect a number of isolated regions, between which the coherence of the phase signal was low. The accuracies of the bridges and branch deletions were tested

by comparing the degree of fit between the unwrapped phase and ICESat GLAS heights before and after they were implemented; if the fit was significantly degraded or outliers were introduced, the deletion/bridge was rejected.

ICESat data were used to refine the interferometric baseline as baseline estimates from orbital data alone are not sufficiently accurate for DEM generation (Zebker et al., 1994). The refined baseline estimate was obtained using a least-squares fit to 1017 ICESat GLAS points (converted to SAR coordinates) that were distributed over the whole of the unwrapped region of ice (Figure 5.1). The unwrapped phase was converted to meters above sea level (a.s.l.) elevation measurements using this refined baseline estimate and the ICESat GLAS points. The DEM was then smoothed using a boxcar average filter with 3x3 smoothing windows in order to reduce high frequency SAR signal noise in the DEM (Joughin et al., 1995). We projected the DEM using the UTM coordinate system and a 50 m posting.

We assessed the accuracy of the InSAR DEM using a further 1035 ICESat GLAS points that were independent of those used to refine the interferometric baselines (Figure 5.1). A linear regression of the InSAR DEM and ICESat heights reveals strong agreement, with an average root mean square (RMS) elevation difference of 7.9 m. The difference between ICESat and InSAR elevation measurements is attributed to a combination of surface elevation changes in the period between SAR and ICESat data acquisition, differences in laser and radar surface penetration depths and independent errors associated with the InSAR and ICESat data.

The vertical precision of the DEM was estimated statistically based on image coherence values and the altitude of ambiguity, and through a comparison with ICESat data. Statistically, the vertical precision of the DEM is estimated to be approximately 0.6 m based on the altitude of ambiguity (43 m) and the high interferogram coherence (mean image coherence of 0.95). A comparison of 160 ICESat and InSAR DEM elevation estimates taken along a 172 km long ICESat track, reveals that the precision of the InSAR DEM (taken as the standard deviation of the residuals) over length scales applicable to sink identification (~5km) is 2.6 m.

5.3.2 Sinks in the InSAR DEM

We used the InSAR DEM to identify the presence of topographic depressions (sinks) based on the assumption that water will pond and fill hollows on the ice sheet surface (Figure 5.2 d and e). We used the hydro-toolset in ArcMAP to identify regions where water would pond on the ice sheet surface under this assumption. Sink areas for the water were defined by identifying either pixels that were lower than all of the surrounding pixels or groups of pixels which all slope inwards to each other. All sinks were then 'filled' to the minimum point at which they would start to drain over the ice surface and this provided a map of the maximum supraglacial lake extent predicted by the DEM in the region.

5.3.3 Supraglacial lakes in optical imagery

To generate a map of the spatial distribution and area coverage of lakes in the region we used 30 m ground-resolution Landsat images provided by the USGS. Four Landsat scenes were processed; two Landsat7 ETM+ scenes from 28/06/2000 and 04/07/2002 and two Landsat5 TM scenes from 07/07/2006 and 08/08/2006. These images were selected as they contained low levels (<2%) of cloud cover and because the images were acquired at different stages of the annual melt season (and thus of lake evolution (Sundal *et al.,* 2009)). Although these images do not coincide with the dates of the DEM, this is not a problem as sinks are persistent features through time (e.g. Echelmeyer *et al.,* 1991).

The Landsat images were enhanced and classified in order to identify supraglacial lakes (Figure 5.2b). Each image was enhanced using a principal components (PC) analysis of data acquired in spectral bands 1, 2, 3, 4, 5 and 7 (band 6 and the panchromatic band were excluded due to differences in resolution- see Lillesand and Kiefer, 1999). The first 3 PC bands contained 99.8% of the image variability from the 6 spectral bands input and were used in the image classification. A mask of the ice area to be analysed was formed to exclude the surrounding land and all water

features extraneous to the ice. The images were classified using the supervised, maximum likelihood technique (Richards, 1999). The training areas used in the classification were user defined and subjected to a separability analysis (Richards, 1999) prior to classification to ensure that the spectral signatures of the classes do not overlap. In the absence of ground-based observations for testing the classification, we took independent, user-defined training classes of each surface type from the Landsat images and constructed confusion matrices (Jensen, 1986) with the classified images, which allowed us to assess the accuracy of the classifications. The water classes were extracted from each scene and combined to create a map of lake locations.

5.3.4 Sink and lake area comparisons

To compare the spatial distributions of the sinks and lakes identified in the above steps (Figure 5.2c) we first manually co-registered the Landsat images to the InSAR DEM using prominent rock outcrop features and isolated the regions covered by both the Landsat images and InSAR DEM (this covers a region of ice 5000 km^2). As a further refinement, we restricted the comparison to locations below an upper altitudinal limit on the basis that the area of the ice sheet surface where lakes form extends only to the limit of summer melting (Sundal *et al,* 2009). We approximate this altitude to be the lower limit of the dry snow zone at the end of the melt season, which we calculate to be at approximately 1500 m a.s.l. in this region using the Landsat image acquired on 08/08/2006. We also excluded the large number of lakes and sinks smaller than 0.0125 km^2, as their locations are sensitive to mis-registrations between the lake and sink datasets, differences in Landsat and DEM resolutions and temporal changes in the ice surface between the Landsat and SAR image acquisitions. To assess the effect of DEM resolution on the degree of agreement between modelled sinks and observed lakes, we applied a boxcar average filter to the original DEM with smoothing windows of 5x5, 9x9 and 19x19 to generate 3 InSAR DEMs with ground-resolutions of 250, 450 and 950 m, respectively.

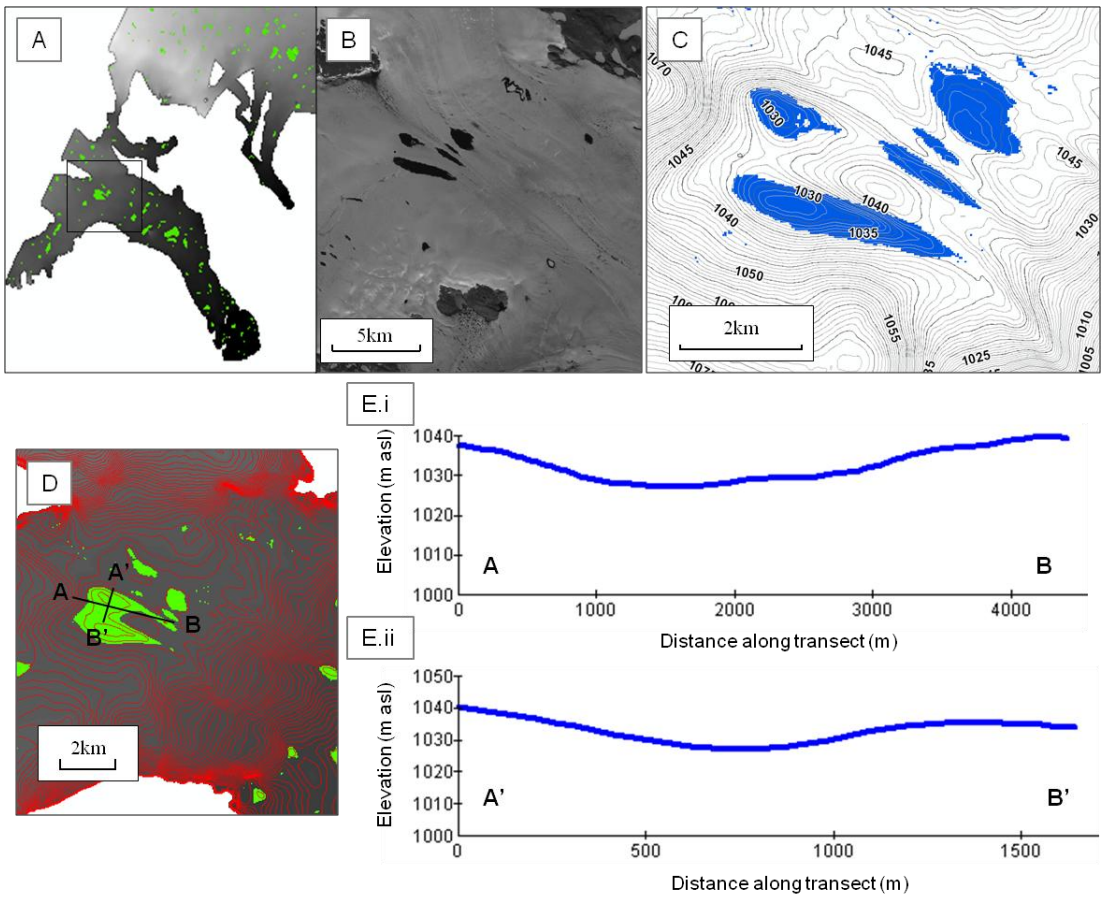

Figure 5.2: A) Shaded relief image of the InSAR DEM, showing sinks in green and the location on Waltershausen Gletscher (black box) of examples of surface lakes observed in Landsat images (b), the coincidence of observed lakes (blue) with surface depressions identified in the DEM (c) and the identification (d) and cross sections (e) of sinks in the DEM.

5.4 Results

Our study provides detailed information about the area and distribution of sinks and lakes within the survey region. Using the DEM, we identified 428 individual sinks with a combined area of 81.4 km^2, equivalent to 1.7% of the reduced study area. The largest sink in the DEM occupies an area of 6.9 km^2, and the average area of sinks we identified was 0.19 km$^{2.}$ On closer inspection, it is evident that the overall size distribution of sinks is negatively skewed, with 85% of the total number of sinks being less than 0.25 km^2 in size. We found no significant correlation between either sink frequency or fractional area and elevation (R^2 of 0.01 and 0.02 respectively). However, the average area of individual sinks does increase with elevation up to an

altitude of 750-1000 m a.s.l., at which point the average area of sinks is twice as large as those found between 0-250 m a.s.l. and 1250-1500 m a.s.l. (Figure 5.3).

Using the Landsat images, we identified 199 lakes with a total area of 29.7 km^2; this is 0.6% of the area included in the study. The largest lake identified has an area of 2.2 km^2, the average size of lakes was 0.15 km^2. In common with sinks, the distribution of lake sizes is negatively skewed, with 88% of all lakes being less than 0.25 km^2 in size. We were able to identify trends in the number density, average size and fractional area of lakes within the study area (Figure 5.3). The average area of lakes generally increased with elevation (R^2 = 0.88), peaking at 0.2 km^2 between 1250-1500 m a.s.l.; this area is an order of magnitude greater than that of lakes between 0-250 m (0.01 km^2). The density of lakes (per 100 km^2) and the fractional area of lakes display similar correlations with elevation, increasing to peaks of 13 (R^2 = 0.79) and 2.1% (R^2 = 0.72), respectively at an altitude of 1000-1250 m a.s.l., and decreasing thereafter.

Comparing the sink and lake datasets as a whole, we found that sinks cover a 64% larger area than lakes, there were over twice as many individual sinks than lakes, that the individual sinks are, on average, 20% larger than the lakes, and that both datasets have size distributions that are skewed towards smaller sizes. A comparison of sinks and lakes in relation to the elevation bands studied shows that the greatest difference between the average area of sinks and lakes occurs at elevations below 1000 m a.s.l., and that between 1250 and 1500 m a.s.l. the average area of lakes was 0.05 km^2 (~20 %) greater than that of sinks. We find there are greater numbers of sinks per 100 km^2 than lakes at all altitudes except between 750 and 1250 m a.s.l., when the number of sinks and lakes per 100 km^2 are approximately equal. The fractional area covered by sinks is larger than that covered by lakes at all elevations. Finally, there are no apparent similarities between altitudinal trends of sinks and lakes (Figure 5.3).

We examined the numbers, sizes, and distributions of the locations where sinks and lakes overlap. In total, we identified 96 locations of coincidence covering an area of 10.6 km^2. The area where lakes and sinks are coincident represents 13.0 % of the

total sink area and 35.6% of the lake area. Figure 5.3 illustrates the extent to which sinks and lakes coincide according to their elevation. Below 250 m a.s.l. there are no areas where sinks and lakes are both identified. Above 250 m a.s.l. the percentage of sink area overlapped by lakes increases sharply with altitude ($R^2 = 0.85$) to a peak of 30.7% between 1000 and 1250 m a.s.l. and thereafter decreases. Above 250 m a.s.l. there is no clear trend between the percentage of the lake area where sinks are found and elevation ($R^2 = 0.12$); the highest percentage is found between 250 and 500 m (49.1%) and the lowest between 500 and 750 m (28.9%). At elevations above 1500 m a.s.l., where lakes do not currently exist, we find that sinks have a higher density (75 per 100 km^2), a smaller average size (0.05 km^2) and occupy a smaller fractional area (0.3%).

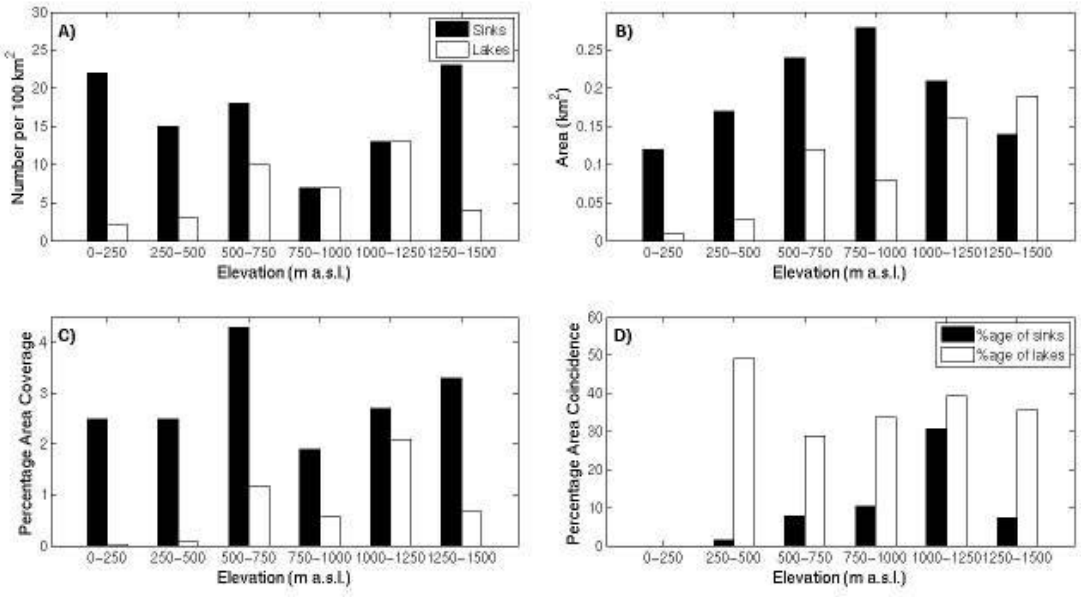

Figure 5.3: Altitudinal trends in topographic sinks (black) and supraglacial lakes (white) A) numbers, B) average size and C) percentage area coverage with altitude above sea level. D) shows the relationships of the percentage of total area of sinks where lakes are found (black) and the percentage of the total area of lakes where sinks are found (white) with altitude above sea level.

We assess some of the error introduced into our analysis by inaccuracy in the classification of lakes in optical imagery and the loss of precision in sink identification due to DEM resolution. An accuracy assessment of the classification of lakes in Landsat imagery provided an estimate that up to 6% of the area identified as

lake in any image belongs to an alternative class; this may account for up to 9% of the area of lakes identified which do not coincide with sinks. We tested the impact of DEM resolution on the agreement between sinks and lakes in the raw data. Reducing the resolution of the InSAR DEM from 150 m to 950 m leads to a decrease in both the total area and the number of sinks by 71.8 % and 98.5 %, respectively (Figure 5.44). At the same time, the average size of sinks increased from 0.02 km^2 to 0.36 km^2. The decrease in DEM resolution from 150 m to 950 m also leads to a 53 % decrease in the lake area where sinks overlap, and a 67% increase in the sink area where lakes overlap (Figure 5.4). By extrapolating trends between DEM resolution and the percentage coincidences of sinks and lakes we suggest that a horizontal resolution of 150m of the DEM may account for a 3% loss in accuracy of lake identification and a 5% gain in accuracy of the percentage of sinks where lakes are also found.

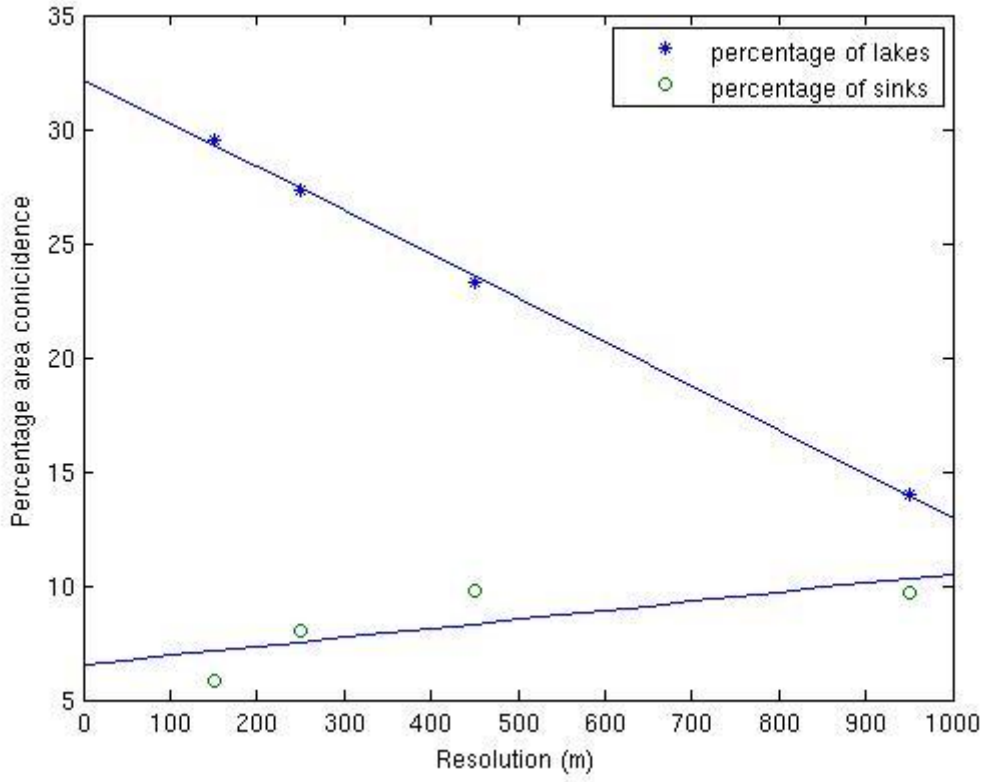

Figure 5.4: Testing the effect of different DEM resolutions on identification and prediction of lake areas. Trend-lines are fitted through both datasets.

5.5 Discussion

Our results give some indication of the processes which govern the formation and distribution of sinks and lakes on the ice surface in northeast Greenland. That there is some agreement between the modelled sinks and observed lakes identified in data acquired 4-11 years apart, suggests that the positions of lakes in this region are persistent. This is in line with observations from the western margin of the GrIS (Echelmeyer *et al.,* 1991; Luthje *et al.,* 2006) and indicates that the positions of the lakes are linked to undulations in the subglacial topography (Echelmeyer *et al.,* 1991; Gudmundsson, 2003). The weak correlation between sink and lake characteristics with altitude however, suggests that, although surface depressions exert a first order control on the position of lakes, the characteristics of sinks have less influence on the size, quantity, and distribution of lakes on a regional scale. The correlation we find between lake characteristics and elevation does, however, provide further insight as to which other factors may control their distribution. Taking elevation as a proxy for surface temperature, ice thickness and surface crevassing, factors which may be controlling the distribution of lakes include the amount and routing of meltwater (Echelmeyer *et al.,* 1991; Luthje *et al.,* 2006) and the ease of hydrofracturing (e.g. Das *et al.,* 2008; van der Veen, 1998).

Some of the differences observed between lakes and sinks may also be due to limitations of our data and analysis. The temporal resolution of the optical imagery used to identify lakes influences the accuracy of estimates of lake areas, numbers and distributions. The observed rapid seasonal evolution of lakes in other regions of the ice sheet (e.g. McMillan *et al.,* 2007; Das *et al.,* 2008; Sundal *et al.,* 2009) suggests that the temporal resolution of the optical images may be insufficient to capture the maximum number and area of lakes within the region. Furthermore, the possibility that the observed relationship between ice surface elevation and lake characteristics may reflect incomplete coverage of the entire span of the melt season in the optical image acquisitions, cannot be discounted. Because surface depressions are required

for lake formation, the surface area of lakes not coincident with sinks must result from misclassifications of lakes in the optical data (e.g. where lake surfaces are frozen) and the inability to detect small and shallow sinks in the DEM, not physical differences between sinks and lakes We estimate that lake misclassifications and the inability to detect small sinks introduce a 12% uncertainty to the percentage area of lakes coincident with sinks and, therefore the inability to detect shallow sinks may have a significant impact. Although our DEM is capable of detecting depressions deeper than ~4m, Sneed and Hamilton (2007) report that up to 91% of the total volume of ponded meltwater in the northwest of Greenland is between 20 cm and 1.5 m deep.

We find that, overall, the efficacy of using sinks as a proxy for the location and surface area of supraglacial lakes in the northeast of Greenland is poor due to the physical differences between sinks and lakes and to limitations of the available data. In comparison to an analysis of lakes at the western margin of the Greenland ice sheet (Luthje *et al.,* 2006), we find a similar ratio of the size of sinks to lakes (3-4 and 3 times greater respectively), However, unlike Luthje *et al.,* (2006), who find that the locations of sinks and lakes compare 'favourably', we find that fewer than half of lake locations are identified in the DEM and less than a quarter of sinks identified in the DEM coincide with lakes. It is possible that this may be associated with glaciological differences in the study regions. For example, the bedrock and ice surface slopes are gradual at the Western margin, whereas in Northeast Greenland they are steep and rapidly changing (Bamber *et al.,* 2003). Such differences affect both uncertainties associated with DEM resolution, and the physical differences between lakes and sinks because the drainage systems and stress regimes of ice in the Northeast are more varied.

Further application of this method to predict, for example, the location of lakes in a warming climate, relies not only on the skill with which we can identify lakes currently forming on the ice sheet surface, but also on the ability to identify sinks above the transient snow line (TSL) where lakes do not currently form. Although our results from above the TSL (Appendix- section 5.8) show that sinks are clearly

identified, there are substantially more sinks in this region exhibiting smaller average area and percentage area coverage than at lower altitudes. Visual inspection reveals that, although there are some large sinks in this region that appear similar to those at lower elevations, the general distribution of sinks above 1500 m a.s.l. appears 'speckled'. We interpret the difference in the distribution of sinks above 1500 m a.s.l. (compared to those below 1500 m a.s.l.) as being a result of noise in the radar signal used to create the DEM. A potential source of such noise is variations in the degree of volume scattering within the firn, such as those associated with the presence of ice lenses forming at variable depths within the snowpack (e.g. Bindschadler and Vornberger, 1992; Rignot, 1995). In consequence, care should be exercised when interpreting the locations of sinks identified above the TSL.

5.6 Conclusions

We have assessed the accuracy of using sinks identified in a DEM to predict the area and location of lakes on the surface of the northeast region of the GrIS through comparison with a dataset of observed lakes. Our data show that the area of sinks is greater than that of lakes, and that applying this methodology would, for example, result in a 64 % overestimate of lake area in this region. We also found that the ability of the methodology to identify the locations of lakes is poor; only 36% of the surface area of lakes was identified. The disagreement arises from a combination of physical differences between sinks and lakes on the ice sheet surface and limitations in both the optical image analysis and the resolution of the DEM. Our analysis of sinks above the TSL revealed that the accuracy of predicting future lake locations is further limited by noise in the DEM, potentially resulting from volume scattering of the radar signal in the snow pack.

The limited accuracy with which lake locations can be predicted using sink locations in northeast Greenland suggests that this method may not be appropriate for models aiming to predict the future impact of supraglacial lake drainage on the ice sheet. However, the results of our study do suggest that there is potential for using sinks to predict and identify lake locations. Refinement of the methodology developed here

could reduce the impact of several of the sources of uncertainty we have identified. We also recognise that this region of the NE GrIS exhibits a more complex glaciology in comparison to large proportions of the GrIS margin due to mountainous subglacial topography, and that this is likely to exacerbate errors associated with our intercomparison of sinks and lake locations. A comparison to similar work in the west of Greenland (Luthje *et al.*, 2006), for example, suggests that the methodology may be more effective in regions of less complex glaciology.

5.7 Limitations

The results presented on the comparison between sinks and lakes in this chapter were subject to the following limitations:

- A key limitation of the comparison conducted between sinks and lakes is that the vertical and horizontal accuracy of the DEM used, although relatively high by comparison to other DEMs (see Chapter 3), was not sufficient to resolve some of the sinks where lakes were observed to form. Furthermore, noise due to volume scattering at high elevations would prevent an accurate prediction of potential lake locations.
- In this chapter, the temporal resolution of the optical imagery used in lake identification, relative to the time taken for lakes to form and drain on the surface of the ice sheet, may have led to an underestimation of the coverage of lakes, thereby introducing inaccuracy into the comparison. However, although this is a limitation to the analysis in this chapter, the results presented in Chapter 6, using higher temporal resolution imagery, suggest that this is not the principal source of inaccuracy when comparing the distribution of lakes and sinks.
- Perhaps one of the largest limitations of the results presented is that the physical differences between lakes and sinks (i.e. that lakes do not necessarily fill a sink) are not accounted for. This will be discussed further in Section 7.4.2.

5.8 Appendix

This appendix contains an additional figure that is referred to in this chapter and in support of the results presented therein.

Sinks above the Transient Snow Line

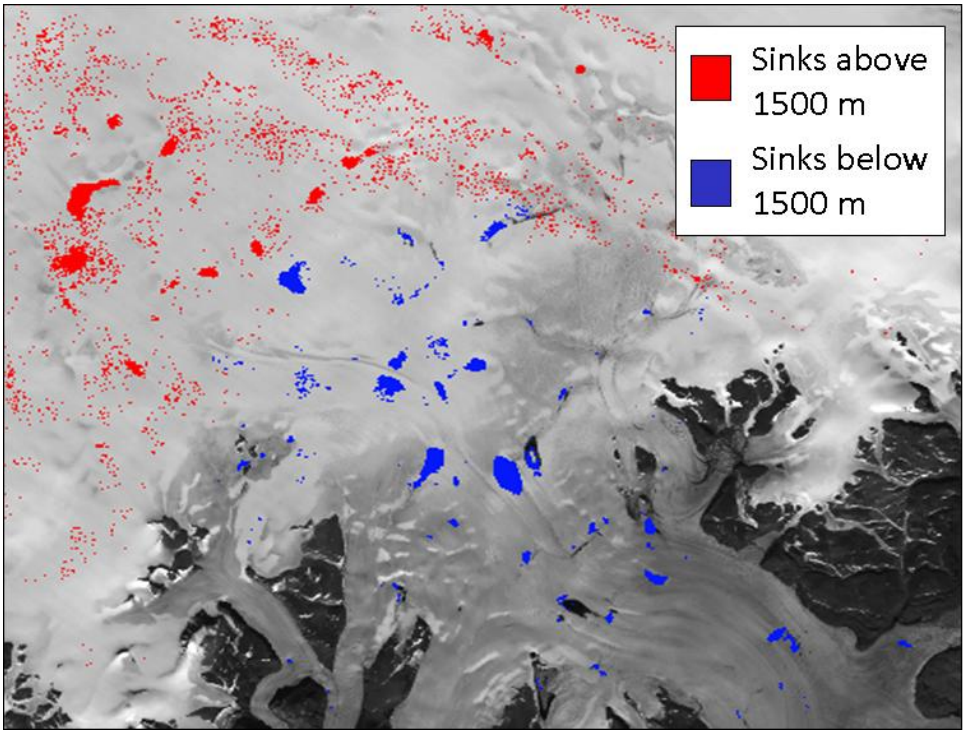

Figure 5.5: Sinks identified in the InSAR DEM of northeast Greenland. Sinks identified above the transient snow line (1500 m a.s.l.) are shown in red and those identified below are shown in blue. The sinks above the transient snow line appear noisy.

Chapter 6: Investigating and predicting supraglacial lake drainage on the Greenland Ice Sheet

In light of the findings reported in Chapter 5, i.e. that there is a poor correspondence between lakes and sinks in the northeast region of the ice sheet, we test our suggestions that this poor match is the result of complex topography in the region and the low temporal resolution of Landsat data. We achieve this by applying the same methodology of identifying sinks to the western, Russell glacier region of the ice sheet (Figure 6.1), where the ice sheet topography and glaciology is, by comparison with the northeast, less complex (i.e. it is less constrained by bedrock topography) and by using daily resolution MODIS imagery to identify lake extents on the ice surface.

We built a high resolution DEM using the data and InSAR methods outlined in Chapter 4/5. Through comparison of 2114 ICEBridge and InSAR DEM data points (see section 6.3.4) we estimated the precision of the DEM, over length scales applicable to mapping sinks (i.e. ~5km) to be 5.8m We identified sinks (topographic depressions) in the DEM using the method described in Chapter 5. We use a dataset of the maximum lake extents in the area compiled from 64 MODIS images from 4 summers (of 2003, 2005, 2006 and 2007) which were classified by A Sundal for Sundal *et al.,* (2009) using methods outlined within.

A total of 870 sinks were identified in the DEM which cover a total area of 656 km^2, or 7 % of total ice surface area included in our study. 560 lakes were identified which cover a total area of 438 km^2 or 4.8% of the area of study. We find a total area where both lakes and sinks are found of 8.2 km^2. This equates to 1% of the area of sinks which coincides with areas where lakes are identified and 47% of the area where lakes are identified which coincides with areas where sinks are found. In terms of the coincidence of individual lakes and sinks, we find that of the 870 sinks identified,

342 (39%) have a lake in them in the MODIS data and of the 560 lakes identified, 323 (58%) form in sinks found in the DEM.

Although the area of lakes overlapped by sinks is an improvement on that reported for our similar study in the northeast region (Chapter 5) (probably due to differences in the nature of glaciology of the 2 regions and the improved temporal resolution of the optical imagery used to identify lake extents), the area of sinks overlapped by lakes is much lower. The accuracy of coincidence between sinks and lakes areas remains insufficient to be used as a tool for identifying or predicting lakes locations now, and in the future. We suggest that the remaining inaccuracy of this method may be attributed to the physical differences governing the formation of lakes and sinks, and the limits of the DEM for accurately identifying sinks (see Chapter 5). The accuracy of this method for identifying and predicting lake locations may be improved by modelling the hydrological processes which govern the size of a given lake on the ice surface (e.g. surface water routing and lake drainage through hydrofracturing) and by using a DEM with higher accuracy and precision than generated here (e.g. LiDAR); although at present, to the best of our knowledge, such a DEM does not exist for this region. Consequently, the next chapter focuses on the application and assessment of an alternative methodology for predicting the future coverage of lakes on the surface of the GrIS.

The remainder of this chapter describes the results of a survey of lake formation and drainage in the west of Greenland using MODIS images and discusses the trends observed and the potential for future lake drainage in a warming climate. This chapter has been prepared for submission to the Journal of Geophysical Research, Earth Surface:

Briggs, K., Nienow, P., Shepherd, A., Naylor, M., Sundal, A., Palmer, S., Bartholomew, I. and Cowton, T. (in prep.) Investigating and predicting supraglacial lake drainage on the Greenland Ice Sheet. *Journal of Geophysical Research, Earth Surface.*

The majority of the work for this chapter was carried out by myself. A Shepherd and P Nienow developed the original ideas for this chapter and provided comments on the manuscript. M Naylor conducted the nearest neighbour cluster analysis. A Sundal and T Cowton processed the MODIS images. I Bartholomew provided the meteorological data from the AWS on Leverett Glacier. A Sole extracted and helped process the IceBridge data. E Rinne extracted and helped with processing of the ICESat data.

The limitations of this work are discussed in section 6.7.

6.1 Abstract

We have used 47 MODIS images to map the formation and drainage of supraglacial lakes during the summer of 2003 over a 9100 km^2 region at the western margin of the Greenland Ice Sheet (GrIS). We identify 312 lakes with a total area of 227 km^2 that form up to an elevation of 1618 metres above sea level (m a.s.l.). Towards high elevations, we observe a decrease in the total area coverage of lakes (from 3.4 % at 1100-1250 m a.s.l. to 1.6 % at >1550 m a.s.l.) due to a decrease in the density of lakes (from 4.7 per 100 km^2 at 1100-1250 m a.s.l. to 1.2 per100 km^2 at >1550 m a.s.l.) and despite of an increase in the average area of individual lakes (from 0.5 km^2 at 1100-1250 m a.s.l. to 1.2 km^2 at >1550 m a.s.l.). Clear trends are observed to exist between lake elevation and the Julian days and the cumulative positive temperatures required for lakes to form and drain. This suggests that it may be possible to predict the timing of lake formation and drainage by elevation which has significant implications for model parameterisation. In this sector of the GrIS, 81% of the supraglacial lakes undergo rapid drainage, and the proportion of lakes which do not drain increases with elevation from 0% below 950 m a.s.l. to 89% at altitudes above 1550 m a.s.l.. We argue that the observed decrease in lake coverage and drainage rates with elevation stems from increases in ice thickness, which controls hydrofracturing and surface relief. The clear trends identified in the distribution and drainage of lakes suggests these trends may be extrapolated to higher elevations and other regions, thereby providing a means of parameterising lakes in ice sheet models.

We also report the simultaneous draining of clusters of lakes; using a nearest neighbour analysis we show that 37% of lakes that drain do so on the same day as others less than 5 km away. Finally, using IceBridge Airborne Topographic Mapper (ATM) data we show the presence of ice surface depressions at altitudes up to 2600 m a.s.l. indicating that lakes have the potential to form well into the ice sheet interior in the event of increasing melt area extents to these regions in a warmer climate. However, in light of our findings of decreasing lake coverage and drainage with elevation, we suggest that the ice sheet conditions may not be favourable for lake drainage at these elevations.

6.2 Introduction

The Greenland Ice Sheet (GrIS) is losing mass from its margins through a combination of increased surface melting (Hanna *et al.,* 2005) and ice discharge (Rignot and Kanagaratnam, 2006) in response to climate warming. The accuracy of model predictions of future mass losses from the GrIS rests on our level of understanding of these responses. However, whilst the processes linking climate to surface melting are well understood, our knowledge of the interplay between climate and ice discharge is limited.

Observations have shown that ice discharge rates fluctuate in response to changes in outlet glacier velocity which are associated with changing ocean conditions (e.g. Holland *et al.,* 2008; Straneo *et al.,* 2010) and surface meltwater inputs to the ice-bed interface (e.g. Zwally *et al.,* 2002; Joughin *et al.,* 2008c; van de Wal *et al.,* 2008; Bartholomew *et al.,* 2010; Sundal *et al.,* 2011). Several studies have suggested that the rapid delivery of surface meltwater to the ice bed leads to increased subglacial water pressures which causes enhanced basal sliding and increased ice velocity (e.g. Zwally *et al.,* 2002; Das *et al.,* 2008; Shepherd *et al.,* 2009). However, over seasonal and interannual timescales the link between melt rates and ice velocities is unclear, with conflicting findings suggesting that increased surface ablation rates may lead to either increases (Zwally *et al.,* 2002) or decreases (Van de Wal *et al.,* 2008; Sundal *et al.,* 2011) in the overall seasonal surface displacement. This may be explained by

differences in the variability of surface meltwater inputs and the evolution of the subglacial drainage system**.**

Model experiments by Schoof (2010) suggest that an increased rate of steady water supply has a limited potential to increase seasonal velocities because the seasonal evolution of the subglacial drainage system enables greater volumes of water to be accommodated and this suppresses water pressures and acceleration. Conversely, larger annual surface displacements occur if water enters the subglacial drainage system in pulses (i.e. strong diurnal melt cycles and rainfall and lake drainage events) over timescales shorter than that required for drainage system evolution (Schoof, 2010). Therefore, to predict the response of ice velocities to surface warming it is important that we are able to parameterise the variability of surface meltwater delivery, and therefore lake drainage events, in ice sheet models.

During the summer, supraglacial lakes are observed to form and drain in the ablation area of the GrIS (e.g. Echelmeyer *et al.,* 1991; Luthje *et al.,* 2006; Box and Ski, 2007; McMillan *et al.,* 2007; Sneed and Hamilton, 2007; Sundal *et al.,* 2009). Lakes develop as surface meltwater ponds in topographic depressions. They form in the same locations year on year implying that the depressions in which they form are surface expressions of subglacial topography (Echelmeyer *et al.,* 1991). Throughout the melt season, lakes begin to develop further inland and at higher elevations, tracking the expansion of the region of surface melting (e.g. Box and Ski, 2007; McMillan *et al.,* 2007; Sundal *et al.,* 2009). In a number of instances, lakes have been observed to drain through crevasses at their bases over the course of just a few hours (Box and Ski, 2007; Das *et al.,* 2008). Lake drainage is thought to occur when the depth and volume of water is great enough to exert sufficient pressure to overcome the stresses keeping a given crevasse closed (e.g. Weertman *et al.,* 1973; Boon and Sharp, 2003; Alley *et al.,* 2005b; van der Veen, 2007; Das *et al.,* 2008). These drainage events have been linked to local in increases velocity (e.g. Joughin, 1996a; Das *et al.,* 2008) which is suggestive of water reaching the bed of the ice sheet, raising subglacial water pressures, and causing hydraulic jacking and enhanced basal sliding.

Sundal *et al.,* (2009) compared lake coverage between warm and cool summers and found that in warmer years lakes form at higher elevations than in cooler years. This prompted the suggestion that in future, warmer climates, lakes may form at elevations beyond their current extent, with the implication that meltwater may be delivered to a larger area of the ice sheet bed and this may impact on ice discharge rates. However, to date there has been no assessment of the elevation to which lakes have the potential to form, the potential extent of their coverage and their potential for draining. Here, we use a combination of optical satellite imagery, and meteorological and topographical data to investigate current trends in lake formation and drainage. The aims of doing so include: identifying the controls on lake formation and drainage events, assessing the potential for extrapolating any observed trends in lake formation and drainage to other regions and higher elevations of the GrIS for model parameterisations of lake distributions, and assessing the likelihood of lakes forming and draining at elevations beyond their current limits in warmer climates.

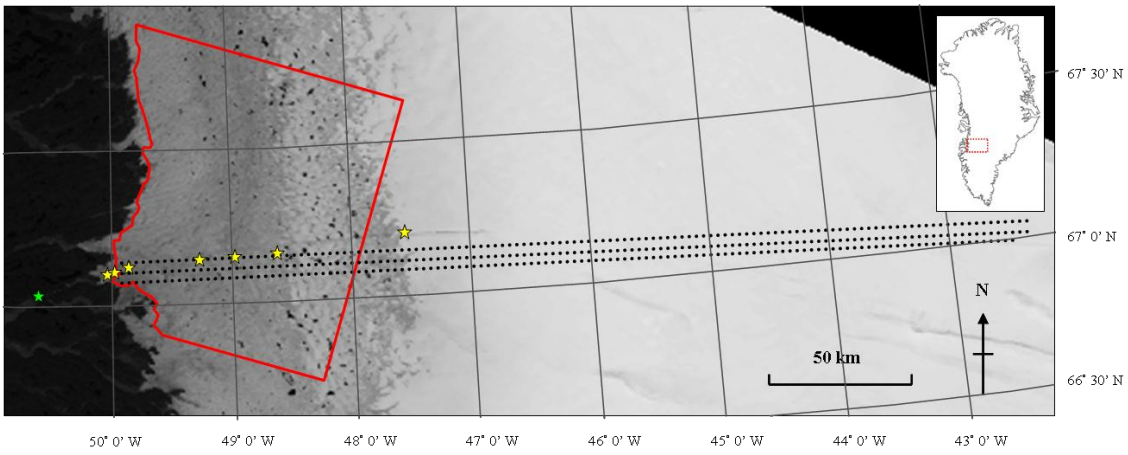

Figure 6.1 : MODIS image (11/07/2003) showing the study region in the southwest of Greenland. The red box delineates the region over which the lake survey was conducted. The green and yellow stars are the locations of the Kangerlussauq and Leverett meteorological and automatic weather stations (AWS) respectively. The black dashed lines are the IceBridge flight lines.

6.3 Methods

The study area is situated in the southwest of Greenland and extends from 66º72 to 67º72 N and between 47º51 and 50º35 W (Figure 6.1). We examine supraglacial

lakes over a 9100 km^2 region of ice, reaching up to an elevation of 1700 m a.s.l., which includes the Russell and Isunguata Sermia glaciers. Surface slopes are examined up to an elevation of 2600 m a.s.l..

6.3.1 MODIS image processing

We use cloud-free MODIS images acquired during the summer of 2003 to investigate the lakes which form and drain on the ice surface. The one-day repeat pass time of MODIS imagery is ideal for studying lake drainage events which are observed to occur in less than a day (Box and Ski, 2007; Das *et al.,* 2008). We chose to use data from 2003 as this was a year with a high number of cloud free images; in total we analysed 47 images acquired between 19/05/2003 (Julian Day (JD) 139) and 12/09/2003 (JD 255).

Data was downloaded from the Level 1 and Atmosphere Archive and Distribution System (LAADS) (http://ladsweb.nascom.nasa.gov/data/search.html). We used bands in the visible spectrum, band 1 (red), band 3 (blue) and band 4 (green), which have respective horizontal resolutions of 250 m, 500 m and 500 m. Image pre-processing was conducted according to the method outlined by Gumley *et al.*, (2007) and included atmospheric correction, resolution sharpening of bands 3 and 4 to 250 m and image geolocation. Initial lake identification was achieved using a fuzzy logic classification based on band 1 and the ratio between band 3 and band 1; band 4 was used for visual analysis (for further details see Sundal *et al.,* 2009). Sundal *et al.,* (2009) estimate the accuracy of lake classification in the same region by comparing lakes classified in a MODIS image with those classified in a higher resolution (15 m) ASTER image acquired on the same day. The total area of lakes identified in the MODIS images exceeded those identified in the ASTER images by 1.6% and a root mean square deviation (RMSD) of 0.22 km^2 was derived. Furthermore, due to the coarse resolution of MODIS images, lakes with an area smaller than approximately 0.1 km^2 are not included in the study. The comparison of ASTER and MODIS images (Sundal *et al.,* 2009) revealed that this accounted for about 12% of the lakes in the ASTER image. The images used in this comparison were acquired in late

summer (01/08/2001), when the percentage of small lakes is likely to be higher earlier in the melt season when lakes are developing (Sundal *et al.,* 2009). This inability to identify small lakes introduces inaccuracy when identifying the timing of lake formation. Furthermore, the classification does not distinguish between frozen lakes and glacier ice. For these reasons we visually inspected the images to precisely identify the day on which lakes first appeared and drained.

6.3.2 DEM generation

To examine the relationship between lake characteristics and elevation we formed a DEM of the region using InSAR (e.g. Zebker and Goldstein, 1986; Kwok and Fahnestock, 1996; Joughin *et al.,* 1996b; Wegmuller *et al.,* 1998) and European Remote Sensing (ERS) satellite SAR data. We use two descending pass ERS-1 and ERS-2 tandem phase image pairs from the 20th and 21st October 1995 and the 2nd and 3rd February 1996 with a combined perpendicular baseline of -115 m. We use ICESat GLAS elevation data (Zwally *et al.,* 2003) to refine the interferometric baseline and to assess the DEM accuracy. We refined the interferometric baseline using 1689 points of know elevation from descending ICESat tracks, and this resulted in a DEM with a root mean square (RMS) altitude error of 19.6m. We regressed a further 1358 points of know elevation from ascending ICESat tracks with the elevations derived from the DEM and this yielded an excellent agreement (R^2 = 0.9942).

6.3.3 Temperature data

We estimated daily surface temperatures across the region in 2003 using air temperature data acquired at Kangerlussuaq airport and atmospheric lapse rates calculated from air temperature data from Kangerlussuaq airport and 7 automatic weather stations (AWS) situated on Leverett glacier in 2009 (Figure 6.1) . We calculate lapse rates by taking the average difference in temperatures between the 7 stations between May and August of 2009. We tested the accuracy of the lapse rates by comparing predicted temperatures against measured temperatures acquired in 2009 and 2010. The average R^2 values from all 7 AWS positions are 0.95 for 2009

and 0.54 for 2010, and the respective average residual error estimates are ± 0.8˚C and ± 1.6˚C.

6.3.4 Slope profiles

To examine the distribution of surface depressions (possible future lake locations) on the ice sheet beyond the limit of current surface melting (and the InSAR DEM), we identify reverse slopes in profiles generated from the IceBridge (ATM) (Krabill, 2009). The data was downloaded from the IceBridge ATM L2 Icessn Elevation, Slope and Roughness, National Snow and Ice Data Center (NSIDC) website (http://nsidc.org/data/ilatm2.html). We used data points acquired from 3 flight lines recorded in May 2010 (Figure 6.1**).** The estimated accuracy of the ATM topography measurements is 10 -20 cm (http://atm.wff.nasa.gov/).

6.4 Results

We identify the formation of 312 lakes with a total surface area of 227 km^2 during the summer of 2003. This equates to 2.5% of the survey area, with an average density of 3.1 lakes per 100 km^2. The average area of individual lakes was 0.7 ± 0.8 km^2 (one standard deviation) and the largest lake identified was 5.1 km^2. Our study region extends up to an elevation of 1700 m a.s.l. and the maximum altitudinal limit for lakes forming during the melt season of 2003 in this area extends to 1618 m a.s.l..

We investigated variations in the altitudinal distribution of lakes in the region using six discrete elevation bands; 650-800 m a.s.l., 800-950 m a.s.l., 950-1100 m a.s.l., 1100-1250 m a.s.l., 1250-1400 m a.s.l., 1400-1550 m a.s.l. and above 1550 m a.s.l.. We find clear trends in the coverage, number and size of lakes with elevation (Figure 6.2). At low elevations (650-800 m a.s.l.), the total fractional coverage of lakes is low (0.6 %) and the population is comprised of a relatively low density (2.0 per 100 km^2) of small lakes (0.19 km^2). However, the coarse resolution of MODIS images means that some percentage of small lakes (0.1 km^2) will not have been detected, and given the tendency towards smaller lakes at lower elevations, the fractional coverage

and density of lakes at low elevations is likely to be greater than we estimate here. The largest fractional coverage of lakes (3.4 %) occurs at mid elevations (1100-1250 m a.s.l.) where there is a high density (4.7 per 100 km^2) of medium-sized lakes (0.5 km^2), and towards high elevations (above1550 m a.s.l.) the fractional coverage decreases (1.6%) and the population is comprised of a low density (1.2 per 100 km^2) of large lakes (1.2 km^2).

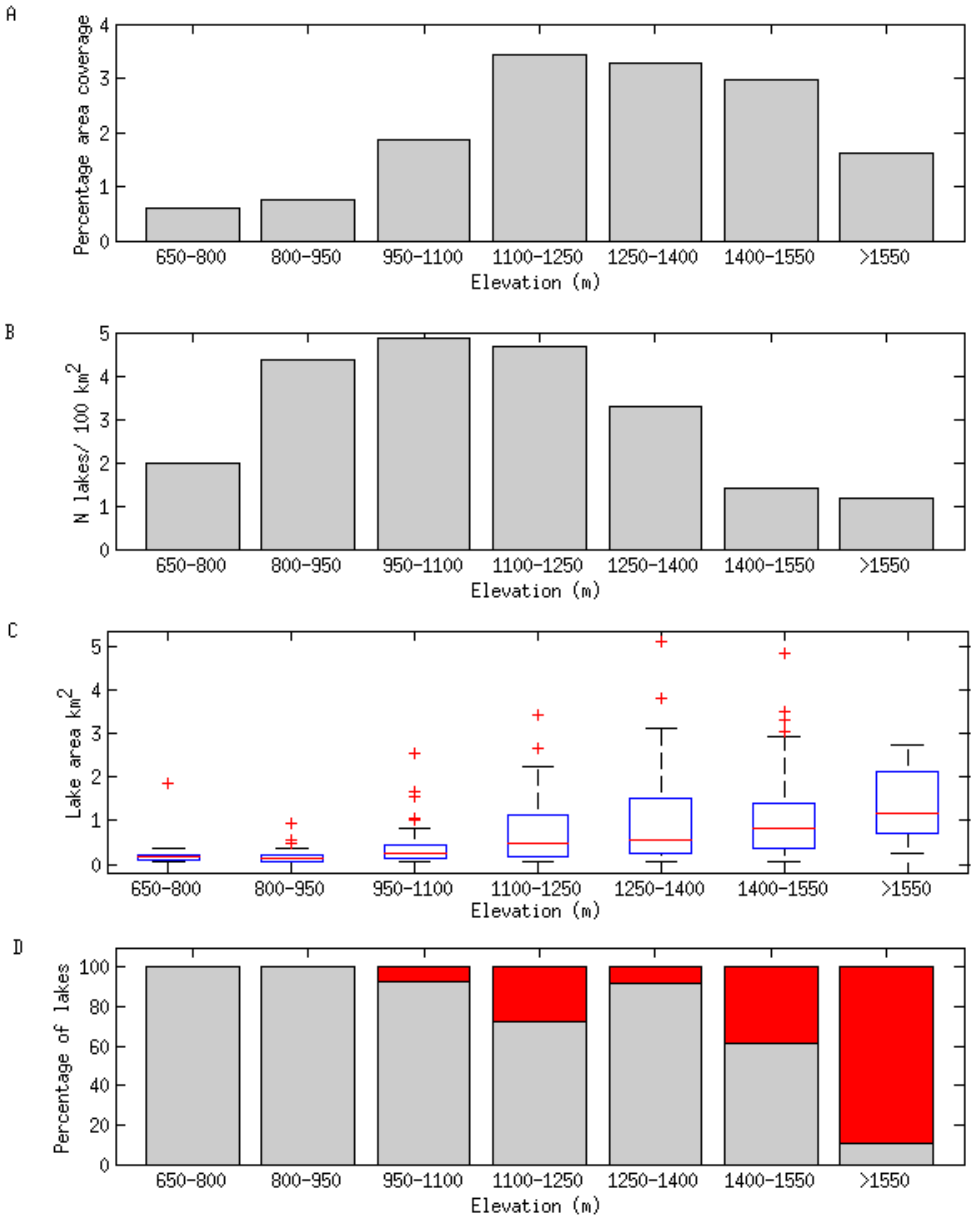

Figure 6.2: A) Fractional coverage of lake area, B) lake density, C) box plots showing the median and inter-quartile ranges (IQR) of lake sizes (the whiskers represent data that are

within 1.5 IQR of the lower and upper quartiles and red crosses mark the outliers) by elevation and D) the percentage of lakes forming on the surface which do (grey) and do not drain (i.e. refreeze at the end of the melt season) (red).

We investigated the relationship between elevation and both the timing of lake initiation and the positive degree days (PDD) (defined as the sum of the mean daily temperatures, t, for all days when $t > 0^{\circ}C$) prior to lake initiation (Figure 6.3a & b). We find that lakes form progressively later in each elevation band (Figure 6.3a). At the lowest elevations (650-800 m a.s.l.) lakes form on average on day 150 ± 2, whereas at elevations greater than 1550 m lakes form on average over a month later, on day 185 ± 7. By examining the PDDs prior to lake formation we are able to account for the time lag of lake formation with altitude. The degree of correlation between the lapse-rate corrected PDDs prior to lake initiation and elevation is not as strong ($R^2 = 0.6$) as that between elevation and the timing of lake initiation ($R^2 = 0.9$) (Figure 6.3b), although we find that more PDDs are required before lakes begin to form at higher elevations (38.0 ± 7.9 ˚C above1550 m a.s.l.) than at low elevations (27.6 ± 10.6˚C between 650 and 800 m a.s.l.).

We investigated lake drainage events relative to elevation and lake sizes, examining the percentage of lakes which drain to those which do not, the timing of lake drainage events and the PDD temperatures before lakes drain. Within our study region 252 (81%) lakes drained suddenly (within consecutive images- i.e. 1- 5 days - Figure 6.3) during the melt season. The lakes which don't drain freeze at the end of the melt season. We find that the proportion of lakes which do not drain increases with elevation (Figure 6.2). Between 650 and 950 m a.s.l. all of the lakes we observed to form also drained, however of the lakes which formed above 1550 m a.s.l., 89% did not drain and these froze over at the end of the melt season. We examined the relationship between the size of lakes which drained and the size of lakes which did not for elevations over 950 m a.s.l. and find that within this sample the lakes which drained are smaller than those which did not (0.8 ± 0.8 km^2 and 1.0 ± 1.1 km^2 respectively) although the difference is not significant at $p = 0.05$.

Of the lakes which did drain, we find that the average day of draining increased with elevation from day 157 ± 5 at elevations between 650 and 800 m a.s.l. to day 194 ±

10 at elevations between 1400 and 1550 m a.s.l. (Figure 6.3c & d). However, only a weak positive trend exists between elevation and the average period over which lakes are present on the ice surface (i.e. the date of draining minus the date of formation) as there is no significant difference (at $p = 0.05$) between the residence times of lakes sited between 800 and 1400 m a.s.l. The average time over which lakes are present on the ice surface is 14.8 ± 10.0 days, with residence times ranging from 1 to 61 days before draining. At low elevations (650 to 800 m a.s.l.) the residence time of lakes (7 ± 6 days) is, on average, 12 days less than that of lakes sited between 1400 and 1550 m a.s.l. (19 ± 10 days).

There are distinct elevation related trends in both the PDDs prior to draining and PDDs while lakes are present on the ice surface (i.e. cumulative PDD temperature at draining minus the cumulative PDD temperature to onset) (Figure 6.3e & f). The PDD temperatures prior to drainage are smallest (62.1 ± 23.7 ˚C total before draining and 34.5 ± 27.3˚C whilst present) at low elevations (650-800 m), largest between 800-950 m (96.9 ± 42.6 ˚C total before draining and 69.0 ± 42.9˚C whilst present) and then decrease steadily thereafter to a minimum at1400 -1550 m a.s.l. (53.5 ± 13.0 ˚C total before draining and 20.3 ± 12.1˚C whilst present).

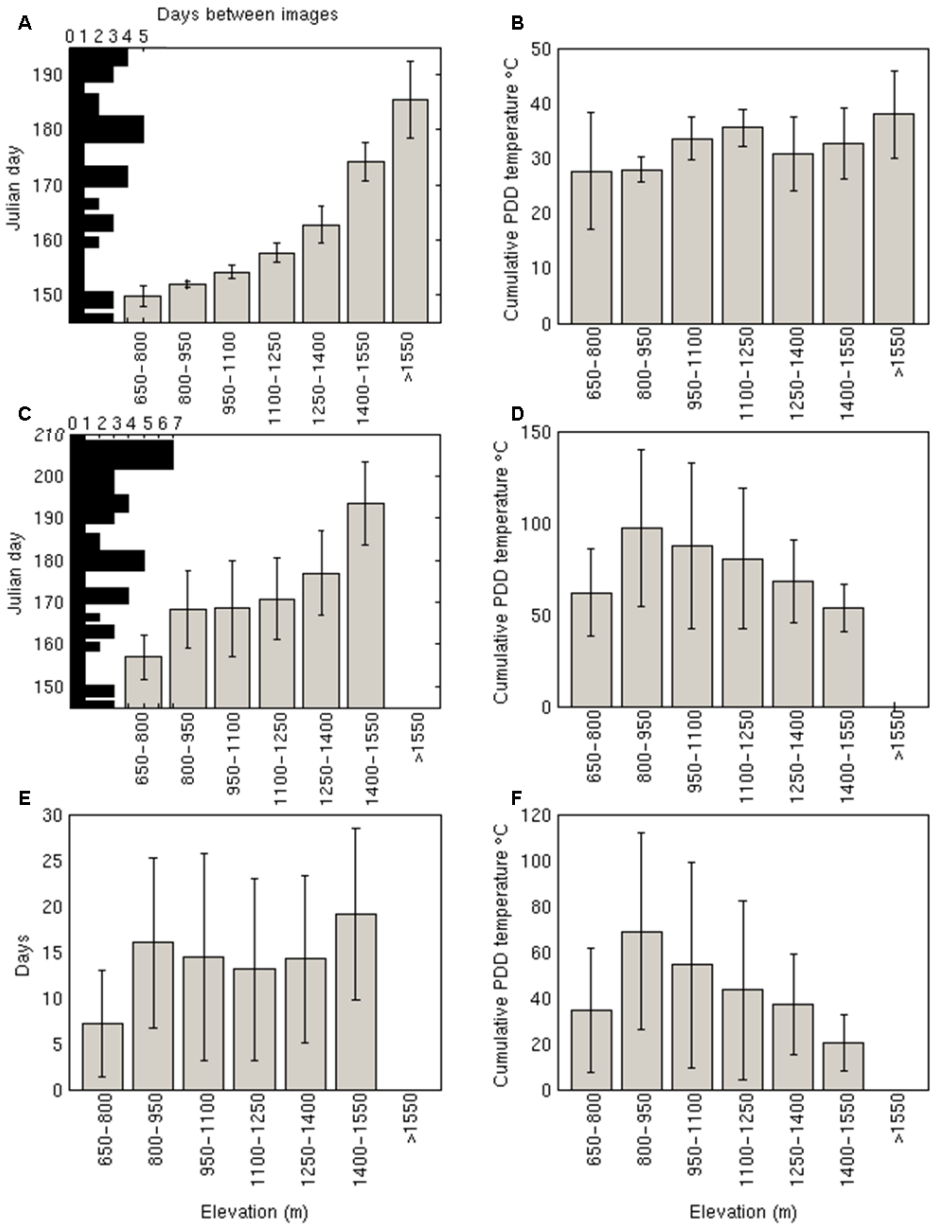

Figure 6.3: Average days (a, c & e) and PDD temperatures (b, d & f) prior to lake filling (a&b), prior to lake drainage (d & c) and between lake formation and drainage (e &f) by elevation band. Vertical error bars represent one standard deviation from the mean. Graphs c, d, e and f do not include data from elevations above 1550 m a.s.l. as only one lake drained at this altitude. Black horizontal bars in a and c show the time gaps between MODIS images.

The MODIS images suggest that neighbouring lakes often drain simultaneously in clusters. We quantitatively demonstrate this clustering effect in lake drainage events using a nearest neighbour analysis (Getis and Boots, 1978) of lakes draining on the same day (Figure 6.4a & b). To provide an assessment of the significance of our

results, we employ bootstrapping (Wu, 1986) to randomly reassign the recorded day of draining to the recorded lake locations, creating 50 new samples of the original data. We then conduct nearest neighbour analyses on the bootstrapped data and calculate the mean and standard deviation of the number of lakes draining on the same day as another. When comparing this to our original nearest neighbour analysis, we interpret that a clustering effect is occurring if the number of lakes that drain in conjunction with their k-nearest neighbour (k=1 being the closest neighbour, k= 2 the second and so on) exceeds one standard deviation from the mean of the bootstrapped dataset.

The results of our cluster analysis shown in Figure 6.4a & b can be partitioned into three groups. The first group of 'local' lakes contains lakes which drain on the same day as their first 3 nearest neighbours, and is characterised by a substantial peak in the number of lakes draining on the same day. A second group of 'regional' lakes contains lakes which drain on the same day as their 4^{th} to ~25^{th} nearest neighbours and also fall beyond 1 standard deviation from the mean of the number of lakes draining on the same day as their k nearest neighbour in the random bootstrapped distribution. A third group of 'distal' lakes, contains lakes which drain on the same day as lakes sited farther than their 25^{th} nearest neighbour number and fall less than 1 standard deviation from the bootstrapped sample mean.

'Local' lake drainage events occurred within an average distance of approximately 5 km. In total 94 or 37% of lakes drained with at least one of its first 3 nearest neighbours or they drained with a lake which had it as one of the other lakes' 3 nearest neighbours. 'Regional' lake drainage events occurred over an average distance of ~15 km. We explored the spatial structure of this intermediate group by re-assigning the position of lakes in latitude (north to south) and longitude (east to west), maintaining the same drainage days and then repeating the nearest neighbour analysis (Figure 6.4c & d). The strength of clustering within this intermediate group is destroyed by reassigning lake positions with longitude but not with latitude; compare the green lines in Figure 6.4c & d. This suggests that the moderate-clustering is related to some effect relevant in an east-west direction only (i.e. the

progression of lake formation and draining with elevation throughout the melt season- see Figure 6.3a & c and Sundal *et al.*, (2009)). In the group of distal lakes, where the number of lakes draining on the same day as their 25th or greater nearest neighbour does not exceed one standard deviation from the mean of the bootstrapped data, any clustering of lake drainage events can be attributed to chance.

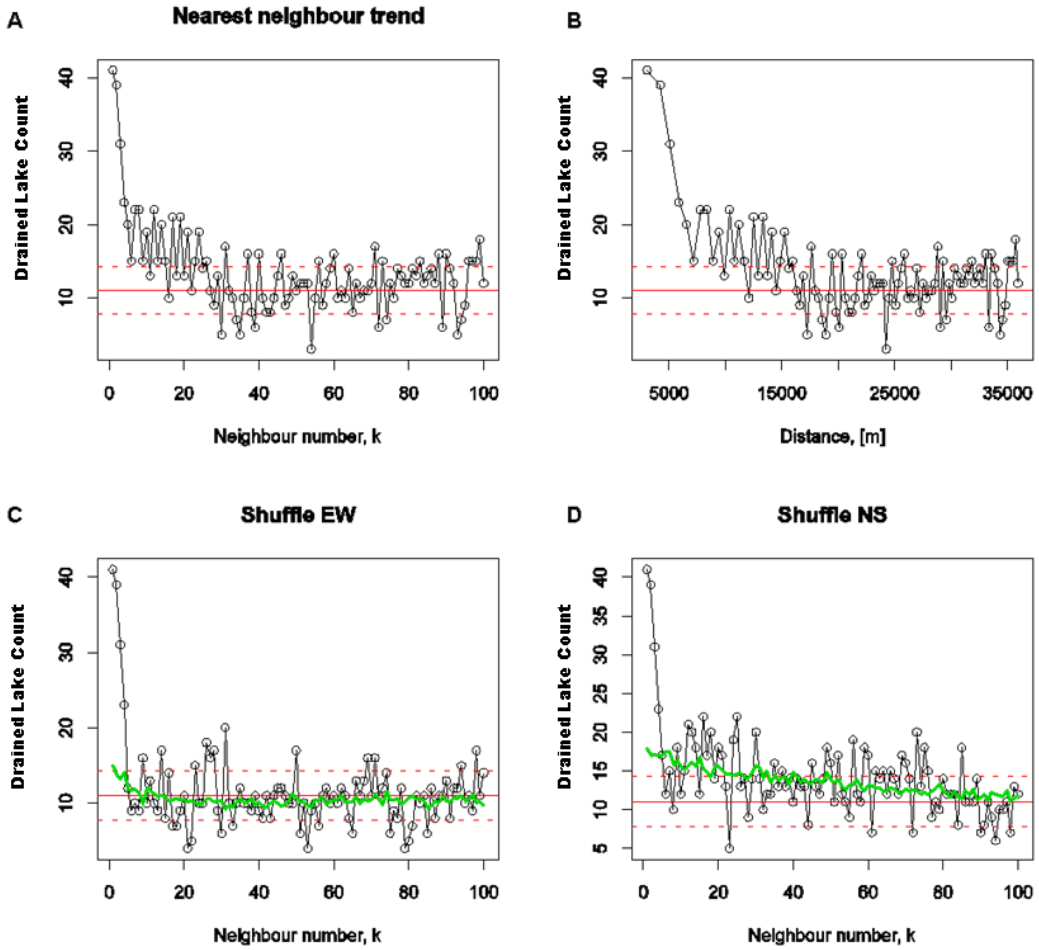

Figure 6.4: Number of lakes that drain with their kth nearest neighbour as a function of a) k and b) mean distance to kth nearest neighbour and as a function of k when shuffled c EW and d) NS. The solid red line represents the sample mean and the red dotted line the standard deviation of the bootstrapped data. The green line in c and d is the moving average (averaged over 50 samples) of the data.

We applied a similar nearest neighbour analysis to lakes draining one day apart (Figure 6.5a) in order to investigate the timescale over which clustered lake drainage events may occur. We observed no significant peak in the number of lakes draining

within one day of any of the nearest neighbours (Figure 6.5a) and so we conclude that clustered lake drainage events do not span consecutive days. We also considered the effect of elevation on clustering (i.e. the first 3 nearest neighbours of a lake) (Figure 6.5b). A higher proportion of lakes drain in clusters at low elevations (700-800 m a.s.l.) and high elevations (1400-1500 m a.s.l.) as compared to those at mid elevations (>60% at high and low elevations relative to 20% at mid elevations).

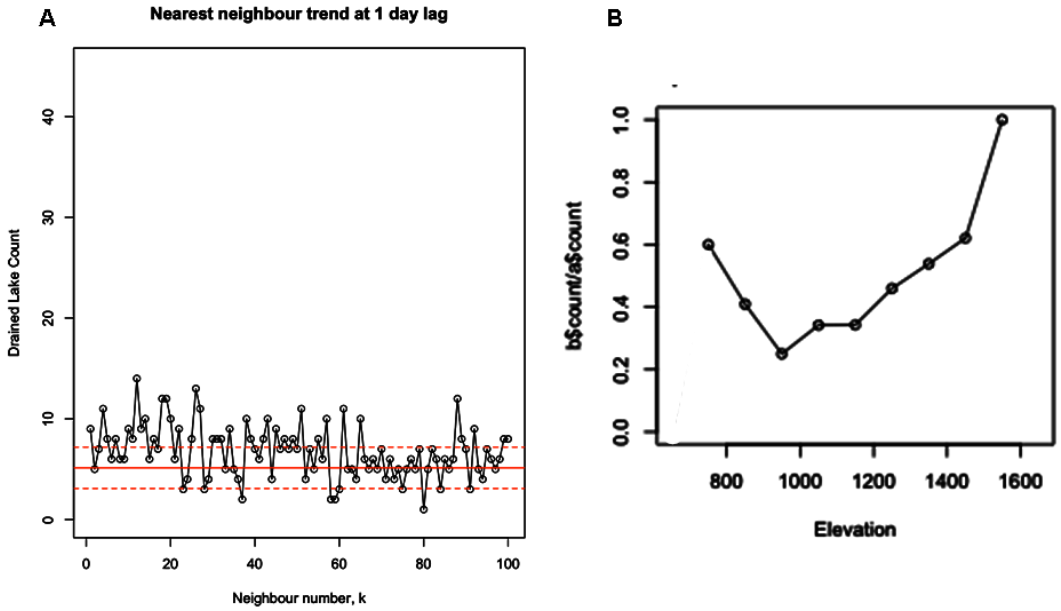

Figure 6.5: A) Number of lakes which drain one day apart from their kth nearest neighbour as a function of k. The solid red line represents the sample mean and the red dotted line the standard deviation of the bootstrapped data. B) The proportion of lakes which drain in clusters by elevation.

We explored the potential for lakes to form at elevations beyond which they form today in the event of a warmer climate by investigating the presence of surface depressions in IceBridge flight lines extending up to 2600 m a.s.l.. In this data we identify any surface depressions by mapping the occurrence of slope reversals along the flight lines. We then analysed the frequencies of reverse slopes with elevation (Figure 6.6a). We find reverse slopes occurring to the highest elevations recorded in the flight lines indicating the potential for lakes to form up to at least this elevation if the regional climate were to warm sufficiently for melting and runoff to occur in this area. We find no clear trend in the frequency of reverse slopes with elevation (Figure 6.6a), although it appears from the profile (Figure 6.6b) that as elevation increases reverse slopes occur at greater intervals and in larger groups indicating that as

elevation increases the number of surface depressions decreases but their sizes increase.

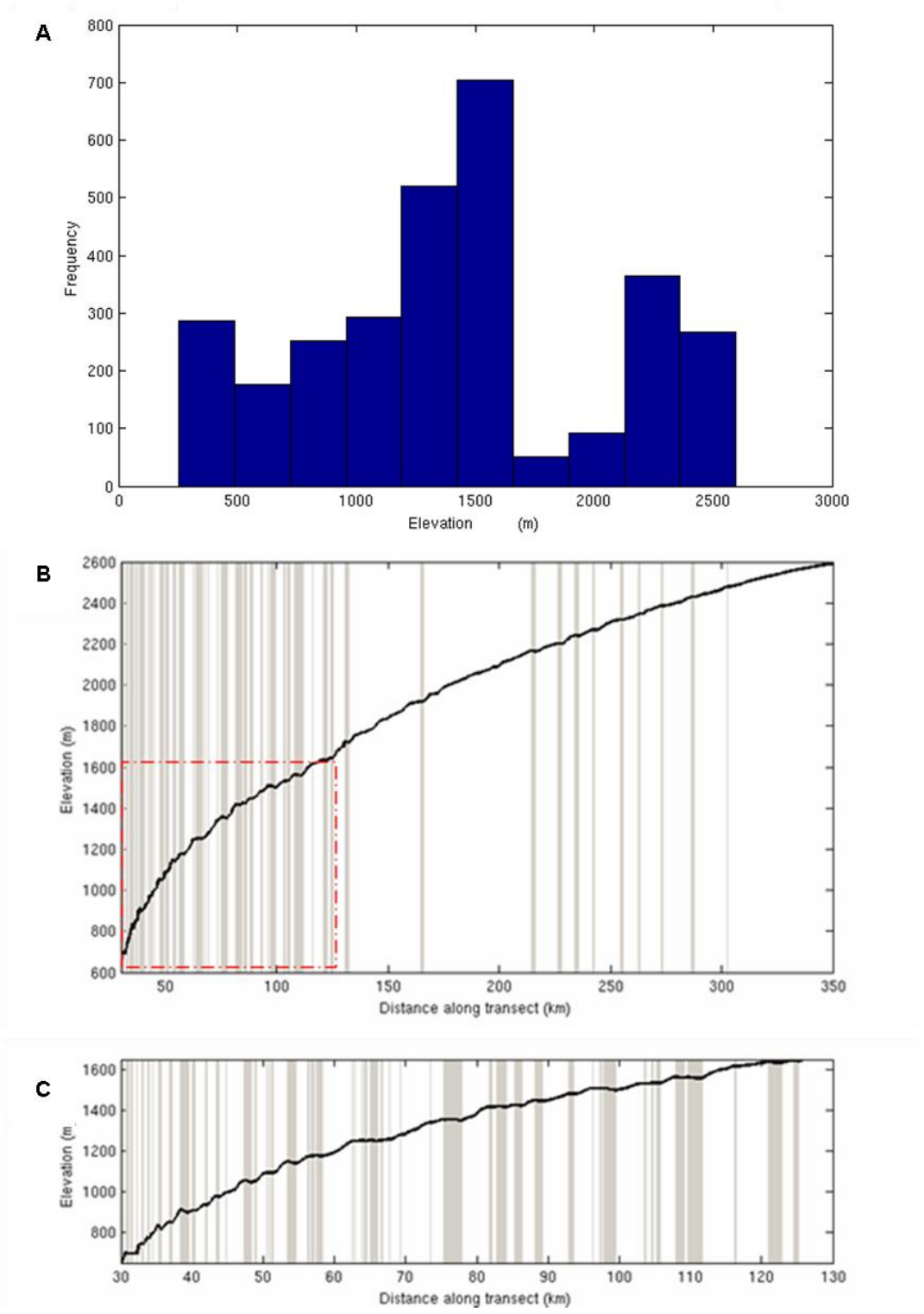

Figure 6.6: A) Frequency distribution of reverse slopes identified in 3 IceBridge ATM lines (locations shown in Figure 6.1). B) Slope profile of one IceBridge ATM line with distance from the margin; the vertical grey lines represent the location of reverse slopes and the red box is the area over which we conduct the current lake analysis and shown in more detail in C.

We investigate the future altitudinal extent of lake formation and drainage using the IPCC forecast of 2ºC warming in Greenland by 2050 (Meehl *et al.*, 2007) as a reference. We apply +2ºC to all the data points in our temperature data for 2003 and extrapolate these temperatures to higher elevations by taking an average of the lapse rates calculated over 1000 m (this gives -0.39ºC/100m, which is comparable to the lapse rates calculated in this region by Steffen and Box (2001)). We find cumulative PDD temperatures comparable to those found at ~1550 m (approximately the limit for lake formation and drainage in 2003) up to 2100 m. Because 2003 was a particularly warm year (the warmest year on record in Greenland between the late 1950's and 2006 (Hanna *et al.*, 2008)), this limit may not be representative of an average limit in 2050.

6.5 Discussion

6.5.1 Distribution of lakes

The fractional coverage of lakes that form on the surface of the GrIS is a function of their density and size. We identify clear trends in each of these parameters with elevation, and we suggest that these trends are related to changes in the ice sheet thickness through the influence it has on surface topography and the propensity of hydrofracturing. Supraglacial lakes have been found to form in depressions that, because they have fixed positions in time, are thought to be the surface expressions of subglacial topography (Echelmeyer *et al.*, 1991). Increasing ice thickness suppresses the expression of subglacial features (Kamb and Echelmeyer, 1986) and so, assuming regular variations in the subglacial topography, this will lead to a decrease in the number of surface depressions. This provides an explanation for the observed decrease in the density of lakes with increasing ice sheet elevations. We recognise, however, that the subglacial relief does vary over the ice sheet bed (Bamber *et al.*, 2001b) and that this too will introduce some spatial variability into the density of surface depressions seen on the ice sheet surface. Furthermore, at low elevations, where the ice is thinner, the observed low density of lakes does not fit

with the above explanation. Instead this may be due to the greater presence of smaller lakes at low elevations which are not detected in the MODIS imagery. In addition, the presence of permanent moulins (e.g. Echelmeyer *et al.,* 1991), which are able to form as a consequence of thinner ice and higher tensile stresses at low elevations, may also lead to fewer areas where water is able to pond.

The high proportion of lakes on the ice sheet surface that drain (89%) suggests the maximum size that lakes reach may be governed by factors which control their drainage. It has been proposed that lakes drain rapidly through their beds by fracturing of water filled crevasses (e.g. Boon and Sharp, 2003; Das *et al.,* 2008). The theory of fracture mechanics suggests that the depth to which a water-filled crevasse may propagate is dependent on the balance between the ice overburden pressure, the far-field tensile stresses and the fluid pressure of water within the crack; if there is a sufficient volume of water in a crack it may propagate to the bed of the ice sheet (e.g. Weertman, 1973; van der Veen, 1998, 2007; Alley *et al.,* 2005b). Since ice overburden pressure increases, and tensile stresses decrease with increasing ice thickness (Kamb and Echelmeyer, 1986), the volume of water required for fracture propagation and lake drainage to occur will increase with increasing ice thickness. Assuming that the surface area of a lake is proportional to its volume (e.g. Amador, 2009), this may explain why larger lakes form at higher elevations.

6.5.2 Lake drainage

The increasing proportion of lakes that do not drain with increasing elevation also may be explained by the impact of ice thickness on the propensity of hydrofracturing. We find no significant difference in the size of lakes which do or do not drain at any elevation. This suggests that the decrease in proportion of lakes which drain with altitude is not governed by limited water supply; although we do recognise that the altitudinal extent of lake formation is limited by availability of surface runoff. This trend may alternatively result from decreased crevassing at higher elevations which stems from reduced tensile stresses. This suggestion is supported by the findings of Catania *et al.,* (2008) who, using ice-penetrating radar

surveys to identify the locations of possible moulins, find that the number of potential moulins (or fractures) reduces towards the ELA and suggest that this is due to decreased tensile stresses and crevasses as ice thickness increases and the influence of bed topography is reduced. It is also interesting to note that, although the lakes which do not drain are present on the ice sheet for a substantially longer amount of time than those that do drain and although it may be expected that they become substantially larger, they do not. This may be due to partial drainage through overland channels.

A substantial proportion (37%) of lakes drain together in clusters. This leads us to believe that the drainage of one lake may trigger the drainage of other lakes nearby and this may due to the effect of melt-induced acceleration of ice flow (e.g. Zwally *et al.,* 2002; Das *et al.,* 2008). Increased flow would lead to an increase in local tensile stresses and thereby increase the likelihood of hydrofracture beneath other nearby lakes containing sufficient volumes of water. The clustering of lake drainage events occurs over length scales of up to 5km, which is comparable to the scale (<10 km) over which longitudinal coupling of velocity changes have been found to occur in this sector of the GrIS (Bartholomew *et al.,* 2010). It is found that higher proportions of lakes drain in clusters at high (1400-1500 m a.s.l.) and low (700-800 m a.s.l.) elevations than at mid elevations. This may be because at low elevations more lakes are close to the threshold for draining at any one time (due to higher tensile stresses and thinner ice), whereas, at high elevations the lake drainage induced speed up may, in many cases, be required to generate stress conditions to enable hydrofracturing (i.e. increased tensile stresses).

6.5.3 Timing of lake drainage events relative to PDD temperatures

The timing/ cumulative PDD temperatures (a proxy for melt) before lake drainage is a function of the timing/ cumulative PDD temperatures at the initiation of lakes, plus the days/ PDD temperatures which occur whilst the lake is present on the ice sheet surface. Our observations show that lakes drain later at higher elevations, in keeping with the findings of Sundal *et al.,* (2009) and this is due to the combined effect of a

later day of formation and a longer duration on the ice sheet surface. Lakes form later at higher elevations as their formation tracks the delayed onset of positive temperatures (and therefore melting) to higher ice sheet elevations. A possible explanation for the shorter lake residence times at lower elevations is that the lakes are typically smaller at the time of drainage and so less melting is required for hydrofracturing and lake drainage; this assertion is supported by our finding that relatively little cumulative melting occurs during this period at low elevations (Figure 6.3f). This explanation does not, however, account for the longer residence times of lakes at higher elevations, despite their typically larger lake sizes (Figure 6.2c). We observe a decrease in the PDD temperatures during the residence times of lakes as compared to lakes at lower elevations elevations. We suggest instead that lakes at higher elevations have longer residence times due to a decrease in melt intensity with increasing elevation which results from increased surface albedo due to an increase in snow cover (e.g. Lang and Braun, 1990; Hock, 2003).

The trends in PDD temperatures with elevation prior to drainage suggests that lake drainage is more sensitive to the PDD temperatures occurring whilst lakes are present on the ice surface rather than those prior to their formation (Figure 6.3b, d & f). As previously mentioned, despite an increase in lake sizes and a probable decrease in surface melt intensity with increasing elevation, the PDD temperature whilst lakes are present on the ice sheet surface decreases with elevation. This can be explained by the general increase in the size of surface hydrological catchment with elevation and distance from the ice margin (Thomsen *et al.*, 1988, 1989) which enables larger volumes of water to be delivered to each lake for a given quantity of surface melting.

6.5.4 Projecting lake formation and drainage to higher elevations

Our results show that surface depressions are present on the ice sheet surface at elevations up to 2600 m a.s.l. (close to the ice divide), which demonstrates that there is a potential for lakes to develop much further inland than they do at present if the area of the ice sheet exposed to seasonal surface melt were to increase (e.g. in a warmer climate). A simple analysis suggests that a 2º C rise in atmospheric

temperature relative to 2003 levels results in melting sufficient for lake formation up to approximately 2100 m, almost 500 m higher than in 2003. However, in light of our other finding which suggests that the frequency of lake drainage tends to decrease with increasing elevation we suggest that the density, fractional coverage and potential for drainage of lakes at 2100 m a.s.l. could be small. This in turn suggests that the potential impact of more widespread lake drainage events on rates of ice flow may also be small. Further years of data and from other regions of the ice sheet are required in order to validate our findings and claims.

6.6 Conclusions

MODIS images from the summer of 2003 have been used to map spatial and temporal trends in the distribution of lakes in the Russell Glacier region, at the west margin of the GrIS. The observations show clear trends in the coverage, density and numbers of lakes with elevation. It was found that lakes increase in coverage, density and size up to mid-elevations (~1100 m a.s.l.), after which, the coverage and density of lakes decreases, and the average size of lakes continues to increase with elevation up to ~1600 m a.s.l. (the limit of lake formation in 2003). Clear trends are observed to exist between lake elevation and the Julian days and the cumulative positive temperatures required for lakes to form and drain. This suggests that it may be possible to predict the timing of lake formation and drainage by elevation which has significant implications for model parameterisation. It was also found that the proportion of lakes which drain decreases from 100% below 950 m a.s.l. to 11% in lakes observed above 1550 m a.s.l.. It is proposed that the trends in the distribution and drainage of lakes with elevation are predominantly the result of changes in ice thickness and horizontal strain rates because of the effect that these have on subduing ice surface topography, tensile stresses and therefore hydrofracturing.

The drainage of lakes in clusters was investigated. It was found that 37% of supraglacial lakes which drained, drained on the same day as lakes less then 5 km away. One possible explanation for why clustering of lake drainage events may occur, is that increased ice velocity following one lake drainage event (Das *et al.,*

2008) will increase local tensile stresses and therefore reduce the threshold volume of water required for hydrofracturing to below the volumes stored in local lakes, allowing them to drain also.

The clear trends found to exist in the distribution and drainage of lakes with altitude in the western, Russell glacier region of the GrIS, may be able to be extrapolated to other regions and higher elevations of the GrIS and thereby provide a means of parameterising supraglacial lake area, density, coverage and drainage in ice sheet models. Using ATM surface profile data from the region we identify surface depressions, and therefore the potential for supraglacial lake development, up to 2600 m. However, our observations of the current distribution of lake formation and drainage with elevation suggest that the ice sheet conditions at high elevations may be less favourable to large areal coverage and drainage of lakes. If this is the case, the potential volume of water which may reach the bed at such altitudes will be small and this may limit any melt induced ice acceleration at these altitudes in future.

6.7 Limitations

The results presented in this chapter were subject to the following limitations:

- Due to the low resolution of the MODIS images (250 m) used to identify the locations and areas of lakes, any small lakes (approximately <0.1 km^2) present on the ice could not be identified automatically (Sundal *et al.*, 2009). By manually identifying the times of lake formation and drainage some of the inaccuracy this may introduce was overcome. There remains however, a limit to the size of lakes which can be identified and this will introduce error into the timing of lake formation and also the mis-identification of many small lakes.

- Because MODIS is an optical imaging sensor, surface conditions are not imaged when there is cloud cover. This led to gaps in the coverage of lake evolution of up to a week (Figure 6.3a & c). This introduces some uncertainty into the timing of lake formation and drainage. However, the gaps in the data

are, on the whole, evenly spread throughout the period of analysis (Figure 6.3a & c) and so will not be a major source of bias in our data.

- Since only one year of data within a single survey area was presented, the findings remain to be validated.

Chapter 7: Synthesis and conclusions

7.1 Introduction

This thesis has investigated seasonal flow variability at marine- and land-terminating glaciers and the physical processes which govern them, in particular the formation and drainage of supraglacial lakes. An incomplete understanding of the physical processes that control ice dynamics has been identified as a major uncertainty in current predictions of the response of the GrIS to climate change (Lemke *et al.*, 2007). In order to improve our understanding of these uncertainties, this thesis has the following objectives:

1. To determine the seasonal velocities of land- and marine-terminating glaciers in the northeast of Greenland using SAR intensity tracking, and to infer the mechanisms controlling their seasonal flow patterns by comparing ice motion with air temperature, supraglacial lake evolution, sea-ice conditions and fluctuations in positions of the ice front (Chapter 4).

2. To investigate the distribution and factors controlling supraglacial lake formation and drainage, and to explore methods for predicting the spread and behaviour of lakes in a warming climate. Specifically the objectives are:

    i) To assess the ability of using a high resolution Digital Elevation Model (DEM) to identify and therefore predict the location of supraglacial lakes in the northeast of Greenland.

    ii) To investigate current spatial and temporal trends in the formation and drainage of lakes in the west of Greenland to predict the future potential for lake drainage events at elevations beyond which they currently form.

This chapter will present a summary and synthesis (Section 7.2) of the principal conclusions derived from this thesis in relation to the objectives outlined in Chapter 3 and above. Section 7.3 places the conclusions into a wider context and Section 7.4 explores the potential for future research to extend the work presented in this thesis.

7.2 Summary of the principal conclusions

7.2.1 Seasonal velocity variability in the northeast of Greenland

Knowledge of the links between GrIS ice dynamics and oceanic and atmospheric forcing is incomplete; this is a major limitation of ice sheet dynamic models and forecasts of future ice sheet changes (Meehl *et al.,* 2007). While some areas in Greenland have been the focus of numerous recent studies (in particular the southeast and west coasts) much less is known about the north east of the ice sheet. The aim of Chapter 4 was to investigate the influence of glacier terminus conditions, and the associated forcing mechanisms, on seasonal ice velocities at land- and marine-terminating glaciers in the northeast of Greenland. The first seasonal dataset of ice velocity for the northeast Zackenberg region of the GrIS is presented. The data set contains velocity estimates for three glaciers, two of which are marine-terminating and one land-terminating. The velocity data was derived from ERS SAR intensity tracking using 18 images acquired between March 1995 and March 1996. Average wintertime velocities of 140±42 myr^{-1} were calculated at land-terminating Wordie Gletscher, and 171±42 myr^{-1} and 248±42 myr^{-1} at marine-terminating Waltershausen and Adolf Hoel Gletschers respectively. Spatial trends in the flow of these glaciers were examined and it was found that Adolf Hoel Gletscher has flow patterns in line with those expected of a marine-terminating glacier and that Wordie and Waltershausen have flow patterns characteristic of land-terminating glaciers. It can be concluded, that although Waltershausen Gletscher terminates in a marine fjord, its subglacial conditions appear largely unaffected by the ocean suggesting that is grounded mostly above sea level.

Seasonal trends in velocity were identified at all three glaciers. Early summer accelerations of 26%, 34% and 16% were observed at Wordie, Waltershausen and

Adolf Hoel Gletschers respectively, which were followed by decelerating flow rates throughout the remainder of the melt season. Using temperature data from a nearby meteorological station and information on the seasonal development of supraglacial lakes, sea ice conditions and ice front positions derived from the SAR imagery, the potential ice velocity forcing mechanisms were investigated. It was found that ice acceleration coincides with the onset of positive temperatures, and that the peak velocities and onset of the subsequent deceleration, coincides with a period of lake drainage at all three glaciers. At some marine-terminating glaciers, seasonal flow variability has been linked to forcing at their termini (e.g Howat *et al.,* 2010). At Adolf Hoel Gletscher, the sea ice in the proglacial fjord was observed to clear and the ice front retreat, during the period of acceleration. However, the terminus position appears stable on an interannual basis and the glacier decelerated during the summer whilst continuing to retreat. Both of these findings are inconsistent with other studies where seasonal flow rates of marine-terminating glaciers are forced from their fronts. It is therefore suggested that all three glaciers appear to respond dynamically to the transfer of surface meltwaters to the bed of the ice sheet, which causes acceleration early in the summer due to increased basal water pressures, followed by deceleration as the subglacial drainage system evolves into a more hydraulically efficient state. These findings are consistent with observation from other land- and 'stable' marine-terminating glaciers in Greenland (e.g. Zwally *et al.,* 2002; van de Wal *et al.,* 2008 Bartholomew *et al.,* 2010; Howat *et al.,* 2010; Anderson *et al.,* 2010).

7.2.2 Comparison of sink and lake locations in the northeast of Greenland

Past research suggests that supraglacial lake drainage provides a means for water to reach the bed of the ice sheet and therefore influence the ice dynamics of the GrIS (e.g. Zwally *et al.,* 2002; Alley *et al.,* 2005b; Das *et al.,* 2008; Howat *et al.,* 2010; Chapter 4). In a warmer climate, it has been postulated that lakes will form higher on the ice sheet surface (Sundal *et al.,* 2009), potentially increasing the influence of supraglacial lake drainage on ice sheet velocities. It is therefore important that future distributions of lakes can be predicted. This forms the principal aim of Chapter 5,

which is to assess the potential for using high resolution DEMs to map the locations and areal extent of supraglacial lakes.

InSAR techniques were used to build a high resolution DEM of the Zackenberg region in the northeast of Greenland. To create the DEM, two descending pass ERS-1 and -2 tandem phase image pairs from the winter of 1995 were used. ICESat GLAS data was used to constrain the DEM. Using this DEM, the areas where lakes may be expected to form were mapped by identifying surface topographic depressions. A comparison was made of the locations and areas of the mapped sinks with lakes identified in four Landsat images acquired between 2000 and 2006. The region covered by the study has a total area of ~5000 km^2 and extends up to 1500 m a.s.l. (the approximate limit of summer melting). Within this region, 428 depressions or sinks were identified in the DEM. The sinks cover an area of 81.4 km^2 and this represents 1.7% of the total ice area included in the analysis. From the optical images, 199 lakes were identified. The lakes cover an area of 29.7 km^2 and this represents 0.6% of the total ice area included in the analysis.

A comparison of the coincidence of locations and areas of lakes and sinks shows that there are 96 locations where both lakes and sinks overlap; this covers a total area of 10.6 km^2, comprising 13% of the total area of sinks and 35.6% of the total area of lakes. This results demonstrate that using sinks to predict the coverage of lakes would lead to a large over-prediction of lake area and also that a large number of lakes would not be identified. Therefore the application of this method to predict lake locations in this part of the GrIS would lead to large inaccuracies. These differences can be attributed to the factors that control the distribution and sizes of lakes (i.e. ice thickness, surface crevassing and surface meltwater availability), and limitations in the quality of the optical data and DEM used to identify the lakes and sinks in this region with complex ice topography. An assessment is provided as to the uncertainty associated with identifying sinks above the current limit of lake formation (~1500 m a.s.l.). At these elevations there appears to be a large amount of noise in the DEM, probably caused by volume scattering of the radar signal in this region. It is concluded that the accuracy of using sinks to predict lake locations in this region may be even worse than below 1500 m a.s.l.

7.2.3 Spatial and temporal trends in lake formation and drainage in the west of Greenland

Chapter 6 begins by repeating a similar analysis to that in Chapter 5, instead for the western margin of the GrIS where the ice surface topography is more subdued, and also, using higher temporal resolution images to identify lakes across the whole of the melt season. Doing so tests the hypotheses set out in the previous chapter, that some of the inaccuracy in lake predictions using sinks stemmed from the limited temporal coverage of images used for identifying lakes and the complex ice surface topography in the northeast region. An InSAR DEM of the region was created, from which sinks were identified. 64 MODIS images from four summers were used to identify lake coverage (Sundal *et al.*, 2009). Sinks were found to cover 7% of the total ice surface area included in the analysis, while lakes cover 4.8%. Only 1% of the area covered by sinks coincides with observed lakes and 47% of the area covered by lakes overlaps with sinks. Although the area of lakes overlapped by sinks is slightly higher than in the northeast, the area of sinks overlapped by lakes is much lower and both remain too inaccurate for the purpose of predicting future lake locations in the absence of substantial methodological or data improvements. In the absence of a procedure for predicting the actual locations and areas of lakes on the ice sheet surface with DEMs, an alternative methodology is investigated for parameterising the distribution of supraglacial lakes by extrapolating the trends observed in current lake distributions.

Chapter 6 examines observed spatial and temporal trends in the formation and drainage of lakes in the western, Russell Glacier region of the GrIS. The aim of this work was to identify the key factors controlling the distribution and drainage of lakes, and assess the potential for future lake development and drainage, at elevations higher than they form at present. In a 9100 km^2 region of the ice sheet margin which extends up to 1700 m a.s.l, 47 MODIS images from the summer of 2003 were used to examine trends in lake formation and drainage with respect to elevation, day and air temperature (as PDD). 312 lakes were identified which cover a total area of 227 km^2 and equate to 2.5% areal coverage of the region. Above 950 m a.s.l., the

percentage area coverage of lakes decreases (1.6% >1550 m a.s.l.) as a result of a decrease in the density of lakes, although the average area of individual lakes increases. The proportion of lakes which drain decreases from 100% below 950 m a.s.l. to 11% above 1550 m a.s.l.. It is proposed that these trends are the result of increasing ice thickness because of the effect that this has on subduing the influence of subglacial topography on ice surface topography (i.e. surface depressions), and tensile stresses and therefore lowering the likelihood of hydrofracturing.

The simultaneous draining of clusters of lakes is reported and this effect is quantified using a nearest neighbour analysis. 37% of lakes were found to drain on the same day as lakes less than 5 km away. No clustering effect was found with lakes draining on consecutive days suggesting that this effect is rapid and short-lived. One possible explanation for why clusters of lake drainage events occur is that increased ice flow velocities, resulting from the drainage of the first lake, increase the ice tensile stresses locally, thereby reducing the threshold volume of water required for hydrofracturing beneath nearby lakes. It is found that higher proportions of lakes drain in clusters at high (1400-1500 m a.s.l.) and low (700-800 m a.s.l.) elevations than at mid elevations. This may be because at low elevations, more lakes are close to the threshold for drainage at any one time (due to higher tensile stresses and thinner ice) and at high elevations, the lake drainage induced speed up is, in many cases, required to generate the conditions necessary to enable hydrofracturing (i.e. increased tensile stresses).

Finally, IceBridge ATM data shows that ice surface depressions exist over 300 km into the ice sheet interior. This indicates that lakes have the potential to form up to at least 2600 m a.s.l. in this region (close to the ice divide) in the event of increased surface temperatures. However, the previous findings of this chapter, suggest that the lake coverage and occurrence of drainage decrease with elevation. As a result, the potential volume of water supplied to the ice bed through this mechanism will likely also decrease.

7.2.4 Synthesis

In summary, the clear link between seasonal ice velocities and glacier hydrology reported here from northeast Greenland (Chapter 4) is similar to findings at other land- and marine- terminating glaciers in Greenland (e.g. Zwally *et al.,* 2002; van de Wal *et al.,* 2008 Bartholomew *et al.,* 2010; Howat *et al.,* 2010; Anderson *et al.,* 2010; Sundal *et al.,* 2011). Supraglacial lake drainage events have been found to be important in Greenland as they enable surface meltwater to reach the bed through thick ice (Das *et al.,* 2008); in Chapter 4 the timing of lake drainage events are found to be correlated with peak velocities and the subsequent onset of ice deceleration, suggesting their significance for ice sheet hydrology and flow rates in this section of the GrIS. It has previously been found that in warmer years more lakes form at higher altitudes on the ice sheet surface (Sundal *et al.,* 2009). This has led to the suggestion that in warmer climates lakes will form higher on the ice sheet surface (Sundal *et al.,* 2009). This will likely cause ice at higher elevations to undergo seasonal speedups (Bartholomew *et al.,* in press), thus increasing the transfer of mass from high to low elevations and increasing the rates of mass loss (Alley *et al.,* 2005b).

Given the potential importance of lake development and drainage, the aim of Chapter 5 was to develop a methodology for predicting future supraglacial lake locations using a DEM to map the locations of surface depressions where water will pond to form lakes. A large number of surface depressions were mapped. However, a comparison with the locations and areas of lakes currently forming on the ice sheet using optical images shows that there is poor agreement between the locations and areas of lakes and sinks in both the northeast and west of Greenland. This is due to limitations in the DEM which prevents depressions from being accurately identified, and the physical differences which exist between lakes and sinks, for example, lakes may drain before they reach the full capacity of the sink. An alternative method for parameterising supraglacial lake distributions and drainage in ice sheet models may be found from extrapolating current trends in the temporal and spatial extent of supraglacial lake evolution. In Chapter 6, patterns of lake formation and drainage are

examined with respect to time and elevation in the west of Greenland using satellite derived optical imagery (MODIS). Statistically significant trends are observed in the fractional area coverage of lakes, their density and size with elevation, suggesting that it may be possible to extrapolate these trends to other regions and higher elevations (i.e. for warmer climate scenarios). Above 950 m a.s.l., it is found that lake coverage and drainage decreases with increasing elevation and therefore ice thicknesses. This suggests that although the temperature and surface conditions may exist for lake formation to occur well into the interior of the ice sheet in future, the ice sheet conditions at these elevations may not be favourable for lake drainage. This would result in an altitudinal limit, above which, lake drainage can no longer occur. This would prevent surface melt water reaching the bed at high elevations and thereby limit the inland extent of hydrologically induced ice speed-ups.

7.3 Wider implications

The conclusions of this thesis, highlighted in the previous section, have a number of implications for the future of the GrIS, its potential effect on sea level change and our ability to model accurately the future evolution of the ice sheet.

7.3.1 Seasonal velocity variability

Ice sheet velocity is critical in terms of mass loss from the GrIS as it governs rates of ice discharge from marine-terminating glaciers (e.g. Rignot and Kanagaratnam, 2006; Rignot *et al.,* 2008; van den Broeke *et al.,* 2009) and the transfer of mass from high to low elevations (e.g. Parizek and Alley, 2004). Observations have shown that rapid and large fluctuations occur in ice flow rates of the Greenland outlet glaciers (e.g. Joughin *et al.,* 2004; Luckman *et al.,* 2006; Rignot and Kanagaratnam, 2006; Howat *et al.,* 2007; 2008). At present these observations cannot be fully explained and this has led to large uncertainties in models predicting mass losses from the Greenland Ice Sheet (Meehl *et al..,* 2007).

Fluctuations in GrIS velocities have been linked to changes in ocean (e.g. Holland *et al.,* 2008; Howat *et al.,* 2008; Nick *et al.,* 2009; Amundson *et al.,* 2010) and

atmospheric conditions (e.g. Zwally *et al.*, 2002; van de Wal *et al.*, 2008; Shepherd *et al.*, 2009; Bartholomew *et al.*, 2010; Howat *et al.*, 2010; Sundal *et al.*, 2011). Ice flow rates at land- and 'stable' marine-terminating margins (i.e. with ice fronts that are neither advancing or retreating on yearly timescales) have been found to respond seasonally to changes in air temperatures and the consequent surface melt rates in Greenland (e.g. Zwally *et al.*, 2002; Bartholomew *et al.*, 2010; Howat *et al.*, 2010; Anderson *et al.*, 2010). It has been inferred that water is transferred from the ice surface to the bed where it enhances basal sliding (e.g. Zwally *et al.*, 2002; Das *et al.*, 2008) and that this effect is regulated on a seasonal basis by the evolution of the subglacial drainage system from an inefficient to an efficient state (e.g. van de Wal *et al.*, 2008; Bartholomew *et al.*, 2010). To date, all of the research into this hydrology-dynamics forcing mechanism in Greenland has focussed on the western and south-eastern margins of the ice sheet (Figure 7.1). The results presented in Chapter 4 imply that similar processes also operate at the northeastern margin of the ice sheet.

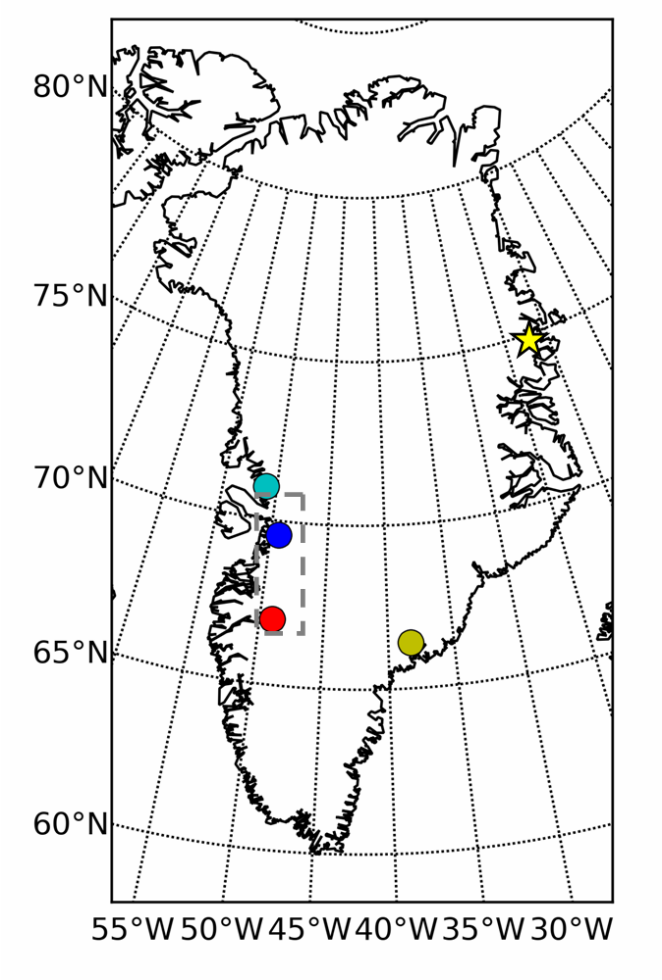

Figure 7.1: The positions of studies looking at seasonal velocity variations in Greenland. Previous studies by van de Wal *et al.*, (2008), Shepherd *et al.*, (2009), Bartholomew *et al.*, (2010) Sundal *et al.*, (2011) (red dot), Zwally *et al.*, (2002) (blue dot), Howat *et al.*, (2010) (light blue dot), Andersen *et al.*, (2010) (green dot) and Joughin *et al.*, (2008c) (grey dotted box). The region covered by the research presented in Chapter 4 is shown by the yellow star.

These findings extend, spatially, our knowledge of the processes controlling flow dynamics across the Greenland Ice Sheet and provide further support for earlier findings of seasonal links between ice dynamics and surface melting in Greenland, especially at marine-terminating margins where few studies of such nature have been conducted (Anderson *et al.*, 2010). Together, these and previous findings suggest these processes are likely to be occurring universally around the ice sheet margin where surface meltwater is generated. Given that observations have shown that surface melting occurs around the whole periphery of the ice sheet in summer (e.g. Fettweis *et al.*, 2007-Figure 7.2) it can be assumed that summer speed-ups are

occurring in these regions also. Observations have also shown that the region of summer melting has increased in past decades (e.g. Fettweis *et al.*, 2007-Figure 7.2) and forecasts suggest that it will continue to increase in future (Meehl *et al.*, 2007). Therefore, in future, more of the ice sheet margin would be expected to experience melt induced seasonal accelerations. In some areas, where runoff is below a threshold described by Schoof (2010) this will increase the overall annual flow velocities and the transfer of mass to low elevations, which in turn will increase rates of surface ablation and ultimately rates of mass loss. However, in areas where runoff is above this threshold, more runoff is expected to cause a deceleration of ice flow. Therefore, understanding these complex interactions between surface melting and ice velocities for the whole of the ice sheet, where melting occurs, is critical for ice sheet modelling and thus forecasts of ice sheet mass balance; the findings in Chapter 4 will facilitate this.

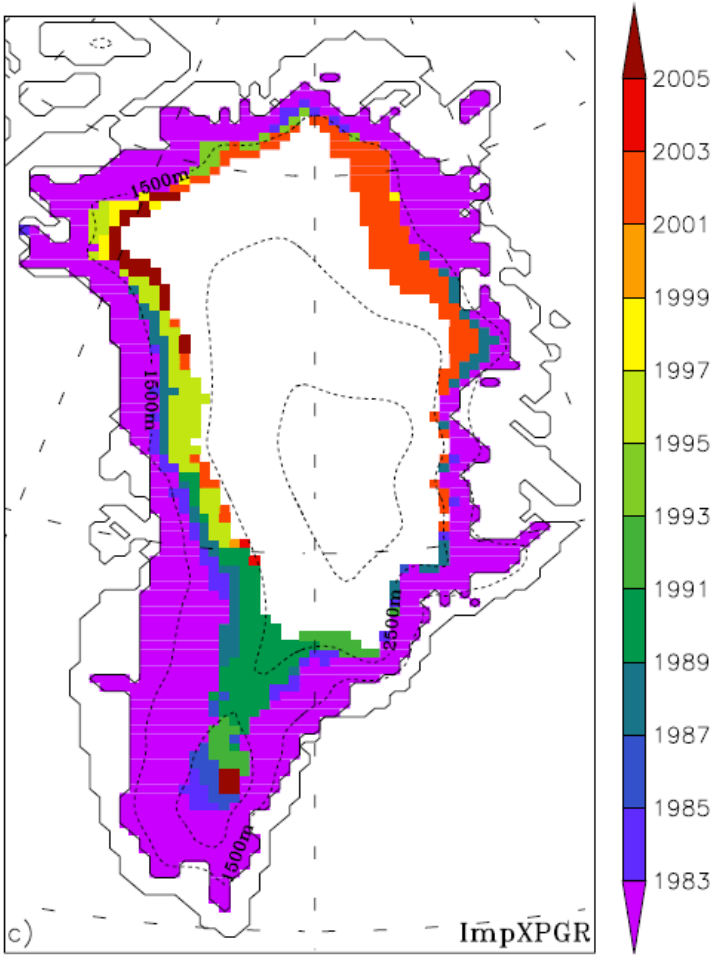

Figure 7.2: A map representing the years in which melt is recorded in a region of the GrIS for the first time. Taken from Fettweis *et al.*, (2007).

7.3.2 Complex tidewater glacier behaviour

Observations have revealed that the most dramatic dynamic changes and mass losses from the GrIS are occurring at the marine-terminating outlet glaciers (e.g. Abdalati *et al.*, 2001; Krabill *et al.*, 2004; Sole *et al.*, 2008; Thomas *et al.*, 2009; Pritchard *et al.*, 2009). However, the dynamics of marine-terminating glaciers are highly complex (e.g. Meier and Post, 1987; Howat *et al.*, 2008; 2010). This is because there are so many factors which can influence their flow dynamics, including: meltwater inputs, ocean temperatures, calving, sea ice concentrations and thickness, ice thickness, subglacial topography and basin geometry, and all these factors vary for each

individual glacier. Although significant steps have been taken to understand the forcing mechanisms of tidewater glacier dynamics in Greenland (e.g. Holland *et al.*,2008; Straneo *et al.,* 2010; Murray *et al.,* 2011), their complexity ensures the processes and behaviour are hard to constrain.

In Chapter 4, a large interannual difference in winter velocities at an apparently stable marine- terminating glacier in the northeast of Greenland are reported. These differences remain unexplained and they serve to highlight another facet of the complexity of tidewater glaciers that, as of yet, is not understood. The limit to our understanding of the dynamics of these glaciers ultimately restricts our ability to represent them comprehensively or accurately in numerical models. Indeed, given the complexity of the behaviour of each individual tidewater glacier, an attempt to comprehensively model the dynamics of the marine-terminating margin of the GrIS may be out of reach. Instead, a means of characterising certain behaviour and simplifying these systems may be the most appropriate method for representing them in ice sheet models.

7.3.3 Predicting the future formation and drainage of lakes

The drainage of supraglacial lakes establishes pathways for water to go from the surface to the bed of the ice where the ice is thick, and overburden pressures large (e.g. Alley *et al.,* 2005b; Das *et al.,* 2008). This is important as it affects ice velocities and mass loss. It has been observed that in warm summers lakes form at higher elevations than in cooler summers (Sundal *et al.,* 2009). As a consequence it has been suggested that in the future, as climate warms (Lemke *et al.,* 2007), lakes will form at higher altitudes than at present and so the area with connections between the surface and bed may increase (Sundal *et al.,* 2009). This could potentially increase the rate of ice flow (Das *et al.,* 2008) and mass loss. Therefore, it is important that we are able to predict lakes which may form and drain at altitudes beyond which they form today.

Although the results presented in Chapter 5 and the beginning of Chapter 6 suggest that this is not currently possible using DEMs, the results presented in Chapter 6

suggest that a prediction of lake formation and drainage at high elevations may be made by extrapolating observed trends in seasonal lake evolution on the ice sheet surface. This work therefore provides a potential methodology for parameterising the distribution and drainage of lakes on the ice sheet surface in models.

The work in Chapter 6 is of further significance as it implies that lakes forming at higher ice sheet elevations, in warmer climates, only have a small chance of draining. This suggests that the transmission of surface meltwater to the bed of the ice, and therefore melt induced acceleration, may not occur at high elevations in a warmer climate. Therefore, a limit to the inland extent of melt induced acceleration may exist. This is significant for forecasting the effects of warming climates and increasing melt area extents on ice velocities as it indicates that the impact of increased surface melting on ice velocities may be spatially restricted. However, conversely, the effect of longitudinal coupling of elevated ice velocities (Price *et al.*, 2008) resulting from lake drainage events at lower elevations, may be expected to induce speed-ups at higher elevations with consequences for tensile stresses i.e. more melt could result in a dynamic response which primes the ice at higher elevations to experience hydrofracture due to increased tensile stresses.

Model and observational studies suggest that once a subglacial drainage system is channelised, ice velocities respond more to short-term spikes in water supply to the bed of the ice, than to changes in mean water flow (Schoof, 2010; Bartholomew *et al.*, in press.). This is because subglacial conduits take several days to enlarge to accommodate meltwater inputs (Schoof, 2010). Therefore, if the volume of water conveyed to the drainage system in a sudden event exceeds its capacity for efficient water evacuation, subglacial water pressure, and therefore basal sliding, will increase (Schoof, 2010). Such sudden events include rainfall and lake drainage events.

Chapter 6 reports that a substantial proportion of draining lakes, drain in clusters over the course of one day (37%). A cluster of lakes draining will lead to a considerably larger volume of water being input into the subglacial system than from just one lake draining. It is likely therefore, that the perturbation to the subglacial drainage system, basal water pressures, basal sliding and ice velocities will also be larger. Furthermore, the net effect on tensile stresses and hydrofracturing up-glacier

(i.e. at higher elevations) of a cluster of lakes draining, as a result of longitudinal coupling (Price *et al.*, 2008), will also be larger than if just one lake drained. Therefore, the drainage of lakes in clusters is potentially important for enabling lake drainage events at high altitudes where few lakes currently drain; this may already be the case, as demonstrated by the large proportion of lakes at high elevations which drain in clusters. Consequently, this clustering effect should be included in ice sheet models of flow dynamics.

7.4 Further work

This thesis has investigated and improved our understanding of the complex processes which control flow variability of the Greenland Ice Sheet. Nevertheless, it is clear that many questions remain and, in relation to the topics addressed in this thesis, there is ample scope for important future work as discussed below.

7.4.1 Future work on velocity variability at the northeast margin of the GrIS

The results presented in Chapter 4 suggest that there is a link between the hydrology and seasonal velocity variations of land- and stable marine- terminating glaciers in the northeast of Greenland. However, the confidence in this suggestion is limited in part by the temporal resolution of the velocity data. Further work, including a field campaign to collect high temporal resolution, ground-based GPS measurements on the glaciers, along with *in-situ* temperature and surface melt data, would enable testing of the findings (c.f. Bartholomew *et al.*, 2010). This would also allow more consistent velocity estimates to be collected which was not possible in this study due to limitations in the spatial coverage of intensity tracking velocity estimates (Figure 4.2) and the lack of available data during the late summer and autumn. Such data would still only allow for a more confident theoretical interpretation of the link between surface hydrology and basal sliding. Forthcoming projects, such as the 'Cryo-egg' project of the University of Bristol (http://sies.bris.ac.uk/~ggbsrl/Cryoegg/home.html), which intend to directly measure the basal environment in Greenland, may provide evidence for the basal hydrological

processes occurring which are currently only inferred. Such 'ground-based' studies are expensive however, and would be difficult in such a remote region, thus limiting their spatial coverage.

The work presented in Chapter 4 could also be extended by broadening the period of study to other years and other glaciers in the region. Doing so would provide a means of investigating interannual differences in seasonal flow variability (similar studies in Greenland are currently restricted to the western margin (Zwally *et al.*, 2002; van de Wal *et al.*, 2008; Sundal *et al.*, 2011) and would provide some context and validation for the findings. In deriving such a dataset of velocity estimates, data from a number of sensors (e.g. Envisat, RADARSAT, Landsat, ASTER) employing a combination of InSAR, optical feature tracking and SAR offset tracking techniques could be used, so as to maximise the number and coverage of velocity estimates.

The limitations in this study resulting from the shortcomings of the meteorological data employed could potentially be overcome by using melt data from coupled climate and surface energy balance models (e.g. Hanna *et al.*, 2005). These models may provide a more accurate representation of the onset of melting, which although not a big problem in the current study due to the low temporal resolution of velocity estimates, would be beneficial in a study with more regular velocity estimates. Furthermore, such data would be valuable for investigating spatial patterns in the link between surface hydrology and glacier velocity and also interannual variability.

An investigation into the subglacial topography of marine-terminating Waltershausen and Adolf Hoel Gletschers would improve any explanation of their flow behaviour as it would provide an indication of to what extent subglacial effective pressures are affected by the depth of the bed below sea level. Such data may be acquired using airborne ground penetrating radar (GPR) surveys (e.g. Gogineni *et al.*, 2001). Such survey data would be invaluable for all marine-terminating glaciers in Greenland, not only for purposes of explaining flow behaviour, but also because it would enable more accurate estimates and model parameterisation of the transition of marine margins to land margins in time (something which is significant for the dynamic behaviour of the ice sheet). The ongoing work of IceBridge hopes to provide this data in the larger tidewater glaciers across the ice sheet (e.g. Sonntag, 2011).

7.4.2 Future work on the use of DEMs to map and predict supraglacial lake coverage

The findings presented in Chapters 5 and 6 report a poor correspondence between the locations of observed lakes and predicted sinks. It may, however, be possible to develop a methodology that would allow DEMs to be used in a predictive capacity for identifying present and future lake locations. This may be achieved by, first of all, accounting for the physical differences between sinks and lakes and also by using a higher resolution DEM. It has been identified that differences between sinks and lakes occur due to differences in the routing and supply of surface meltwater to a sink, the presence of deeply incised subaerial streams that drain lakes and hydrofracturing of ice in the lake bed (Chapter 5). These differences may be accounted for by modelling the depth of water in lakes at which hydrofracturing will occur (e.g. Krawczynski *et al.*, 2009) and by modelling the surface hydrological network using a high resolution DEM combined with modelled surface melt rates to examine the delivery of water to and from lakes (e.g. Palmer *et al.*, 2011).

Given the level of inaccuracy in detecting sink basins (Chapter 5), the resolution of the InSAR DEM used in this study would not be sufficient to fully capture the surface hydrological network and model accurately the routing of surface runoff. In order to capture this and the small/shallow lakes not detected in the InSAR DEM, a higher resolution DEM must be employed. One possibility would be to use airborne laser altimetry with sufficiently close flightline spacing to be able generate a continuous DEM. As airborne laser altimetry has the potential to create DEMs with horizontal resolutions of a few metres and vertical accuracies of less than 10 cm (Knoll and Kerschner, 2009) it would provide very precise mapping of potential lake sites. However, due to the intensive nature of acquiring such a DEM, the potential to produce a map of sinks on an ice sheet-wide scale would be unfeasible.

7.4.3 Future work on understanding and predicting supraglacial lake drainage events

Because the trends observed in lake distribution and drainage reported in Chapter 6 are based on only one year of data from one section of the ice sheet margin, they lack validation. In order to strengthen the outcomes, the analysis conducted in Chapter 6 could be repeated in other areas and in other years in order to validate the observed trends. Repeating the analysis over several years of data would allow for a comparison of patterns in lake drainage events in relatively warm and cool years which may provide an indication as to what causes some lakes to drain and not others. For example, if a selection of lakes does not drain in both cool and warm years alike, this may suggest that the reason for this is not driven by the availability of melt but instead by some structural control of the ice (i.e. its thickness or local tensile stress regime and hence a lack of fractures). By repeating the analysis in several other regions of the ice sheet, it could be determined if the drainage behaviour observed in the Russell region was similar in other regions and whether the patterns observed could be reliably extrapolated across the ice sheet.

To further the understanding of the controls on lake drainage events it would be valuable to investigate the relationship between the volume of water in lakes at the point of draining and the surface stress gradients, and in turn, the relationship of this to ice thickness and elevation. In Chapter 6 the potential importance of this in controlling lake drainage is implied, although the data to develop the argument further is lacking. To do so would require analysis of individual lake characteristics and drainage events. For example, lake volume and depths have previously been derived by measuring the depletion of surface reflectance with increased depth in multispectral image signals (e.g. Box and Ski, 2007; Sneed and Hamilton, 2007; Georgiou *et al.*, 2009). Stress gradients may be calculated from surface velocity maps (e.g. Fastook *et al.*, 1995; Bindschadler *et al.*, 1996) and ice thickness data, as mentioned previously, from GPR (e.g. Gogineni *et al.*, 2001). GPR data has previously been used by Catania *et al.*, (2008) to identify the presence of potential moulins in relation to lakes, suggesting that the number of moulins decreases towards the interior of the ice sheet.

7.5 Concluding remarks

This thesis has investigated key processes which affect the interaction between the climate and ice dynamics of the GrIS and are therefore a key control on the ice sheet's current and future mass balance. It has helped to clarify the processes governing seasonal flow velocities at land- and marine-terminating margins and adds to other suggestions that surface melt-driven velocity variations are likely widespread and perhaps universal across the ablation zone of the GrIS. It has also generated further evidence of the complexity of the processes that control the motion of marine-terminating glaciers thatas yetr cannot be predicted with confidence. Finally, this thesis has demonstrated that parameterising supraglacial lake distribution and evolution using DEMs may not be feasible from current datasets, but significant insights are possible by extrapolation of statistical trends in their current distribution and behaviour.

A critical failing in the current ability to forecast sea level rise, stems from inaccuracies in the modelling of ice dynamics at the ice sheet scale as a result of the failure of current models to incorporate the necessary processes (Meehl *et al.*, 2007). The findings of this thesis provide new observations which can be utilised to improve the accuracy of sea-level rise projections produced by the next generation of ice sheet models.

References

Abdalati, W. Krabill, W., Frederick, E., Manizade, S., Martin, C., Sonntag, J., Swift, R., Thomas, R., Wright, W. and Yungel, J. 2001. Outlet glacier and margin elevation changes: near-coastal thinning of the Greenland ice sheet. *Journal of Geophysical Research***. 106**(D24), 33729-33741.

Abdalati, W., Krabill, W., Frederick, E., Manizade, S., Martin, C., Sonntag, J., Swift, R., Thomas, R., Wright, W. and Yungel, J. 2002. Airborne laser altimetry mapping of the Greenland ice sheet: application to mass balance assessment. *Journal of Geodynamics.* **34** (3-4), 391-403.

Al-Rousan, N. and Petrie, G. 1998. System calibration, geometric accuracy testing and validation of DEM and orthoimage data extracted from SPOT stereopairs using commercially available image processing systems. *International Archives of Photogrammetry and Remote Sensing.* **34**(4), 8-15.

Alsdorf, D. E. and Smith, L. C. 1999. Interferometric SAR observations of ice topography and velocity changes related to the 1996, Gjálp subglacial eruption, Iceland. *International Journal of Remote Sensing*. **20**, 3031-3050.

Alley, R. B., Clark, P. U., Huybrechts, P. and Joughin, I. 2005a. Ice-sheet and sea-level changes. *Science.* **310,** 456-460.

Alley, R. B., Dupont, T. K., Parizek, B. R. and Anandakrishnan, S. 2005b. Access of surface meltwater to the beds of sub-freezing glaciers: Preliminary insights. *Annals of Glaciology.* **40,** 8-14.

Amador, N.S. 2009. *Spatial and temporal characteristics of supra-glacial melt lakes in west-central Greenland from satellite optical remote sensing.* MSc thesis. The Ohio State University. Pp 52.

Amundson, J. M., Fahnestock, M., Truffer, M., Brown, J., Lüthi, M. P., and Motyka, R. J. 2010. Ice mélange dynamics and implications for terminus stability, Jakobshavn Isbræ, Greenland. *Journal of Geophysical Research.* **115,** F01005.

Anderson, M. L., Larsen, T. B., Nettles, M., Elosegui, P., van As, D., Hamilton, G. S., Stearns, L. A., Davis, J. L., Ahlstrom, A. P., de Juan, J., Ekstrom, G., Stenseng, L., Khan, S. A., Forsberg, R. and Dahl-Jensen, D. 2010. Spatial and temporal melt variability at Helheim Glacier, East Greenland, and it effect on ice dynamics. *Journal of Geophysical Research.* **115,** F04041, doi:10.1029/2010JF001760.

Atwood, D. K., Guritz, R. M., Muskett, R. R., Lingle, C. S., Sauber, J. M. and Freymueller, J. T. 2007. DEM control in Arctic Alaska with ICESat laser altimetry. *IEEE Transactions on Geoscience and Remote Sensing.* **45,** (11), 3710-3720.

Bamber, J. L., Ekholm, S., Krabill, W. B. 2001a. A new high-resolution digital elevation model of Greenland fully validated with airborne laser altimeter data. *Journal of Geophysical Research.* **106,** (B4), 6733-6745.

Bamber, J. L., Layberry, R. L. and Gogineni, S. P. 2001b. A new ice thickness and bed data set for the Greenland ice sheet. 1. Measurement, data reduction and errors. *Journal of Geophysical Research.* **106,** D24, 33,773-33,780.

Bamber, J. L., Baldwin, D. J. and Gogineni, S. P. 2003. A new bedrock and surface elevation dataset for modelling the Greenland ice sheet. *Annals of Glaciology.* **37,** 351-356.

Barrand, N. E., Murray, T., James, T. D., Barr, S. L. and Mills, J. P. 2009. Optimising photogrammetric DEMs for glacier volume change assessment using laser-scanning derived ground-control points. *Journal of Glaciology.* **55,** 189. 106-116.

Bartholomaus, T. C., Anderson, R. S, and Anderson, S. P. 2007. Response of glacier basal motion to transient water storage. *Nature Geoscience.* **1,** 33-37.

Bartholomew, I., Nienow, P., Mair, D., Hubbard, A., King, M. A. and Sole, A. 2010. Seasonal evolution of subglacial drainage and acceleration in a Greenland outlet glacier. *Nature Geoscience.***3,** 408-411.

Bartholomew, I., Nienow, P., Sole, A., Mair, D., Cowton, T., King, M. A. and Palmer, S. In press. Seasonal variations in Greenland ice sheet motion: Inland extent and behaviour at higher elevations. *Earth and Planetary Science Letters.*

Benn, D. I., Warren, C. R. and Mottram, R. H. 2007. Calving processes and the dynamics of calving glaciers. *Earth-Science Reviews.* **82,** 143-179.

Bindschadler, R. A. and Scambos, T. A. 1991. Satellite-image-derived velocity field of an Antarctic Ice Stream. *Science.* **252,** 242-246.

Bindschadler, R. and Vornberger, P. 1992. Interpretation of SAR imagery of the Greenland Ice Sheet using coregistered TM imagery. *Remote Sensing of the Environment.* **42,** 167-175.

Bindshcadler, R., Vornberger, P., Blakenship, D., Scambos, T. and Jacobel, R. 1996. Surface velocity and mass balance of Ice Streams D and E, West Antarctica. *Journal of Glaciology*. **42,** (142), 461-475.

Bindshadler, R. A., Fahnestock, M., and Sigmund, A. 1999. Comparison of Greenland ice sheet topography measured by TOPSAR and airborne laser altimetry. *IEEE Transactions on Geoscience and Remote Sensing*, **37,** (5), 2530-2535.

Bingham, R. G., Nienow, P. W. and Sharp, M. J. 2003. Intra-annual and intra-seasonal flow dynamics of a High Arctic polythermal valley glacier. *Annals of Glaciology.* **37,** 181-188.

Bingham, R. G., Nienow, P. W., Sharp, M. J. and Boon, S. 2005. Subglacial drainage processes at a High Arctic polythermal valley glacier. *Journal of Glaciology.* **51 (172),** 15-24.

Boon, S. and Sharp, M. 2003. The role of hydrologically-driven ice fracture in drainage system evolution on an Arctic glacier. *Geophysical Research Letters.* **30**(18), 1916, doi:10.1029/2003GL018034.

Box, J. E. and Ski, K. 2007. Remote sounding of Greenland supraglacial melt lakes: Implications for subglacial hydraulics. *Journal of Glaciology.* **53**(181), 257-265.

Box, J. E., Bromwich, D. H., Veenhuis, B. A., Bai, L.-S., Stroeve, J. C., Rogers, J. C., Steffen, K., Haran, T. and Wang, S.-H. 2006. Greenland Ice Sheet surface mass balance variability (1988-2004) from calibrated polar MM5 output. *Journal of Climate.* **19,** 2783-2800.

Box, J. E., Yang, L., Bromwich, D. H. and Bai, L-S. 2009. Greenland ice sheet surface air temperature variability: 1840-2007. *Journal of Climate.* **22,** 4029-4049.

Brenner, A. C., DiMarzio, J. P. and Zwally, H. J. 2007. Precision and accuracy of satellite radar and laser altimeter data over the continental ice sheets. *IEEE Transactions on Geoscience and Remote Sensing.* **45**(2), 321-331.

Budd, W. F., Keage, P.L. and Blundy, N. A. 1979. Empirical studies of ice sliding. *Journal of Glaciology.* **23,** 157-170.

Cappelen, J., Jørgensen, B. V. Laursen, E. V., Stannius, L. S. and Thomsen, R. S. 2001. The observed climate of Greenland 1958-99 with climatological normals 1961-1990. *Danish Meteorological Institute Technical Report.* 00-18.

Catania, G.A., Neumann, T. A. and Price, S. F. 2008. Characterizing englacial drainage in the ablation zone of the Greenland ice sheet. *Journal of Glaciology.* **54** (187), 567-578.

Chen, J. L., Wilson, C. R. and Tapley, B. D. 2006. Satellite gravity measurements confirm accelerated melting of Greenland ice sheet. *Science.* **313** (5795), 1958-1960.

Church, J. A., Gregory, J. M., Hurbrechts, P., Kuhn, M., Lambeck, K., *et al.*, 2001. Changes in sea level. In: *Climate change 2001: The scientific basis. Contribution of working group I to the third assessment report of the Intergovernmental Panel on Climate Change.* Eds. Houghton, J. T., Ding, Griggs, D. J., Noguer, M., van der Linden, P. J., Dai, X., Maskell, K. and Johnson, C. A. Cambridge University Press, Cambridge, United Kingdom and New York, NY, USA, 881pp.

Chylek, P., Dubey, M. K., and Lesins, G. 2006. Greenland warming of 1920-1930 and 1995-2005. *Geophysical Research Letters.* **33,** L11707.

Constantini, M. 1998. A novel phase unwrapping method based on network programming. *IEEE Transactions on Geoscience and Remote Sensing*, **36** (3), 813-821.

Copland, L., Mueller, D. R. and Weir, L. 2007. Rapid loss of the Ayles Ice Shelf, Ellesmere Island, Canada. *Geophysical Research Letters.* **34,** L21501.

Csatho, B. M., Bolzan, J. F., van der Veen, C. J., Schenk, A. F. and Lee, D-C. 1999. Surface velocities of a Greenland outlet glacier from high-resolution visible satellite imagery. *Polar Geography.* **23**(1), 71-82.

Csatho, B., Schenk, T., Shin, S. W. and van der Veen, C. J. 2002. Investigating long-term behaviour of Greenland outlet glaciers using high resolution satellite imagery. *Geoscience and remote sensing symposium, 2002. IGARSS '02. 2002 IEEE International.* **2,** 1047 – 1050.

Cuffey, K. M. and Marshall, S. J. 2000. Substantial contribution to sea-level rise during the last interglacial from the Greenland ice sheet. *Nature.* **404,** 591- 594.

Culter, P. M. 1998. Modelling the evolution of subglacial tunnels due to varying water input. *Journal of Glaciology.* **44(148),** 485-497.

Das, S. B., Joughin, I., Behn, M. D., Howat, I. M., King, M. A., Lizarralde, D. and Bhatia, M. P. 2008. Fracture propagation to the base of the Greenland Ice Sheet during supraglacial lake drainage. *Science.* **320,** 778-781.

Davis, C. H., Kluever, C. A. and Haines, B. J. 1998. Elevation change of the Southern Greenland Ice Sheet. *Science.* **279**(5359), 2086-2088.

Davis, C. H., Kluever, C. A., Haines, B. J., Perez, C. and Yoon, Y. T. 2000. Imporved elevation-change measurement of the southern Greenland ice sheet from satellite radar altimetry. *IEEE Transactions on Geoscience and Remote Sensing.* **38,** (3), 1367-1378.

De Lange, R., Luckman, A. and Murray, T. 2007. Improvement of satellite radar feature tracking for ice velocity derivation by spatial frequency filtering. *IEEE Transactions on Geoscience and Remote Sensing.* **45 (7),** 2309-2318.

Derauw, D. 1999. DInSAR and coherence tracking applied to glaciology: the example of Shirase Glacier. In *Proceedings of the workshop FRINGE '99,* Liege, Belgium.

DiMarzio, J., Brenner, A., Schutz, R., Shuman, C. A. and Zwally, H. J. 2007a. *GLAS/ICESat 500 m laser altimetry digital elevation model of Antarctica.* Boulder, Colorado USA: National Snow and Ice Data Center. Digital media.

DiMarzio, J., Brenner, A., Schutz, R., Shuman, C. A. and Zwally, H. J. 2007b. *GLAS/ICESat 1 km laser altimetry digital elevation model of Greenland.* Boulder, Colorado USA: National Snow and Ice Data Center. Digital media.

Dwyer, J. L. 1995. Mapping tide-water glacier dynamics in East Greenland using Landsat data. *Journal of Glaciology.* **41(139),** 584-595.

Echelmeyer, K., Clarke, T. S. and Harrison, W. D. 1991. Surficial glaciology of Jakobshavn Isbræ, West Greenland: Part I. Surface morphology. *Journal of Glaciology.* **37 (127),** 368-392.

Eiken, T., Hagen, J. O. And Melvold, K. 1997. Kinematic GPS survey of geometry changes on Svalbard glaciers. *Annals of Glaciology.* **24,** 157-163.

Ettema, J., van den Broeke, M. R., van Maijgaard, E., van de Berg, W. J., M., Bamber, J. L., Box, J. E. and Bales, R. C. 2009. Higher surface mass balance of the Greenland ice sheet revealed by high-resolution climate modelling. *Geophysical Research Letters.* **36,** L12501.

Fahnestock, M., Abdalati, W., Joughin, I., Brozena, J. and Gogineni, P. 2001. High geothermal heat flow, basal melt and the origin of rapid ice flow in central Greenland. *Science.* **294,** 2338-2342.

Fastook, J. L., Brecher, H. H. and Hughes, T. J. 1995. Derived bedrock elevations, strain rates and stresses from measured surface elevations and velocities: Jakobshavn Isbrae, Greenland. *Journal of Glaciology*.**41** (137), 161-173

Ferretti, A., Monti-Guarnieri, A., Prati, C., Rocca, F. and Massonnet, D. 2007. *InSAR Principles: Guidelines for SAR Interferometry processing and interpretation.* ESA publications, ESTEC, The Netherlands.

Fettweis, X., van Ypersele, J. –P., Gallée, H., Lefebre, F. And Lefebvre, W. 2007. The 1979-2005 Greenland ice sheet melt extent from passive microwave data using an improved version of the melt retrieval XPGR algorithm. *Geophysical Research Letters.* **34,** L05502.

Forbes, J. 1859. *Occasional papers on the theory of glaciers*. Edinburgh: Adam and Charles Black. Pp278

Forsberg, R., Keller, K., Nielsen, C. S., Gundestrup, N., Tscherning, C. C., Norvang Madsen, S. and Dall, J. 2000. Elevation change measurements of the Greenland Ice Sheet. *Earth and Planets Space*. **52,** 1049-1053.

Fountain, A. G. And Wlader, J. S. 1998. Water flow through temperate glaciers. *Reviews in Geophysics*. **36,** 299-328.

GAMMA remote sensing. 2008. *Documentation- theory. SAR processing*. Version 1.4. MSP documentation. MSP users guide. GAMMA Remote Sensing Research and Consulting AG, Bern. March 2008.

Georgiou, S., Shepherd, A., McMillan, M. and Nienow, P. 2009. Seasonal evolution of supraglacial lake volume from ASTER imagery. *Annals of Glaciology*. **50**(52), 95- 100.

Getis, A. and Boots, B. 1978. *Models of Spatial Processes*. Cambridge: Cambridge University Press.

Gogineni, S., Tammana, D., Braaten, D., Leuschen, C., Akins, T., Legarsky, J., Kanagaratnam, P., Stiles, J., Allen, C. and Jezek, K. 2001. Coherent radar ice thickness measurements over the Greenland ice sheet. *Journal of Geophysical Research*. **106,** D24, 33,761-33,772.

Goldstein, R. M., Zebker, H. A. and Werner, C. L. 1988. Satellite radar interferometry: two-dimensional phase unwrapping. *Radio Science*. **23**(4), 713-720.

Goldstein, R. M., Engelhardt, H., Kamb, B. and Frolich, R. M. 1993. Satellite radar interferometry for monitoring ice sheet motion: Application to an Antarctic ice stream. *Science*. **262,** 1525-1530.

Goldstein, R. M. and Werner, C. L. 1998. Radar interferogram filtering for geophysical applications. *Geophysical Research Letters*. **25**, 4035-4038.

Gregory, J. M., Huybrechts, P., Raper, S. C. B. 2004. Threatened loss of the Greenland ice-sheet. *Nature*. **428,** 616.

Greve, R. 2000. On the response of the Greenland ice sheet to greenhouse climate change. *Climate Change.* **46,** 289-303.

Gudmundsson, G. H. 2003. Transmission of basal variability to a glacier surface. *Journal of Geophysical Research.* **108 (B5),** 2253, doi: 10.1029/2002JB002107.

Gumley, L., Descloitres, J. and Schmatlz, J. 2007. *Creating reprojected MODIS true color images: A tutorial.* 19pp., URL ftp://ftp.ssec.wisc.edu/pub/IMAPP/MODIS/TrueColor (accessed November 2008).

Hall, D. K., Williams, R. S., Luthcke, S. B. and Digrolamo, N. E. 2008. Greenland ice sheet surface temperature, melt and mass loss: 2000-06. *Journal of Glaciology.* **54** (184), 81-93

Hanna, E., Huybrechts, P., Janssens, I., Cappelen, J., Steffen, K. and Stephens, A. 2005. Runoff and mass balance of the Greenland Ice Sheet: 1958-2003. *Journal of Geophysical Research.* **110,** D13108.

Hanna, E., Huybrechts, P., Steffen, K., Cappelen, J., Huff, R., Shuman, C., Irvine-Fynn, T., Wise, S. and Griffiths, M. 2008. Increased runoff from melt from the Greenland Ice Sheet: a response to global warming. *Journal of Climate.* **21,** 331-341.

Hanna, E., Cappelen, J., Fettweis, X., Huybrechts, P., Luckman, A. and Ribergaard, M. H. 2009. Hydrologic response of the Greenland ice sheet: the role of oceanographic warming. *Hydrologic Processes.* **23,** 7-30.

Hatzianastassiou, N. Cleridou, N. and Vardavas, I. 2001. Polar cloud climatologies from ISCCP C2 and D2 Datasets. *Journal of Climate.* **14,** 3851-3562.

Higgins, A. K., 1991. North Greenland glacier velocities and calf ice production. *Polarforschung.* **60(1),** 1-23.

Hock, R. 2003. Temperature index melt modelling in mountain areas. *Journal of Hydrology*. **282,** 104-115.

Hock, R. and Hooke, R. L. 1993. Evolution of the internal drainage system in the lower part of the ablation area of Storglaciären, Sweden. *Geological Society of America.* **105(4),** 537-546.

Hofmann, C., Schwäbisch, M., Och, S. Wimmer, C. and Moreira, J. R. 1999. Mulit-path P-band interferometry- first results. *Proceedings, Fourth International Airborne Remote Sensing*, Ottawa, **2**, 732-737.

Holland, D. M., Thomas, R. H., Young, B. D., Ribergaard, M. H. and Lyberth, B. 2008. Acceleration of Jakobshavn Isbræ triggered by warm subsurface ocean waters. *Nature Geoscience.* **1,** 659-664.

Holzapfel, R., Kopp, W. and Wegener, K. 1939. Meteorologie. In: Wegener, K. (ed): Wissenschaftliche Ergebnisse der deutschen Grönland- Expedition Alfred Wegener 1929 und 1930/31. Band IV. F.A. Brockhaus/Leipzig.

Houghton, J.T., Ding, Y., Griggs, D. J., Noguer, M., van der Linden, P. J., Dai, K., Maskell, K., and Johnson, C. A. 2001. *Climate change 2001:The scientific basis. Contribution of working group I to the third assessment report of the Intergovernmental Panel on Climate Change*. Cambrige University Press, Cambridge, United Kingdom and New York, NY, USA, 881pp.

Howat, I. M., Joughin, I., Tulaczyk, S. and Gogineni, S. 2005. Rapid retreat and acceleration of Helheim Glacier, east Greenland. *Geophysical Research Letters.* **32,** L22502.

Howat, I., Joughin, I. and Scambos, T. A. 2007. Rapid changes in ice discharge from Greenland outlet glaciers. *Science.* **315,** 1559-1561.

Howat, I. M., Joughin, I., Fahnestock, M., Smith, B. E. and Scambos, T. A. 2008. Synchronous retreat and acceleration of southeast Greenland outlet glaciers 2000-2006: ice dynamics and coupling to climate. *Journal of Glaciology.* **54(187),** 646-660.

Howat, I. M., Box, J. E., Ahn, Y., Herrington, A. and McFadden, E. M. 2010. Seasonal variability in the dynamics of the marine-terminating outlet glaciers. *Journal of Glaciology.* **56(198),** 601-613.

Hubbard, B. and Nienow, P. 1997. Alpine subglacial hydrology. *Quaternary Science Reviews.* **16,** 939-955.

Huybrechts, P. and de Wolde, J. 1999. The dynamic response of the Greenland and Antarctic ice sheets to multiple-century climatic warming. *Journal of Climate.* **12,** 2169-2188.

Iken, A. 1981. The effect of the subglacial water pressure on the sliding velocity of a glacier in an idealized numerical model. *Journal of Glaciology.* **27** (97), 407-421.

Iken, A. and Bindschadler, R. A. 1986. Combined measurements of sub-glacial water pressure and surface velocity of Findelengletscher, Switzerland: conclusions about drainage system and sliding mechanism. *Journal of Glaciology.* **32(110),** 101-119.

Iken, A., Röthlisberger, H., Flotron, A. and Haerberli, W. 1983. The uplift of Unteraargletscher at the beginning of the melt season – a consequence of water storage at the bed? *Journal of Glaciology.* **39,** 15-25.

Jensen, J. R. 1986. *Introductory Digital Image Processing.* Prentice-Hall, Englewood Cliffs, New Jersey. Pp 379.

Jiskoot, H. T., Murray, T. and Luckman, A. 2003. Surge potential and drainage basin characteristics in East Greenland. *Annals of Glaciology.* **36,** 142-148.

Johannessen, O. M., Khvorostovsky, K., Miles, M. W. And Bobylev, L. P. 2005. Recent ice-sheet growth in the interior of Greenland. *Science.* **310, (**5750), 1013-1016

Johansson, A. M., Brown, I. A. and Jansson, P. 2010. Multi-temporal, multi-sensor investigations of supra-glacial lakes on the Greenland ice sheet. *Proceedings of the ESA Living Planet Symposium Bergen, Norway 28 June- 2 July 2010.*

Joughin, I. R. and Winebrenner, D. P. and Fahnestock, M. A. 1995. Observations of ice-sheet motion in Greenland using satellite radar interferometry. *Geophysical Research Letters.* **22**(5), 571-574.

Joughin, I., Tulaczyk, S., Fahnestock, M. and Kwok, R. 1996a. A mini-surge on the Ryder Glacier, Greenland, observed by satellite radar interferometry. *Science.* **274,** 228-230.

Joughin, I., Winebrenner, D., Fahnestock, M., Kwok, R. and Krabill, W. 1996b. Measurement of ice-sheet topography using satellite-radar interferometry. *Journal of Glaciology.* **42 (140),** 10-22.

Joughin, I., Fahnestock, M., Ekholm,M. and Kwok, R. 1997. Balance velocities of the Greenland ice sheet. *Geophysical Research Letters.* **24**(23), 3045-3048.

Joughin, I. R., Kwok, R. and Fahnestock, M. A. 1998. Interferometric estimation of three-dimensional ice-flow using ascending and descending passes. *IEEE Transactions on Geoscience and Remote Sensing*. **36**, 25-37.

Joughin , I., Fahnestock, M., Kwok, R., Gogineni, P. and Allen, C. 1999. Ice flow of Humboldt, Peterman and Ryder Gletscher, northern Greenland. *Journal of Glaciology.* **45** (150), 231-241.

Joughin, I., Abdalati, W. and Fahnestock, M. 2004. Large fluctuations in speed on Greenland's Jakobshavn Isbræ glacier. *Nature.* **432,** 608-610.

Joughin, I., Howat, I. M., Fahnestock, M., Smith, B., Krabill, W., Alley, R. B., Stern, H. and Truffer, M. 2008a. Continued evolution of Jakobshavn Isbræ following its rapid speedup. *Journal of Geophysical Research.* **113,** F04006.

Joughin, I., Howat, I., Alley, R. B., Ekstrom, G., Fahnestock, M., Moon, T., Nettles, M., Truffer, M. and Tsai, V. C. 2008b. Ice-front variation and tidewater behaviour on Helheim and Kangerdlugssuaq Glaciers, Greenland. *Journal of Geophysical Research.* **113,** F01004.

Joughin, I., Das, S. B., King, M. A., Smith, B. E., Howat, I. M. and Moon, T. 2008c Seasonal speedup along the Western flank of the Greenland Ice Sheet. *Science.* **320,** 781-783.

Joughin, I., Smith, B. E., Howat, I. M., Scambos, T. and Moon, T. 2010a. Greenland flow variability from ice-sheet-wide velocity mapping. *Journal of Glaciology.* **56 (197),** 415-430.

Joughin, I., Smith, B. E. and Abdalati, W. 2010b. Glaciological advances made with interferometric synthetic aperture radar. *Journal of Glaciology.* **56**(200), 1026-1042.

Kääb, A. 2005. *Remote sensing of mountain glaciers and permafrost creep.* Schrifternreihe Physische Geographie. **48**, pp**.**266

Kääb, A. and Weber, M. 2004. Development of transverse ridges on rockglaciers. Field measurements and laboratory experiments. *Permafrost and Periglacial Processes.* **15**(4), 379-391.

Kääb, A., Huggel, C., Paul, F., Wessels, R., Raup, B., Kieffer, H. and Kargel, J. 2002. Glacier monitoring from ASTER imagery: accuracy and application. *Proceedings of EARSeL-LISSIG- Workshop observing our Cryosphere from space.* Bern, March 11-13-2002. 43-53.

Kamb, B. 1987. Glacier surge mechanism based on linked cavity configuration of the basal conduit system. *Journal of Geophysical Research.* **92**(B9), 9083-9100.

Kamb, B. and Echelmeyer, K., 1986. Stress-gradient coupling in glacier flow: 1. Longitudinal averaging of the influence of ice thickness and surface slope. *Journal of Glaciology.* **32,** 267-284.

Khan, S. A., Whar, J., Bevis, M., Velicogna, I. and Kendrick, E. 2010. Spread of ice mass loss into northwest Greenland observed by GRACE and GPS. *Geophysical Research Letters.* **37,** L06501

Knoll, C. And Kerschner, H. 2009. A glacier inventory for South Tyrol, Italy, based on airborne laser scanning. *Annals of Glaciology.* **50**(53), 46-52.

Koning, D. M. and Smith, D. J. 1999. Movement of King's Throne rock glacier, Mount Rae area, Canadian Rocky Mountains. *Permafrost and Periglacial Processes.* **10**(2), 151-162.

Krabill, W. B. 2009. Updated 2011. *IceBridge ATM L2 Icessn Elevation, Slope, and Roughness,* [May 2010]. Boulder, Colorado USA: National Snow and Ice Data Center. Digital media.

Krabill, W., Thomas, R., Martin, C. F., Swift, R. N. and Frederick. 1995. Accuracy of airborne laser altimetry over the Greenland ice sheet. *International Journal of Remote Sensing.* **16**(7), 1211-1222.

Krabill, W., Abdalati, W., Frederick, E., Manizade, S., Martin, C., Sonntag, J., Swift, R., Thomas, R., Wright, W. and Yungel, J. 2000. Greenland Ice Sheet: high-elevation balance and peripheral thinning. *Science.* **289** (5478), 428-430.

Krabill, W., Hanna, E., Huybrechts, P., Abdalati, W., Cappelen, J., Csatho, B., Frederick, E., Manizade, S., Martin, C., Sonntag, J., Swift, R., Thomas, R. and Yungel, J. 2004. Greenland ice sheet: Increased coastal thinning. *Geophysical Research Letters.* **31,** L24402.

Krawczynski, M. J., Behn, M. D., Das, S. B. and Joughin, I. 2009. Constraints on the lake volume required for hydro-fracture through ice sheets. *Geophysical Research Letters.* **36,** L10501, doi:10.1029/2008GL036765.

Kwok, R. and Fahnestock, M. M. 1996. Ice sheet motion and topography from radar interferometry. *IEEE Transactions on Geoscience and Remote Sensing.* **34**(1), 189-200.

Lang, H. and Braun, L. 1990. On the information content of air temperature in the context of snow melt estimation. In: Molnar, L., (Ed), *Hydrology of Mountainous Areas,* Proceedings of the Strbske Pleso Workshop, Czechoslovakia, June 1988. IAHS Publication No. 190. 347- 354.

Lemke, P., Ren, J., Alley, R. B., Allison, I., Carrasco, J., Flato, G., Fujii, Y., Kaser, G., Mote, P., Thomas, R. H. and Zhang, T. 2007. Observations: Changes in Snow, Ice and Frozen Ground. In: *Climate Change 2007: The Physical Science Basis. Contribution of Working Group I to the Fourth Assessment Report of the Intergovernmental Panel on Climate Change* [Solomon, S., Qin, D., Manning, M. Chen, Z., Marquis, M., Averyt, K. B., Tignor, M. and Miller, H. L. (eds.)]. Cambridge University Press, Cambridge, United Kingdom and New York, NY, USA.

Letreguilly, A., Reeh, N. and Huybrechts, P. 1991. The Greenland ice sheet through the last glacial – interglacial cycle. *Palaeogeography, Paleoclimatology and Palaeoecology*. **90,** 385-394.

Lillesand, T. M. and Keifer, R. W. 1999. *Remote sensing and image interpretation.* 4th Edition. Wiley. Pp736.

Lucchitta, B. K. and Ferguson, H. M. 1986. Antarctica: measuring glacier velocity from Satellite Images. *Science*. **234,** 1105-1108.

Lucchitta, B. K., Rosanova, C. E. and Mullins, K. F. 1995. Velocities of Pine Island Glacier, West Antarctica, from ERS-1 SAR images. *Annals of Glaciology*. **21,** 277-283.

Luckman, A. and Murray, T. 2005. Seasonal variation in velocity before retreat of Jakobshavn Isbrae, Greenland. *Geophysical Research Letters.* **32,** L08501, doi: 10.1029/2005GL022519

Luckman, A., Murray, T., Jiskoot, H., Pritchard, H. and Strozzi, T. 2003. ERS SAR feature tracking measurement of outlet glacier velocities on a regional scale in East Greenland. *Annals of Glaciology.* **36,** 129-134.

Luckman, A., Murray, T., de Lange, R. and Hanna, E. 2006. Rapid and synchronous ice-dynamic changes in East Greenland. *Geophysical Research Letters.* **33,** L03503.

Luckman, A., Quincey, D. and Beven, S. 2007. The potential of satellite radar interferometry and feature tracking for monitoring flow rates of Himalayan glaciers. *Remote Sensing of the Environment.* **111,** 172-181.

Luthcke, S. B., Zwally, H. J., Abdalati, W., Rowlands, D. D., Ray, R. D., Nerem, R. S., Lemoine, F. G., McCarthy, J. J. and Chinn, D. S. 2006. Recent Greenland ice mass loss by drainage system from satellite gravity observations. *Science.* **314,** 1286-1289.

Luthje, M., Pederson, L. T., Reeh, N. and Greuell, W. 2006. Modelling the evolution of supraglacial lakes on the West Greenland ice-sheet margin. *Journal of Glaciology*. **52 (179),** 608-618.

Madson, S. N., Martin, J. M. and Zebker, H. A., 1995. Analysis and evaluation of the NASA/ JPL TOPSAR across-track interferometric SAR system. *IEEE Transactions on Geoscience and Remote Sensing.* **33,** 383-391

Mair, D., Nienow, P., Sharp, M. J., Wohlleben, T. and Willis, I. 2002. Influence of subglacial drainage system evolution on glacier surface motion: Haut Glacier d'Arolla, Switzerland. *Journal of Geophysical Research.* **107,** B8, 2175.

Mair, D., Nienow, P., Willis, I. and Sharp, M. 2008. Spatial patterns of glacier motion during a high-velocity event: Haut Glacier d'Arolla, Switzerland. *Journal of Glaciology*. **47 (156),** 9-20.

Massom, R. and Lubin, D. 2006. *Polar Remote Sensing. Volume II: Ice Sheets.* Springer Berlin Heidelberg, pp 39-136.

Massonnet, D. and Feigl, K. L. 1998. Radar interferometry and its application to changes in the Earth's surface. *Reviews of Geophysics.* **36,** 441-500.

Meehl, G. A., Stocker, T. F., Collins, W. D., Friedlingstein, P., Gaye, A. T., Gregory, J. M., Kitoh, A., Knutti, R., Murphy, J. M., Noda, A., Raper, S. C. B., Waterson, I. G., Weaver, A. J. and Zhao, Z.-C., 2007. Global climate projections. In: *Climate Change 2007: The Physical Science Basis. Contribution of Working Group I to the Fourth Assessment Report of the Intergovernmental Panel on Climate Change* [Solomon, S., Qin, D., Manning, M. Chen, Z., Marquis, M., Averyt, K. B., Tignor, M. and Miller, H. L. (eds.)]. Cambridge University Press, Cambridge, United Kingdom and New York, NY, USA.

Meier, M. F. 1960. Mode of flow of Saskatchewan Glacier, Alberta, Canada. *US Geological Survey Professional Paper.* **351**

Meier, M. F. And Post, A. 1987. Fast tidewater glaciers. *Journal of Geophysical Research.* **92(B9),** 9051-9058.

Meier, M., Lundstrom, S., Stone, D., Kamb, B., Engelhardt, H., Humphrey, N., Dunlap, W. W., Fahnestock, M., Krimmel, R. M. and Walters, R. 1994. Mechanical and hydrologic basis for the rapid motion of a large tidewater glacier 1. Observations. *Journal of Geophysical Research.* **99**(B8), 15219-15229. Doi:10.1029/94JB00237.

Mohr, J. J., Reeh, N. and Madsen, S. N. 1998. Three-dimensional glacial flow and surface elevation measures with radar interferometry. *Nature*. **391,** 273-276.

Motyka, R., J., Hunter, L., Echelmeyer, K. A. and Connor, C. 2003. Submarine melting at the terminus of a temperate tidewater glacier, LeConte Glacier, Alaska, U.S.A. *Annals of Glaciology*. **36**(11), 57-65.

McMillan, M., Nienow, P., Shepherd, A., Benham, T. and Sole, A. 2007. Seasonal evolution of supra-glacial lakes on the Greenland Ice Sheet. *Earth and Planetary Science Letters.* **262,** 484-492.

Murray, T., Scharrer, K., James, T. D., Dye, S. R., Hanna, E. Booth, A. D., Selmes, N., Luckman, A., Hughes, A. L.C., Cook, S. and Huybrechts, P. 2010. Ocean regulation hypothesis for glacier dynamics in southeast Greenland and implications for ice sheet mass changes. *Journal of Geophysical Research.* **115,** F03026, doi:10.1029/2009JF001522.

Nick, F., M., Vieli, A., Howat, I. M. and Joughin, I. 2009. Large-scale changes in Greenland outlet glacier dynamics triggered at the terminus. *Nature Geoscience.* **2,** 110-114.

Nienow, P., Sharp, M. and Willis, I., 1998. Seasonal changes in the morphology of the subglacial drainage system, Haut Glacier d'Arolla, Switzerland. *Earth Surface Processes and Landforms.* **23,** 825-843.

Otto-Bliesner, B. L., Overpeck, J. T., Marshall, S. J., Miller, G. 2006. Simulating Arctic climate warmth and icefield retreat in the Last interglaciation. *Science.* **311,** 1751-1753.

Overpeck, J. T., Otto-Bliesner, B. L., Miller, G. H., Muhs, D. R., Allet, R. B. and Kiehl, J. T. 2006. Paleoclimatic evidence for future ice sheet instability and rapid sea-level rise. *Science.* **311,** 1747-1750.

Paar, G., Bauer, A. and Kauffmann, V. 2001. Rock glacier monitoring using terrestrial laser scanning. Abstract. *Proceedings, 1st European Permafrost Conference,* Rome, 58-59.

Palmer, S., Shepherd, A., Nienow, P. and Joughin, I. 2011. Seasonal speedup of the Greenland Ice Sheet linked to routing of surface water. *Earth and Planetary Science Letters.* **302,** 423-428.

Parizek, B. R. and Alley, R. B. 2004. Implications of increased Greenland surface melt under global-warming scenarios: ice sheet simulations. *Quaternary Science Reviews.* **23,** 1013-1027.

Parry, M. L., Canziani, O. F., Palutikof, J. P. and co-authors. 2007. *Climate change 2007: Impacts, adaptation and vulnerability. Contribution of working group II to the fourth assessment report of the Intergovernmental Panel on Climate Change.* Parry, M. L., Canziani, O. F., Palutikof, J. P., van der Linden, P.J. and Hanson, C. E., Eds., Cambridge University Press, Cambridge, UK.

Paterson, W. S. B. 1994. *The Physics of Glaciers.* Pergamon Press/ Elsevier Ltd., Oxford, 3rd ed., 480 pp.

Pattyn, F. and Derauw, D. 2002. Ice-dynamic conditions of the Shirase Glacier, Antarctica, inferred from ERS SAR interferometry. *Journal of Glaicology.***48** (163), 559-565

Pfeffer, W. T. 2007. A simple mechanism for irreversible tidewater glacier retreat. *Journal of Geophysical Research.* **112,** F03S25

Phalippou, L. and Wingham, D. G. 1999. HSRRA: An advanced radar altimeter for ocean and Cryosphere monitoring. *Proceedings of CEOS SAR Workshop, October 26-29.* ESA, Noordwijk, The Netherlands/Centre National d'Etudes spatiale, Toulouse, France.

Pitkänen, T. and Kajuutti, K. 2004. Close-range photogrammetry as a tool in glacier changes detection. *ISPRS International Archives of Photogrammetry, Remote Sensing and Spatial Information Sciences,* XXXV (B7), 769-773.

Pritchard, H., Murray, T., Luckman, A., Strozzi, T. and Barr, S. 2005. Glacier surge dynamics of Sortebræ, east Greenland, from synthetic aperture radar feature tracking. *Journal of Geophysical Research.***110,** F03005, doi:10.1029/2004JF000233.

Pritchard, H. D., Arthern, R. J., Vaughan, D. G. And Edwards, L. A. 2009. Extensive dynamic thinning on the margins of the Greenland and Antarctic ice sheets. *Nature.* **461,** 971-975.

Price, S. F., Payne, A. J., Catania, G. A. and Neumann, T. A. 2008. Seasonal acceleration of inland ice via longitudinal coupling to marginal ice. *Journal of Glaciology.* **54 (185),** 213-219.

Rabus, B. T. and Lang, O. 2003. Interannual surface variations of Pine Island Glacier, West Antarctica. *Annals of Glaciology.* **36,** 205-214

Ramillien, G., Lombard, A., Cazenave, A., Ivins, E. R., Llubes, M., Remy, F. and Biancale, R. 2006. Interannual variations of the mass balance of the Antarctica and Greenland ice sheets from GRACE. *Global and Planetary Change.* **53** (3), 198-208.

Reeh, N., Thomsen, H. H., Higgins, A. K. and Weidick, A. 2001. Sea ice and the stability of north and northeast Greenland floating glaciers. *Annals of Glaciology.* **33,** 474- 480.

Rees, W. G. 2001. *Physical Principles of Remote Sensing.* Second Edition. Cambridge University Press, UK. Pp 343

Ribergaard, M. H. 2007. *Oceanographic Investigations off West Greenland 2006.* NAFO Scientific Council Documents 07/001.

Richards, J. A. 1999. *Remote Sensing Digital Image Analysis.* Springer-Verlag, Berlin. pp. 240.

Rignot, E. 1995. Backscatter model for the unusual radar properties of the Greenland Ice Sheet. *Journal of Geophysical Research.* **100 (E5),** 9389-9400.

Rignot, E. 1996. Tidal motion, ice velocity and melt rate of Petermann Gletscher, Greenland, measured from radar interferometry. *Journal of Glaciology.* **42**(142), 476-485.

Rignot, E. and Kanagaratnam, P. 2006. Changes in the velocity structure of the Greenland Ice Sheet. *Science.* **311,** 986-990.

Rignot, E., Jezek, K. C. and Sohn, H. G. 1995. Ice flow dynamics of the Greenland ice sheet from SAR interferometry. *Geophysical Research Letters.* **22**(5), 575-578

Rignot, E., Gogineni, S., Krabill, W. and Ekholm, S. 1997. North and north-east Greenland ice discharge from satellite radar interferometry. *Science.***276**(5314), 934-937.

Rignot, E., Gogineni, S., Joughin, I. and Krabill, W. 2001. Contribution to the glaciology of northern Greenland from satellite radar interferometry. *Journal of Geophysical Research.* **106**(D24), 34007-34019.

Rignot, E., Box, J. E., Burgess, E. and Hanna, E. 2008. Mass balance of the Greenland ice sheet from 1958 to 2007. *Geophysical Research Letters.* **35,** L20502.

Rignot, E., Koppes, M and Velicogna, I. 2010. Rapid submarine melting of the calving faces of West Greenland glaciers. *Nature Geoscience.* **3,** 187-191.

Rignot, E., Velicogna, I., van den Broeke, M. R., Monaghan, A. and Lenaerts, J. 2011. Acceleration of the contribution of the Greenland and Antarctic ice sheets to sea level rise. *Geophysical Research Letters.* **38,** L05503, doi:10.1029/2011GL046583.

Ritz, C., Fabre, A. and Letreguilly, A. 1997. Sensitivity of a Greenland ice sheet model to ice flow and ablation parameters: Consequences for evolution through the last climatic cycle. *Climate Dynamics.* **13,** 11-24.

Rosanova, C. E., Lucchitta, B. K., Ferringo, J. G. 1998. Velocities of Thwaites Glacier and smaller glaciers along the Marie Byrd Land coast, West Antarctica. *Annals of Glaciology.* **27,** 47-53.

Rosen, P. A., Werner, C. W. and Hiramatsu, A. 1994. Two–dimensional phase unwrapping of SAR interferograms by charge connection through neutral trees. in *Proceedings of IGARSS '94, Pasadena, 8-12 August, 1994.*

Rosen, P. A., Hensley, S., Joughin, I. R., Li, F. K., Madsen, S. N., Rodríguez, E. and Goldstein, R. M. 2000. Synthetic Aperture Radar Interferometry. *Proceedings of the IEEE.* **88**, 333-382.

Schoof, C. 2010. Ice-sheet acceleration driven by melt supply variability. *Nature.* **468,** 803-806.

Sharp, M. 2005. Subglacial drainage. *Encyclopaedia of Hydrological Sciences.* 2587-2600.

Shepherd, A., Hubbard, A., Nienow, P. King, M., McMillan, M. and Joughin, I. 2009, Greenland ice sheet motion coupled with daily melting in late summer. *Geophysical Research Letter.* **36,** L01501.

Shuman, C. A., Zwally, H. J., Schutz, B. E., Brenner, A. C., DiMarsio, J. P., Suchdeo, V. P. and Fricker, H. A. 2006. ICESat Antarctic elevation data: Preliminary precision and accuracy assessment. *Geophysical Research Letters.* **33,** L07501, doi:10.1029/2005GL025227.

Slobbe, D. C., Ditmar, P. And Lindenbergh, R. C. 2009. Estimating the rates of mass change, ice volume change and snow volume in Greenland from ICESat and GRACE data. *Geophysical Journal International.***176,** 95-106.

Sneed, W. A. and Hamilton, G. S. 2007. Evolution of melt pond volume on the surface of the Greenland Ice Sheet. *Geophysical Research Letters.* **34,** L03501, doi:10.1029/2006GL028697.

Sohn, H.-G., Jezek, K. C. And van der Veen, C. J. 1998. Jakobshavn Glacier, West Greenland: 30 years of spaceborne observations. *Geophysical Research Letters.* **25 (14),** 2699-2702.

Sole, A., Payne, T., Bamber, J., Nienow, P. And Krabill, W. Testing hypotheses of the cause of peripheral thinning of the Greenland Ice Sheet: is land-terminating ice thinning at anomalously high rates? *The Cryosphere.* **2,** 205-218.

Sonntag, J. 2011. Spring 2011 IceBridge Flight Plans. 17 February 2011 draft. Accessed on 27/05/2011 ftp://atm.wff.nasa.gov/outgoing/oibscienceteam/flightplans20110217.pdf

Stearns, L. A. and Hamilton, G. S. 2007. Rapid volume loss from two East Greenland outlet glaciers quantified using repeat stereo satellite imagery. *Geophysical Research Letters.* **34,** L05503, doi:10.1029/2006GL028982.

Stearns, L. A., Hamilton, G. S. and Reeh, N. 2005. Multi-decadal record of ice dynamics on Daugaard Jensen Gletscher, East Greenland, from satellite imagery and terrestrial measurements. *Annals of Glaciology.* **42(1),** 53-58.

Stebler, O., Barmettler, A., Divis, L., Small, D., Schwerzmann, A. Meier, E. and Nüesch, D. 2004. Swiss Alpine Airborne SAR Experiment (SASARE) part I: Multi-baseline polarimetric SAR interferometry studies at L- and P- band. *Proceedings IEEE International Geoscience and Remote Sensing Symposium (IGARSS).* Anchorage, Alaska, **2,** 1116-1120.

Steffen, K. and Box, J. 2001. Surface climatology of the Greenland ice sheet: Greenland climate network 1995-1999. *Journal of Geophysical Research.* **106,** D24, 33,951-33,964. doi:10.1029/2001JD900161

Steffen, K., Nghiem, S. V., Huff, R. and Neumann, G. The melt anomaly of 2002 on the Greenland ice sheet from active and passive microwave satellite observations. *Geophysical Research Letters.* **31,** L20402.

Straneo, F., Hamilton, G. S., Sutherland, D. A., Stearns, L. A., Davidson, F., Hammill, M. O., Stenson, G. B. and Rosing-Asvid, A. 2010. Rapid circulation of warm subtropical waters in a major glacial fjord in East Greenland. *Nature Geoscience.* **3,** 182-186.

Straneo, F., Curry, R. G., Sutherland, D. A., Hamilton, G. S., Cenedese, C., Vage, K. and Stearns, L. A. 2011. Impact of fjord dynamics and glacial runoff on the circulation near Helheim Glacier. *Nature Geoscience.* Advanced publication.

Strozzi, T., Luckman, A., Murray, T., Wegmüller, U. and Werner, C. L. 2002. Glacier motion estimation using SAR offset-tracking procedures. *IEEE Transaction on Geoscience and Remote Sensing.***40 (11),** 2384-2391.

Sundal, A. V. 2008. Part II: Supporting document. Determining supra-glacial lake area from MODIS satellite images. Masters Thesis. Submitted to the University of Edinburgh. August 2008.

Sundal, A. V., Shepherd, A., Nienow, P., Hanna, E., Palmer, S. and Huybrechts, P. 2009. Evolution of supra-glacial lakes across the Greenland Ice Sheet. *Remote Sensing of the Environment.***113,** 2164-2171.

Sundal, A. V., Shepherd, A., Nienow, P., Hanna, E. Palmer, S. Huybrechts, P. 2011. Melt-induced speed-up of Greenland ice sheet offset by efficient subglacial drainage. *Nature*. **469**, 521-524.

Tedesco, M. 2007. Snowmelt detection over the Greenland ice sheet from SSM/I brightness temperature daily variations. *Geophysical Research Letters*. **34**, L02504.

Thomas, R. H. 2004. Force-perturbation analysis of recent thinning and acceleration of Jakobshavn Isbræ, Greenland. *Journal of Glaciology.* **50(168),** 57-66.

Thomas, R. H., Abdalati, W., Akins, T. L., Csatho, B. M., Frederick, E. B., Gogineni, S. P., Krabill, W. B., Manizade, S. S. and Rignot, E. J. 2000. Substantial thinning of a major east Greenland outlet glacier. *Geophysical Research Letters.* **27 (9),** 1291-1294.

Thomas, R., Akins, T., Csatho, B., Fahnestock, M., Gogineni, P., Kim, C. And Sonntag, J. 2000. Mass balance of the Greenland Ice Sheet at high elevations. *Science.* **289,** 426-428.

Thomas, R., Rignot, E., Casassa, G., Kanagaratnam, P., Acuna, C., Akins, T., Brecher, H., Frederick, E., Gogineni, P., Krabill, W., Manizade, S., Ramamoorthy, H., Rivera, A., Russell, R., Sonntag, J., Swift, R., Yungel, J. and Zwally, J. 2004. Accelerated sea-level rise from West Antarctica. *Science.* **306,** (5694), 225-258.

Thomas, R., Frederick, E., Krabill, W., Manizade, S. and Martin, C. 2006. Progressive increase in ice loss from Greenland. *Geophysical Research Letters.* **33,** L10503.

Thomas, R., Davis, C., Frederick, E., Krabill, W., Li, Y., Maizade, S. and Martin, C. 2008. A comparison of Greenland ice-sheet volume changes derived from altimetry measurements. *Journal of Glaciology.* **54** (185), 203-212.

Thomas, R., Frederick, E., Krabill, W., Manizade, S. and Martin, C. 2009. Recent changes on Greenland outlet glaciers. *Journal of Glaciology.* **55(189),** 147-162.

Thomsen, H. H., Thorning, L. and Braithwaite, R. 1988. Glacier hydrological conditions on the inland ice north-east of Jakobshavn/Ilulisat, West Greenland. *Rapport Grølands Geologiske Undersøgelse*. **138,** mapsheet

Thomsen, H. H., Thorning, L. and Olesen, O. B. 1989. Applied glacier research for planning hydro-electric power, Ilulissat/Jakobshavn, West Greenland. *Annals of Glaciology.* **13,** 257-261.

Toutin, T. and Cheng, P. 2002. Comparison of automated digital elevation model extraction results using along-track ASTER and across-track SPOT stereo-images. *Optical Engineering.* **41**(9), 2102-2106

Trabant, D. C., Krimmel, R. M., Echelmeyer, K. A., Zirnheld, S. L. and Elsberg, D. H. 2003. The slow advance of a calving glacier: Hubbard Glacier, Alaska, USA. *Annals of Glaciology.* **36,** 45-50

Vachon, P. W., Geudtner, D., Gray, A. L., Mattar, K., Brugman, M. and Cumming, I. G. 1996. Airborne and spacborne SAR interferometry: Application to the Athabasca glacier area. *Proceedings, IGARSS '96,* Lincoln, Nebraska, 2255-2257.

Van de Wal, R. S. W. and Ekholm, S. 1996. On elevation as input for mass balance calculations of the Greenland ice sheet. *Annals of Glaciology.***23,** 181-186.

Van de Wal, R. S. W., Boot, W., van den Broeke, M. R., Smeets, C. J. P. P., Reijmer, C. H., Donker, J. J. A. and Oerlemans, J. 2008. Large and rapid melt-induced velocity changes in the ablation zone of the Greenland Ice Sheet. *Science.* **321,** 111-113.

Van den Broeke, M., Bamber, J., Ettema, J., Rignot, E., Schrama, E., van de Berg, W. J., van Maijgaard, E., Velicogna, I. and Wouters, B. 2009. Partitioning recent Greenland Mass Loss. *Science.* **326,** 984-986.

Van der Veen, C. J. 1998. Fracture mechanics approach to penetration of surface crevasses on glaciers. *Cold Regions Science and Technology*. **27,** 31-47.

Van der Veen, C. J. 1999. *Fundamentals of Glacier Dynamics.* A. A. Balkema Publishers, Rotterdam. 462 pp.

Van der Veen, C. J. 2007. Fracture propagation as means of rapidly transferring surface meltwater to the base of glaciers. *Geophysical Research Letters.* **34,** L01501

Velicogna, I. 2009 Increasing rates of ice mass loss from the Greenland and Antarctic ice sheets revealed by GRACE. *Geophysical Research Letters.* **36,** L19503.

Velicogna, I. and Wahr, J. 2005. Greenland mass balance from GRACE. *Geophysical Research Letters.* **32,** L18505, doi:10.1029/2005GL023955

Velicogna, I. and Wahr, J. 2006. Acceleration of Greenland ice mass loss in spring 2004. *Nature.* **443,** 329-331.

Vieli, A., Funk, M. and Blatter, H. 2001. Flow dynamics of tidewater glaciers: a numerical modelling approach. *Journal of Glaciology*. **47** (159), 595-606.

Vieli, A., Jania, J., Blatter, H. and Funk, M. 2004. Short-term velocity variation on Hansbreen, a tidewater glacier in Spitsbergen. *Journal of Glaciology*. **50 (170),** 389-398.

Warren, C. R. and Glasser, N. F. 1992. Contrasting response of South Greenland glaciers in response to recent climate change. *Arctic and Alpine Research.* **24(2),** 124-132.

Weertman, J. 1973. Can a water-filled crevasse reach the bottom surface of a glacier? *ISAH Publication 95* (Symposium at Cambridge 1969-*Hydrology of Glaciers*), 139-145.

Wegmüller, U., Werner, C. and Strozzi, T. 1998. SAR interferometric and differential interferometric processing chain. *Geoscience and Remote Sensing Proceedings, 1998, IGARSS '98.* Seattle, USA. *1998 IEEE International.*

Wegmüller, U., Werner, C., Strozzi, T. and Wiesmann, A. 2002. *Phase unwrapping with GAMMA ISP* (technical report). GAMMA Remote Sensing AG, Bern, Switzerland.

Weidick, A. 1988. Surging glaciers in Greenland- a status. *The Geological Survey of Greenland: Report No. 140.* 106-110.

Weidick, A. 1995. *Satellite Image Atlas of the World: Greenland.* US government print office, Washington, D. C.

Welch, R. 1990. 3-D terrain modelling for GIS applications. *GIS World.* **3**(5), 26-30.

Werner, C., Wegmüller, U., Strozzi, T. and Wiesmann, A. 2005. Precision estimation of local offsets between pairs of SAR SLCs and detected SAR images. *Geoscience and Remote Sensing Symposium, 2005. IGARSS '05. Proceedings. 2005 IEEE International*. **7,** 4803-4805.

Willis, I. C. 1995. Intra-annual variations in glacier motion: a review. *Progress in Physical Geography*. **19(1),** 61-106.

Wimmer, c., Siegmund, R., Schwäbisch, M. and Moreira, J. R. 2000. Generation of high-precision DEMs of the Wadden Sea with airborne interferometric SAR. *IEEE Transactions on Geoscience and Remote Sensing.* **38,** 2234-2245.

Wingham, 1995. Elevation change of the Greenland ice sheet and its measurement with satellite radar altimetry. *Philosophical Transactions of the Royal Society of London- A.* **352**(1699), 335-346.

Wouters, B., Chambers, D. and Schrama, E. J. O. 2008. GRACE observes small-scale mass loss in Greenland. *Geophysical Research Letters.* **35,** L20501.

Wu, C. F. J. 1986. Jackknife, bootstrap and other resampling methods in regression analysis. *Annals of Statistics.* **14**(4), 1261-1295.

Young, N. W. and Hyland, G. 2002. Velocity and strain rates derived from InSAR analysis over the Amery Ice Shelf, East Antarctica. *Annals of Glaciology.* **34,** 228-234.

Zebker, H. A. and Goldstein, R. M. 1986. Topographic mapping from interferometric synthetic aperture radar observations. *Journal of Geophysical Research.* **91, B5,** 4993-4999.

Zebker, H. A., Werner, C. L., Rosen, P.A. and Hensley, S. 1994. Accuracy of topographic maps derived from ERS-1 interferometry. *IEEE Transactions on Geoscience and Remote Sensing.* **GE-32**(4), 823-836.

Zwally, J. H., Bindschadler, R. A., Brenner, A. C., Major, J. A. and Marsh, J. G. 1989. Growth of Greenland ice sheet: measurement. *Science.* **246** (4937) 1587-1589.

Zwally, H. J., Abdalati, W., Herring, T., Larson, K., Saba, J. and Steffen, K. 2002. Surface melt-induced acceleration of Greenland Ice Sheet flow. *Science.* **297,** 218-222.

Zwally, H.J., R. Schutz, C. Bentley, J. Bufton, T. Herring, J. Minster, J. Spinhirne, and R. Thomas. 2003 updated 2009. /GLAS/ICESat L1B Global Elevation Data V018/. data used: 2008-2009. Boulder, CO: National Snow and Ice Data Center. Digital media.

Zwally., H. J., Giovinetto, M. B., Li, J., Cornejo, H. G., Beckley, M. A. , Brenner, A. C., Saba, J. L. and Yi, D. 2005. Mass changes of the Greenland and Antarctic ice sheets and shelves and contributions to sea-level rise: 1992-2002. *Journal of Glaciology.* **51** (175), 509-527.

Zwally, H. J., Li, J., Brenner, A. C., Beckley, M., Cornejo, H. G., DiMarzio, J., Giovinetto, M. B., Neumann, T. A., Robbins, J., Saba, J. L., Yi, D. and Wang, W. 2011. Greenland ice sheet mass balance: distribution of increased mass loss with climate warming; 2003-07 versus 1992-2002.